LUND UNIVERSITY

MASTER'S THESIS

DEPARTMENT OF MECHANICAL ENGINEERING
DIVISION OF MATERIALS ENGINEERING
FACULTY OF ENGINEERING, LTH
DECEMBER 2017

Catalytic ortho- to parahydrogen conversion in liquid hydrogen

AUTHOR: Emil Karlsson

SUPERVISOR:
MONIKA HARTL, EUROPEAN SPALLATION SOURCE AB, LUND

SUPERVISOR:
HOSSEIN SINA, LUND UNIVERSITY, MATERIALS ENGINEERING

EXAMINER:
SRINIVASAN IYENGAR, LUND UNIVERSITY, MATERIALS ENGINEERING

ISRN LUTFD2/TFMT--17/5056--SE

EUROPEAN SPALLATION SOURCE

Acknowledgement

This thesis has been conducted at the European Spallation Source facilities in cooperation with the Division of Materials Engineering at the Lund Institute of Technology.

Firstly, I would like to give a special thanks to my supervisor at the ESS, Monika Hartl for making this thesis possible and for all invaluable support and knowledge she has provided during this project. I would like to give an acknowledgement to the target and materials group at the European Spallation Source at Lund.

Thanks to Guenter, Cryrille, Christoph, Yongjoong, Anna and Harald for sacrificing their time to help me when needed during this project, providing their knowledge and for sharing their laboratory facilities and equipment with me during this project. A warm thank you to the rest of the employees that I have met under my time here at ESS for making me feel welcome and a part of the ESS.

Finally, I would like to give my deepest gratitude to professor Srinivasan Iyengar for introducing me to this project and for all the support and knowledge that he has provided. I would also like to thank my supervisor at the Division of materials Engineering Hossein Sina for his support.

Abstract

The kinetics of the catalytic conversion of ortho- to parahydrogen was studied for the two catalysts, IONEX® and OXISORB®. The study also involved the optimization of an experimental technique for the conversion of orthohydrogen in a static setup. The main focus of the optimization being directed towards the analytical setup, where the acquisition of information and interpretation of the data were two main points for optimization. The rate of conversion is an important factor regarding the choice of catalyst for the future ESS hydrogen loop. A parahydrogen concentration of 99.5% has been determined as the lowest concentration yield from the catalytic conversion process. Both catalyst showed a good performance for the conversion of ortho- to parahydrogen, where a concentration of 99.7 to 99.8% parahydrogen was obtained from the experiments.

The kinetics for the catalyzed conversion of orthohydrogen using IONEX® and OXISORB® was determined to be based on first order exponential equations. The kinetics of IONEX® was described by a single first order exponential function. While the conversion of OXISORB® showed to be a function of two first order equations, which exhibits an independence as well as a codependence on one another.

The kinetics of conversion for the catalyst showed that the IONEX® catalyst is more efficient in converting ortho-hydrogen into parahydrogen. This is shown from the specific rate and the space velocity of the catalyst, based on the conditions of the experiment and the ESS hydrogen loop respectively.

Both catalysts appear to be suitable options for the future ESS hydrogen loop, where both catalysts possess the catalytic strength to compensate for the back conversion of parahydrogen during moderation of the emitted neutrons. The study shows that the IONEX® catalyst is the most efficient option but the final assessment would require a study of the long-term degenerative effects of the catalysts which could not be determined from the limited number of experiments carried out in this work.

Nomenclature

A_1	Amplitude of the exponential equation
a	Vibrational ground state
b	Vibrational excited state
C	Concentration of reactant
c	Velocity of light in vacuum
C_{CL}	Calibrated leak for the leak detector
CF_1	The first combined function from the empirical modeling.
CF_2	The second combined function from the empirical modeling.
C_{Ortho}	Corrected concentration of orthohydrogen
C_0	Initial concentration of reactant
$^{\circ}C$	Degrees Celsius
D	Lens diameter
D_{3d}^6	Point group of corundum
D_L	Lens diameter
F	F-number of a lens
f	Focal length of a lens
F_{Bypass}	Flow rate of the catalyst bypass loop
F_{Mod}	Flow rate of the moderator loop
H	Hydrogen
H_2	Hydrogen molecule
$H2B$	Experiments involving the characterization of the hydrogen signal using backscattering geometry
H_2^O	Orthohydrogen

$H_{2_{END}}^{O}$	Final concentration of orthohydrogen determined at the end of the catalytic conversion experiment
$H_{2_{INIT}}^{O}$	Initial concentration of orthohydrogen determined at the start of the catalytic conversion experiment
H_2^P	Parahydrogen
$H_{2_{END}}^{P}$	Final concentration of parahydrogen determined at the end of the catalytic conversion experiment
$H_{2_{INIT}}^{P}$	Initial concentration of parahydrogen determined at the start of the catalytic conversion experiment
$H2T$	Experiments involving the characterization of the hydrogen signal using transmission geometry
γ_{assym}	Anti symmetric stretch of the silicon oxygen bond
γ_{sym}	Symmetric stretching vibrations of the Si-O-Si lattice in solid silica
i	Index for a specific experiment
ION	Experiments involving IONEX® as the catalyst material
I_{Ortho}	Integrated intensity of orthohydrogen (J: 0➔2)
I_{Para}	Integrated intensity of parahydrogen (J: 1➔3)
I_0	Incident light onto the filter
I_1	Transmitted light from a filter
J	Rotational state
K	Kelvin
k	Rate constant
k_{Bond}	Force constant of the molecular bond
λ	Wavelength
m_{Cat}	Amount of catalyst in the catalytic conversion experiments

$m_{Cat_{Tot}}$	Total amount of catalyst for the ESS liquid hydrogen conversion loop
m_{H_2}	Mass of the relative hydrogen amount
m_{Tot}	Combined moment of atomic spins in a molecule
N	Number of atoms in a molecule
n	Order of the rate equation
n_{box}	Boxcar width a computational setting for the Raman spectrometer, related to adjacent smoothing
$n_{\frac{Bypass}{Moderator}}$	Fraction of how many circulations a hydrogen molecule can make in the catalyst bypass loop compared to the moderator loop.
n_{H_2}	Amount of hydrogen in the catalytic conversion experiments
$n_{scans\,to\,average}$	Number of scans collected for a single measurement for the Raman spectrometer
ν	Frequency
ν_{H-H}	Vibration of the hydrogen-hydrogen bond
OD	Optical density
OXI	Experiments involving OXISORB® as the catalyst material
P_{H_2}	Hydrogen pressure measured in the storage cylinder
q_G	Leak evaluation
ϖ	Wavenumber
R	Gas constant
R_S	Residual signal
R_{Sp}	Space velocity, representing the rate of the catalytic reaction based on the hydrogen and catalyst amount used in the experiment.

R_{Tot}	Catalytic rate which represents the conversion rate of the total catalyst amount, the rate is based on the determined amount of catalyst for the ESS liquid hydrogen loop and the space velocity of the catalytic reaction.
S	Total spin configuration of a molecule
S_{CL}	Calibrated leak signal
Seg_1	Curve represented by the first linear segment determined from the catalytic conversion using OXISORB® as catalyst
Seg_2	Curve represented by the second linear segment determined from the catalytic conversion using OXISORB® as catalyst
S_L	Signal leak
T	Temperature
t	Conversion time for the empirical model
t_{Bypass}	Time required for a hydrogen molecule to travel around the catalyst bypass loop
t_{eq}	Time when equilibrium is reached for the catalytic conversion experiments
$t_{integration}$	Integration time for the Raman spectrometer
t_{Mod}	Time required for a hydrogen molecule to travel around the entire moderator loop
t_{scan}	Acquisition time for a single measurement using Raman spectroscopy
t_1	Time factor of the exponential equation
$t_{\frac{1}{2}}$	Half-life for the catalytic conversion of orthohydrogen
τ	Rate constant of the conversion of orthohydrogen obtained from the linear fitting of the natural logarithm
U	Reduced atomic mass
V_{Cyl}	Volume of storage cylinder

v_n	Vibrational quantum number
x	Conversion time
Ψ_E	Electronic wave function
Ψ_N	Nuclear wave function
Ψ_R	Rotational wave function
Ψ_T	Translational wave function
Ψ_{Tot}	Total wave function
Ψ_V	Vibrational wave function
y_0	The offset value in the exponential equation
y_E	Extrapolated ratio of ortho and para hydrogen, based on the determined exponential equation
y^{Isomer}	Final percentage of the hydrogen isomer, determined from the fitted exponential equation

Abbreviations

Al_2O_3	Aluminum oxide
CCD	Charge Coupled Device
CrO	Chromium(II) oxide
2-D	Two dimensional
ERIC	European Research Infrastructure Consortium
ESS	European Spallation Source
Fe_2O_3	Iron(III) oxide
FFT-CCD	Full Frame Transfer Charge Coupled Device
IRF	Instrumental response function
mbar	Millibar
mg	Milligram
ml	Milliliter
mm	Millimeter
mmol	Millimole
meV	Millielectron volt
mW	Milliwatt
µm	Micrometer (micron)
NIR	Near infra-red
nm	Nanometer
NMR	Nuclear magnetic resonance
OM	Optical modes of the symmetric vibrations in silica
RT	Room temperature
R1	Fluorescent band caused by impurities in the crystal lattice of sapphire
R2	Fluorescent band caused by impurities in the crystal lattice of sapphire
SMA	Subminiature Version A
UV	Ultra violet

Table of Contents

1 Introduction

The European spallation source (ESS) a European Research Infrastructure Consortium (ERIC) is in process with one of the largest science and technology projects of its kind. With the construction of the world's largest neutron source being one of the cornerstones of the project. Capabilities of the ESS will greatly exceed any present neutron source facility of today with the delivery of unmatched brightness to the two dozen neutron instruments to enable world leading research. The ERIC is composed of 15 European countries, with the host countries being Sweden and Denmark. The Neutron source facility is located in Lund, Sweden.

Neutrons are produced by bombarding accelerated protons on a heavy metal target. The protons will be absorbed by the target which will result in the emission of neutrons from the target. The emitted neutrons have a high internal energy and is referred to as fast neutrons. These neutrons need to be transformed into neutrons with a more suitable energy for the instruments, such as cold neutrons. The transformation of the fast neutrons into cold neutrons is achieved by allowing the emitted neutrons to pass through a moderating material, where the fast neutrons lose a fraction of its energy with every interaction with the moderation material until the neutrons possess a suitable energy.

The moderating material will be liquid hydrogen, where the hydrogen will be in the form of parahydrogen. The presence of parahydrogen is essential to achieve maximum brightness from the moderator. A concentration of at least 99.5 percent parahydrogen is required to obtain maximum brightness. Orthohydrogen is formed from the interaction between parahydrogen and the fast neutrons, along with the extremely slow natural conversion rate of ortho- to parahydrogen. This presents the need for a catalyzed process to ensure the required parahydrogen concentration of 99.5 percent in the liquid hydrogen moderator.

To address this issue, the ESS is designing an external conversion loop where orthohydrogen is converted into parahydrogen by using a catalyst. For the catalyzed conversion, the ESS has two types of catalysts at their disposal which has shown to be promising regarding the conversion of ortho- to parahydrogen. There are however still aspects regarding the catalysts and the conversion kinetics in liquid hydrogen which is still not fully known. This presents an interest in the kinetics and the comparison between the two catalysts.

From the requirement of the parahydrogen concentration and the conversion loop is a desire to confirm that the parahydrogen concentration in the liquid hydrogen that is fed into the moderator consists of the required minimum of 99.5 percent. Presenting an interest of developing a method for continuous measurement of the amount of parahydrogen and how to implement that into the conversion loop.

1.1 Aim and scope

The aim of this master thesis is divided into three parts. The first part involves the optimization of the experimental setup. This includes the sample cell and cryostat setup along with the Raman spectroscopy system. Along with a design of a computational process, for the data collection and interpretation to the experimental setup. The optimization is required in order to obtain an accurate process for the characterization of the parahydrogen concentration. The second part focuses on the process to measure catalyzed conversion of ortho- to parahydrogen and determine the kinetics for the reaction at cryogenic temperature. Including the characterization of the background along with the ortho- and parahydrogen Raman signal. From the measured kinetics of the catalyzed conversion is a specific catalytic rate determined for both catalysts. Lastly, an evaluation regarding the catalytic ability of the catalysts based on the conditions of the ESS hydrogen loop is performed. To classify the relative characteristics of the catalysts and if the desired requirements can be met.

1.2 Delimitations

The conversion process is exothermic and the available setup cannot provide with a constant temperature throughout the experiment. Therefore, has the decision been made that the catalytic conversion will be performed at 16 ±1K instead of 20K, which is the operating temperature for the future ESS hydrogen loop. This serves as a safety factor to the limited cooling capabilities of the sample cell, in order to assure that the temperature does not exceed the boiling point of hydrogen. This could cause the sample cell to break from the increased pressure due to the evaporation of liquid hydrogen inside the cell.

1.3 Disposition of the report

The report begins with a literary review starting with hydrogen. The focus in this section is on the two forms- ortho- and parahydrogen regarding the background, general characteristics, symmetry requirements, thermodynamic aspects and the procedure of the conversion process, followed by a general description of the catalysts and the counteracting process of back conversion. The last section of the review will focus on the characterization method, known as Raman spectroscopy. Including the background behind the analysis method, technical application and optics and general advantages and disadvantages of the method.

Following the review is the presentation of the experimental part of the thesis. This section presents the details of the equipment and procedures used in this work.

The results from the experiments are presented and discussed, followed by conclusions about the kinetics of hydrogen conversion and a final assessment of the two catalysts under the experimental conditions in this work, as well as the conditions for the future ESS hydrogen loop.

2 Theory

The following section will focus on the background and principles of the two major sections in this thesis. The first section of this chapter will focus on the theory regarding hydrogen and the catalytic conversion process. The last segment of this chapter will focus on the background and principles regarding the analysis method of Raman spectroscopy.

2.1 Hydrogen

Hydrogen is the simplest and most abundant element in the universe. The hydrogen atom (H) as its most common isotope consists of a nucleus consisting of a single proton surrounded by a single electron. Pure hydrogen is found as a diatomic molecule (H_2), the hydrogen atoms are covalently bonded to one another with a bond length of roughly 7.4 nm. Hydrogen has two additional isotopes, deuterium and tritium which contains one and two additional neutrons respectively in its core. Deuterium is a stable isotope but less common compared to hydrogen while tritium is an unstable and radioactive isotope of hydrogen [1–3]. An illustration of the hydrogen molecule is shown in figure 1.

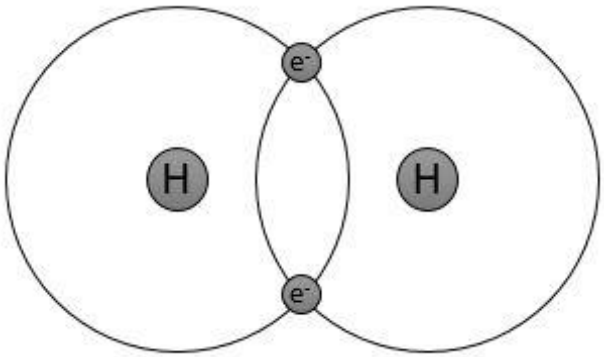

Figure 1: Illustration of a hydrogen molecule.

Hydrogen is a versatile element and is an important component in several chemical reactions, such as the Haber process to produce ammonia and hydrogenation processes for the removal of sulfur from petrochemical fuels. Other applications for hydrogen rather than being a reactant in chemical reactions, is the use of hydrogen as a fuel, mainly in rockets. In recent times, the use of hydrogen has increased in interest as an alternative fuel for cars [2–5]. Hydrogen has also been referred to as an excellent moderating material for uses in high intensity neutron spallation sources to produce cold and thermal neutrons [6–8]. The efficiency of liquid hydrogen as a moderating material has gained significant interest and studies has shown that the efficiency is greatly dependent on the spin configuration of the hydrogen molecule [8–10]. The effect of the molecular spin configuration has also been recognized as a key factor for the stability of liquid hydrogen [11].

2.1.1 Hydrogen isomers

Each hydrogen atom possesses an accumulative spin of ½. The arrangement of the individual atomic spins of the hydrogen molecule, results in two isomers of molecular hydrogen, called orthohydrogen and parahydrogen. The term "isomer" is used to describe a molecule composed of the same number of atoms, with identical atomic number and mass but in different energy states. The two isomers are characterized by specific symmetry requirements and that they exhibit differences in physical properties such as heat capacity, electrical conductivity and neutron scattering capabilities. The energy difference between the two hydrogen isomers is reported to be 14.8 meV [6,12].

2.1.2 Isomer symmetry

The characterization of the hydrogen isomers is based on symmetry requirements for the protons of the hydrogen molecule. The hydrogen molecule consists of two protons which are indistinguishable from one another with the accumulative spin of ½. Particles with half integer spin like the proton is regarded as a fermion. With fermions follows the constriction by the Pauli exclusion principle, which requires that the total wave function of fermions must be antisymmetric [1,5,13,14]. The following contributions to the total wave function is presented below:

$$\Psi_{Tot} = \Psi_T \, \Psi_V \, \Psi_R \, \Psi_E \, \Psi_N$$

The total wave function (Ψ_{Tot}) is a combination of the translational (Ψ_T), vibrational (Ψ_V), rotational (Ψ_R), electronic (Ψ_E) and nuclear (Ψ_N) wave functions. The characteristics of the hydrogen molecule is governed by the symmetry of the individual wave functions, where the translational vibrational and electronic wave functions (Ψ_T, Ψ_V and Ψ_E) are symmetric for a diatomic molecule. This results in that either the rotational (Ψ_R) or nuclear (Ψ_N) wave functions must be antisymmetric in order to fulfill Pauli exclusion principle [5,15].

The nuclear wave function is governed by the spin configuration of the hydrogen isomers. The spin configuration (S) can either be symmetric (S=1) or antisymmetric (S=0). The number of states are dependent on the possible configurations of the atomic spins in the molecule. For molecular hydrogen, each atom has a spin of ½ which can be considered as either +½ or -½. The symmetric configuration (S=1), is referred to as the triplet state and has three possible configurations that results in an overall parallel symmetry of the combined atomic spins, (m_{Tot} = +1, 0 and -1). The antisymmetric configuration (S=0) is called the singlet state, where only one configuration is possible for the individual spins to assume an antiparallel configuration (m_{Tot} = 0) [5,13,14,15].

An illustration for the possible configurations of the "triplet" and "singlet" states of hydrogen is presented in figure 2.

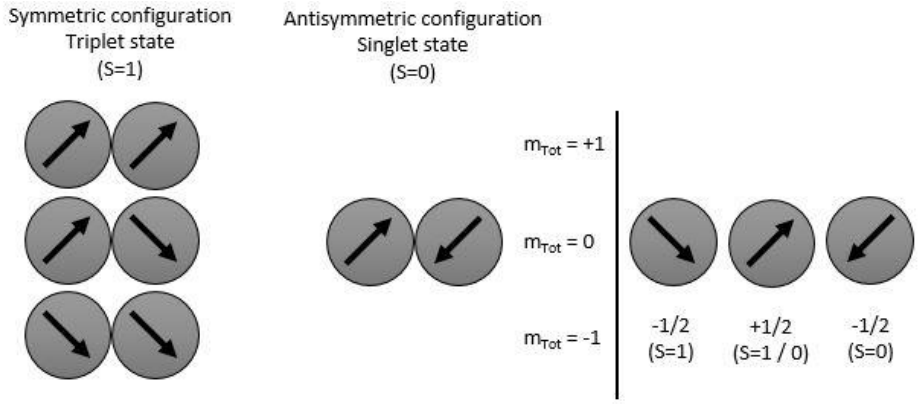

Figure 2. The spin configurations of the "triplet" and "singlet" states, together with an illustration of the resulting moment for the combined (left side) and the individual (right side) spins.

From the symmetry requirements resulting in the two following states is the triplet state is represented by the orthohydrogen isomer, while the singlet state represents the parahydrogen isomer.

The nuclear characteristics of ortho- and parahydrogen leads to the following symmetry requirements for the rotational wave function. The rotational wave function is governed by the rotational states (J) of the molecule in which the odd rotational states (J=1,3,5) belong to the antisymmetric wave function, while the even rotational states (J=0,2,4) represent the symmetrical wave function [1,5,13]. This results in the following symmetry requirements regarding the nuclear and rotational wave functions of the hydrogen isomers:

$$Ortho: \Psi_{TOT} = \Psi_{Rotational}(Anti)\Psi_{Nuclear}(Sym)$$

$$Para: \Psi_{TOT} = \Psi_{Rotational}(Sym)\Psi_{Nuclear}(Anti)$$

The orthohydrogen isomer belongs to the antisymmetric rotational wave function while the rotational wave function of parahydrogen is symmetric, which fulfills the requirement of the total wave function being antisymmetric.

2.1.3 Isomeric equilibrium

The symmetry of ortho- and parahydrogen results in the following distribution of the two isomers. The hydrogen molecule can either exist in the singlet state or in one of the three triplet states. The condition that the hydrogen molecule can adopt any of the four possible states has shown to result in an equal distribution of the hydrogen molecules among the four states [14,16]. With all states equally populated, 75 percent of the hydrogen molecules occupy the triplet states (orthohydrogen) and 25 percent occupy the singlet state (parahydrogen). The distribution of 75:25 percent is referred to as normal hydrogen, at room temperature [13,14]. The equilibrium distribution of the hydrogen isomers has shown to be temperature dependent.

At lower temperatures is the singlet state (parahydrogen) thermodynamically favored, since it is the lowest energetic state of the hydrogen isomers [13]. The shift in equilibrium as a function of temperature transpires from the distribution of normal hydrogen (75:25%), which is the highest attainable distribution of the hydrogen isomers and represents the equilibrium at room temperature. At lower temperatures is the equilibrium pushed towards an increased ratio of parahydrogen and reaches a distribution of 0.2% orthohydrogen and 99.8% parahydrogen at 20K [13].
An illustration of the temperature dependence on the equilibrium concentration of ortho- and parahydrogen is shown in figure 3.

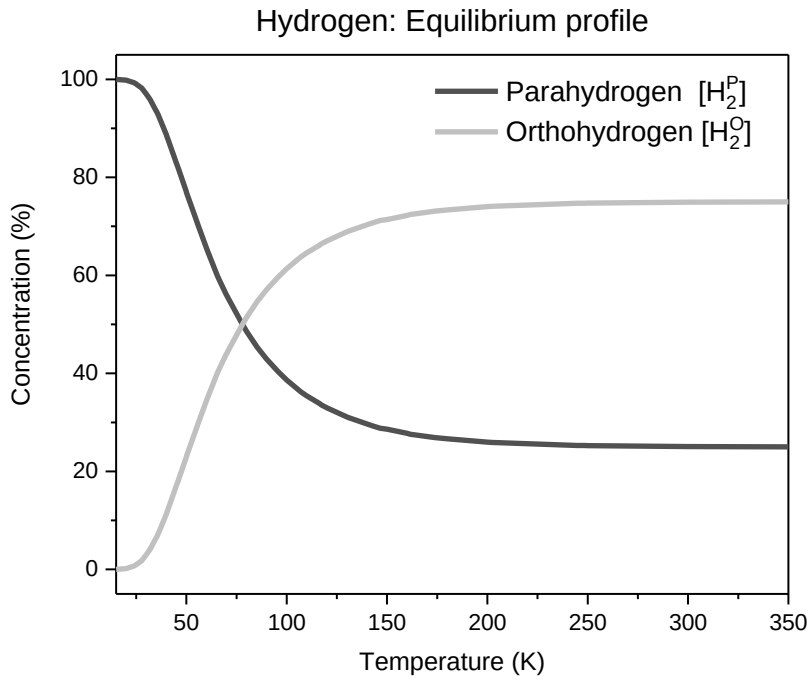

Figure 3:Equilibrium concentration profile of the ortho- and parahydrogen isomers as a function of temperature. Based on experimental data in ref [17].

As reported in literature, parahydrogen is almost completely favored at the boiling point of hydrogen (20.27K). However, obtaining pure hydrogen by lowering the temperature is an extremely slow process, where natural conversion has been reported to take days [5,13,15,16]. The slow approach to equilibrium results in the possibility of obtaining non- equilibrium mixtures of hydrogen. The slow process is due to the difficult transition of ortho- to parahydrogen. The transition is restricted by the requirement of a spin flip in the hydrogen molecule. The spin flip involves the transition of an ortho molecule, with symmetric configuration of the atomic spins (S=1) to the antisymmetric configuration of parahydrogen (S=0), which is restricted due to the preservation of angular momentum of the hydrogen molecule.

To achieve the conversion of an orthohydrogen molecule to a parahydrogen molecule a magnetic field gradient is required allowing the spin flip to transpire [5,13]. This is commonly facilitated by the addition of a magnetic catalyst, in which the presence of a magnetic sites provides the magnetic gradient required to enable the conversion.

2.1.4 The conversion process

The conversion of ortho- to parahydrogen can be accomplished either through a homogeneous (uncatalyzed) or heterogeneous (catalyzed) process. It requires the presence of a magnetic field which enables the transition from one nuclear spin state to another. The conversion process is exothermic, with a heat evolution of approximately 670 J/g. The emitted heat from the conversion process is higher than the heat of evaporation which is 440 J/g [17,18]. The exothermic reaction when parahydrogen is formed from orthohydrogen leads to the evaporation of liquid hydrogen. This emphasizes the need for cooling to maintain the hydrogen in the liquid state during the conversion process.

2.11.4.1 Uncatalyzed conversion

Conversion without a catalyst involves the interaction between orthohydrogen molecules. If the molecules are in close enough proximity to one another, the resulting interaction can provide a magnetic gradient is strong enough the spin flip can be facilitated. The magnetic gradient is a result of the nuclear spin and rotational moment. This results in natural conversion which can only transpire from the interaction between orthohydrogen molecules, since parahydrogen does not possess a magnetic moment. The uncatalyzed process is described by the following relationship:

$$\frac{d[H_2^O]}{dt} = -k[H_2^O]^2$$

The change in orthohydrogen (H_2^O) is related to the square of the orthohydrogen concentration. The process is bimolecular and dependent on the concentration of orthohydrogen. The uncatalyzed rate of conversion has been estimated to be in the range of a few percent in the magnitude of hours [1,5,16–18].

2.1.4.2 Catalyzed conversion

Catalyzed conversion was theoretically proposed by Wigner, considering the magnetic induced transition of the nuclear spin configuration in hydrogen. This was later observed by Farkas for the catalyzed conversion using oxygen [5,14,19,20]. The catalytic conversion of orthohydrogen has been studied for several types of catalysts and states of aggregation, ranging from interactions in gas phase to solid state interactions [1,5,11,18–22]. The conversion process regarding the adsorption of liquid hydrogen on a solid catalyst surface is of particular interest. The presence of a magnetic substance leads to a significant increase of the conversion rate. This is a result of the stronger magnetic moment. For example the magnetic moment of a oxygen molecule is approximately 2000 times greater than the magnetic moment of hydrogen [5].

The conversion process occurs when a hydrogen molecule is close enough to the magnetic lattice, causing a dipolar interaction between the magnetic moment of the hydrogen atoms and the magnetic center so that spin flip can occur [5,14]. The process of catalytic conversion is presented as a first order process which takes place within a few seconds to minutes. The relative strength of catalytic conversion is proportional to the square of the magnetic moment of the catalytic center and the molecules being converted [1,20,23].

This thesis will investigate the kinetics of conversion using the two catalysts IONEX® and OXISORB®, where the two magnetic centers originates from chromium(II) and iron(III), which has a magnetic moment of 4.90 and 5.92 Bohr magnetons respectively [23,24]. This indicates that the relative efficiency of iron(III) ions, present in the iron(III) oxide (Fe_2O_3) catalyst IONEX® is greater than the chromium(II) ions in the OXISORB® catalyst, which consists of chromium(II) oxide (CrO) deposited on a silica carrier [23].

2.1.4.3 Adsorption

Adsorption has an important role in catalytic conversion using a solid catalyst. It has been reported in literature that orthohydrogen is preferentially adsorbed on solid surfaces, due to the hindered rotation of the molecule. This results in the fast desorption of parahydrogen from the catalyst [21]. The conversion has been found to occur only in the first adsorbed layer of hydrogen [20]. When a hydrogen molecule is adsorbed on a surface the mobility of the molecule is affected by a barrier between the catalyst surface and the hydrogen molecule [19]. The rotational degree of freedom is reduced to one, where the rotation of the molecule is either parallel or perpendicular to the surface. The orientation between the orthohydrogen molecule and the catalyst surface appears to have an effect on the rate of conversion. A parallel orientation is reported to result in a higher rate of conversion, compared to when the molecule is in a perpendicular orientation to the catalyst surface [25]. This is related to the increased surface of the hydrogen molecule exposed to the magnetic lattice.

2.1.5 Catalyst information

The two catalysts IONEX® and OXISORB® are used for the catalytic conversion of ortho- to parahydrogen. General information regarding these catalysts is given in the following sections.

2.1.5.1 IONEX®

IONEX® is a catalyst composed of iron(III) oxide (Fe_2O_3) with a water content less than 2% and a density of 1.32 g/cm^3. The catalyst has a measured surface area of 216 m^2/g and has a reported space velocity of 1200 cm^3 of H_2/min/cm^3. The catalyst has a mesh size of 30 x 50 (600-300 µm). IONEX® is stable in normal atmosphere, at low humidity, as moisture degrades the catalytic activity. Regeneration of the catalyst can be done by exposing the catalyst to a flowing stream of dry hydrogen at 160°C for 16 hours.

2.1.5.2 OXISORB®

OXISORB® consists of a silica gel carrier doped with 2-3% chromium(II) oxide (CrO). The catalyst has a relative density of 0.7 g/cm^3 and is very reactive to oxygen and moisture. As a result, it cannot be used in air or in the presence of any moisture. An inert atmosphere is therefore required for handling the catalyst. The catalyst is commonly used as an oxygen remover in gloveboxes. Regeneration of OXISORB® can be performed by exposing the catalyst to a stream of dry hydrogen at 200-500°C. The surface area of the catalyst has been determined to be 560 m^2/g. An estimated space velocity has been presented by [18], where two monolayers of normal hydrogen is fully converted in 5.1 minutes which corresponds to 4 mmol of H_2/min/g.

2.1.6 Back conversion

Using parahydrogen as a moderating medium for the production of cold neutrons leading to the following reaction, in which the parahydrogen molecules are converted to orthohydrogen [26]. This is referred to as back conversion and is due to the dissociation of the hydrogen isomers into atomic hydrogen. During recombination to molecular hydrogen the distribution of 3:1 ortho- to parahydrogen is adopted due to the elevated energy of the dissociated hydrogen [26]. The rate of back conversion for the ESS liquid hydrogen moderator is estimated to 3 mol/minute. The rate is based on the moderator design and the rate of back conversion reported in literature [26].

2.1.7 Hydrogen spectra

The information obtained using Raman spectroscopy is commonly presented as a graph, where the intensity of the scattered photons is presented as a function of the Raman shift. The intensity of the peaks in the obtained spectrum represents the number of photons registered at the specific Raman shift from the incident beam. The Raman shift is presented as the wavenumber (cm^{-1}) and is related to the frequency difference between the incident and scattered photons. The spectra of a hydrogen sample show the rotational and vibrational movements of the hydrogen molecule, where the transition of even rotational quantum numbers represents parahydrogen and the transition of uneven quantum numbers represents orthohydrogen [1,6,12,27].

The rotational transition (S(J)) of the first and second order transitions for ortho- and parahydrogen, which has observed using Raman spectroscopy and reported in literature is presented in table 1.

Table 1: The specific Raman shift of the first two rotational levels for ortho-and parahydrogen.

Rotational quantum number (J)	Transition (J ➔ J+2)	Shift (cm^{-1})	Isomer
0	(0 ➔ 2)	354[1, 2], 355[3]	Para
1	(1 ➔ 3)	587[1, 2], 586[3]	Ortho
2	(2 ➔ 4)	>(800)[1], 814[2], 812[3]	Para
3	(3 ➔ 5)	>(1000)[1], 1034[2], 1032[3]	Ortho

[1] [6,27], [2] [1], [3] [12]

Table 1 shows the observed positions of the rotational transitions, where the characterization has been conducted using an excitation source with a wavelength of 532 nm and 488 nm respectively [12,27].

The concentration of the ortho- and parahydrogen is determined by integrating the observed first and second order rotational peaks in the obtained spectra. The population of the lower rotational levels becomes more favored at cryogenic temperatures, which represents the energetic ground state of the hydrogen isomers. The low energy ground states are represented by the first order rotational levels for parahydrogen (J=0) and orthohydrogen (J=1) respectively [1,12,19,27,28].

The vibrational states of hydrogen are presented in table 2.

Table 2: The specific Raman shift for the first four vibrational levels in hydrogen [1].

Vibrational quantum number (v_n)	Shift (cm^{-1})
0	4162
1	3926
2	3696
3	3468

The vibrational ground state is represented by the vibrational quantum number ($v_n = 0$) which corresponds to a Raman shift of 4162 cm^{-1}. The other vibrational states in the table represents elevated vibrational states, the likelihood to observe these states at cryogenic temperatures is low, due to the energetic ground states becoming favored at lower temperatures.

2.2 Analysis methods for ortho-parahydrogen characterization

The ortho- parahydrogen ratio can be determined through different techniques, such as Nuclear Magnetic Resonance (NMR) spectroscopy, thermal measurements related to the conductivity or enthalpy of the isomers and neutron scattering [6,18,20,22]. However, recent studies have proposed Raman spectroscopy as an alternative method for determining the relative amounts of ortho- and parahydrogen [6,12]. The fundamentals of Raman spectroscopy, both theoretical and experimental are summarized in the following section.

2.3 Raman spectroscopy

Raman spectroscopy, dates back to the early 20th century. The method is based on the scattering of light by a sample which is irradiated with monochromatic light. The scattered light is collected and led to a detector which registers the number of individual counts as a function of the difference in frequencies between the scattered and incident light [29]. The scattered light is related to the individual movement of the molecules in the irradiated sample, which results in specific peaks in the corresponding spectrum. Hence, Raman spectroscopy can be used as a quantitative method to analyze and characterize the substrate in a bulk sample, by identifying the individual signals generated by each component [30,31].

Raman spectroscopy is a versatile analytical method which introduces the possibility of examining a sample, regardless of physical state, ambient temperature, or sample enclosure. The only requirement is that the enclosure is transparent to the incident light. Raman spectroscopy can be used as an in-situ analysis method for following chemical processes. Increased interest in Raman spectroscopy [30] at the current juncture is due to its advantages, improvements in the technique and the development of better analytical equipment.

2.3.1 Theory

Upon irradiation of a sample with light, interactions may occur between the molecules in the sample and the photons from the incident light [30,31,32]. From the interaction, light can either be absorbed or scattered by the sample. The phenomenon of absorption or scattering of light depends on the energy of the incident photons and if the energy is consistent with the energy difference between the ground state and the excited state of the molecules in the sample. Absorption requires that the energy of the photon agrees with the energy difference between the energetic states of the molecule, while the scattering of photons is not dependent on the energies to match with one another. [30,31].

The scattering of light occurs when photons interact with a molecule and the energy of the incident photons is transferred to the molecule, creating a short-lived complex. The complex is referred to as the virtual state, with significantly higher energy, but without any significant nuclear movement to compensate for the increase in energy. The equilibrium electron configuration of the molecule does not correspond to the new electron arrangement of the virtual state.

Because of the elevated electron arrangement and the unfavorable nuclear distribution, the virtual state is very unstable. Therefore, is the energy which is gained from the interaction with the incident photons quickly irradiated from the virtual state as scattered light. The energy of the virtual state and the distortion of the electron cloud are closely related to one another, since both are dependent on the frequency of the incident light. This presents an opportunity to modify the frequency of the incident light depending on the nature of the measurement. Increasing the frequency can improve a weak signal of a Raman spectrum. However, it can also result in fluorescence and sample degradation due to the increased intensity of the incident light [30,31].

Raman spectroscopy uses light of a single frequency to excite the molecules in a sample and measure the scattered light from the excited molecules [29]. The measured scatter from the molecules is presented either as the difference in wavelength (λ), frequency (ν), or wavenumber (ϖ) to the incident beam. The connections between these three units are described by the following relationships:

$$\lambda = \frac{c}{\nu} \quad (cm)$$

$$\nu = \frac{c}{\lambda} \quad (Hz)$$

$$\varpi = \frac{\nu}{c} = \frac{1}{\lambda} \quad (cm^{-1})$$

In Raman spectroscopy, the measured scatter is often presented in terms of energy, with the wavenumber (ϖ) being the most common parameter used in literature [29].

Data obtained from a Raman spectroscopy measurement are commonly presented as intensity versus the Raman shift (cm^{-1}), where the Raman shift is a measure of the energy difference between the incident light and the scattered light. It is usually described as the shift in energy (Δcm^{-1}), but is more commonly expressed as (cm^{-1}), wavenumber (ϖ, cm^{-1}) or Raman shift (cm^{-1}). The term Raman shift will hereafter be the parameter referred to in this thesis.

The scattering of light can be inelastic or elastic. The elastic scatter describes the relaxation of a distorted electron cloud with no nuclear motion. Elastic scatter results in a small to no change between the scattered light in relation to the incident light. The elastic scattering of light is referred to as Rayleigh scattering and is the most dominant effect in Raman spectroscopy.

The inelastic scatter is referred to as Raman scatter and it is a less common phenomenon where only one in every 10^6 to 10^8 photons will be affected by inelastic scattering [29,30].

Raman scattering is a weak process and is the result of movement of the nuclei due to the interaction between the light and the electrons of the molecule. The motion of the nuclei requires more energy compared to the distortion of electrons, which leads to a change in energy of the molecule to either a higher or lower energy state. Depending on the initial energy state of the molecule which either can be in the ground state (a) or an excited state (b). Inelastic scatter from the virtual state can therefore result in the possibility of a promotion from the ground state to an excited state (a → b), meaning that energy is absorbed by the molecule from the interaction with the incident light, which is referred to as Stokes scattering. The other possibility is the transition from an excited state to the ground state (n → m), where energy is transferred from the molecule to the scattered light, which is called anti-Stokes scattering [29–32].

An illustration of the phenomenon of the scattering processes is shown in figure 4.

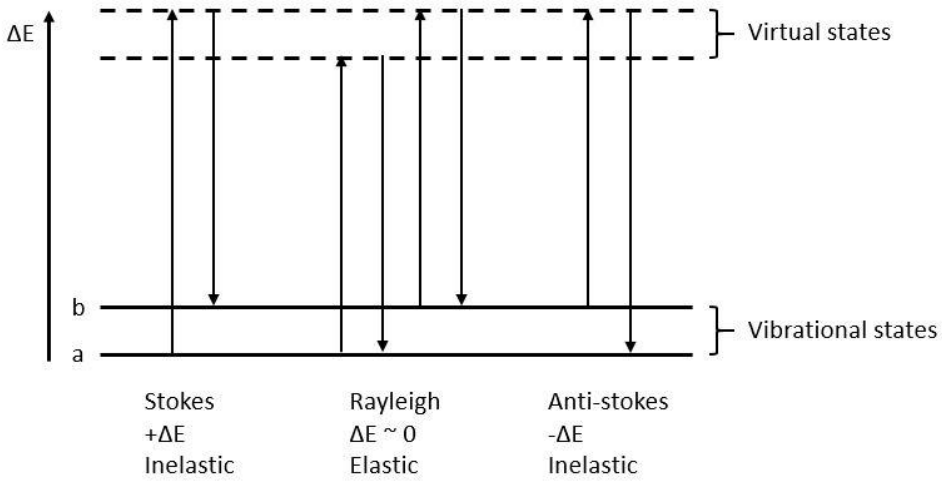

Figure 4: Illustration of the elastic and inelastic scattering in Raman spectroscopy.

Before excitation, most of the molecules in the initial state are likely to be in the ground state [30]. This means that stokes scattering is a more dominant process compared to anti-Stokes scattering and provides a stronger signal.

The signal obtained is a result of the inelastic scattering of light, due to the change in energy by transition between the rotational and vibrational states of a molecule. The energy of a molecule, apart from electronic energy is related to the translational, vibrational, and rotational energies. The translation energy is related to the movement of a molecule in a three-dimensional space, resulting in three degrees of freedom. The rotational energy is for linear molecules, such as the hydrogen molecule is described by two degrees of freedom [31].

The only possible rotations for a linear molecule is around or about its own axis, the degrees of freedom for the vibrational energy of a hydrogen molecule is given by:

$$3 * N - 5$$

The variable (N) is the number of atoms in the molecule. This leaves one vibrational freedom for the linear hydrogen molecule which is related to the simple stretching of the bond between the hydrogen molecules (H-H) [31]. The vibration frequency of the H-H bond can be calculated by Hooke's law:

$$\varpi = \frac{1}{2\pi c} * \sqrt{\frac{k_{Bond}}{U}}$$

From Hooke's law is (k_{Bond}) defined as the force constant for the bond, (U) represents the reduced mass of the atoms and (c) the velocity of light. The frequency for the vibration of a hydrogen molecule is approximately 4160 cm^{-1}. The following equation indicates that the vibrational frequency is dependent on bond strength and the size of the molecule. This implies that molecules composed of lighter atoms or with a stronger bond between the atoms will have a higher frequency compared to molecules with heavier atoms or weaker bond strength [31].

2.3.2 Advantages and disadvantages with Raman spectroscopy

Raman spectroscopy has many advantages, allowing easier sample analysis, regardless of the physical state. Raman spectroscopy can detect molecules dispersed in solutions, which enables the possibility of examining molecules in aqueous solutions [33]. The spectroscopic method can examine samples in varying temperatures and in enclosed containers transparent to light. Studies regarding vibrations in molecules with covalent bonds are stronger in Raman scattering compared to infrared absorption [30]. Symmetrical vibrations are Raman active only, due to the mutual exclusion principle. which dictates that a vibration can only be Raman or infrared active but not both. With Raman spectroscopy lasers are normally used as the excitation source, which allows the modification of the frequency of the incident light to enhance the obtained signal. However, Raman scattering is a weak process with one in every 10^6-10^8 photons being scattered [30]. This makes the analysis method very sensitive to interfering phenomena such as fluorescence, which is much stronger compared to Raman scattering [33].

Fluorescence is a result of the frequency of the excitation source being in the visible region, which is a common design for lasers used with Raman spectroscopy. Fluorescence can be avoided by increasing the frequency of the excitation source, pushing the frequency towards the UV region. Using lasers with a higher frequency does not only result in a higher equipment cost but can also lead to photo degradation, which will interfere with the measurement. The sample becomes degraded by the intensive irradiation which reduces the number of molecules available for Raman scattering. Fluorescence and photo degradation are the two main challenges of Raman Spectroscopy, but their interference has been minimized by the development of new techniques, better sensors and light sources.

2.3.3 Techniques and instrumentation

The key components in Raman spectroscopy are the excitation source, collection technique and detection instrumentation [34,35]. Each component can be customized, permitting continuous improvement to the method.

2.3.3.1 Excitation source

As mentioned previously, the intensity of scattered light is related to the frequency of the incident light, which makes the light source an important feature in Raman spectroscopy [33]. Lasers are most commonly used as the excitation source, with an operational frequency in the range 400 to 1064 nm. The most common types of lasers use a frequency in the UV-visible region. Lasers provides a monochromatic source that has a high-power output. Polarized light with a small band gap, a small focal diameter has shown improvement over the inherent weak signal of Raman scattering and contributes to the possibility of getting data with high resolution. The use of high frequency lasers has been shown to be a good solution for minimizing the interference from fluorescent effects [34,35].

2.3.3.2 Collection techniques

The collection techniques commonly used in Raman spectroscopy are based on the understanding that light is scattered as a sphere from the sample, upon interaction with the incident beam. Scattered light is collected at a preset angle from the incident light and the sample. The two most common angels of collection are either at an 90° or 180° angle from the sample. The collection at 180° is referred to as traditional and backscattering geometry [34,35]. The importance of these geometries is to reduce the collection of Rayleigh scattering and the interference of the incident laser light, which are more intensive compared to the weaker Raman scattering and becomes more important for the characterization of vibrations at lower frequencies, closer to the frequency of the incident light [34]. In this thesis scattered light will be collected using the traditional backscattering geometry.

2.3.3.3 Optical components

The use of optical components such as filters, lenses and fibers has been proven to be a good solution to enhance the signal of Raman scattering and is regarded as crucial part in the collection setup, which will be described in the next couple of sections [34].

2.3.3.3.1 Lenses

Lenses enables the possibility of collecting more scattered light as well as extrapolating the focal distance of the excitation source. The power of a lens is given by:

$$F = \frac{f}{D}$$

In the following relationship is (F) referred to as the F-number, (D) represents the collection diameter of the of the lens and (f) is related to the focal length of the lens. The F-number is used as a measure of the lens capabilities. A high F-number is desirable for lenses that are used to extrapolate the focal point. While low F-numbers are favored for lenses used to collect the scattered data [35].

2.3.3.3 2 Filters

Filters are used to enhance the emitted light by filtration of light with unwanted frequency. Common filters used in Raman spectroscopy are notch and band pass filters. These two types of filters work as a counterbalance to one another and is used to enhance the excitation light as well as the collected signal [35]. The notch filter rejects specific frequencies at a specific range while frequencies outside that range can pass through, which is used to reject unwanted frequencies from the collected scatter, such as Rayleigh scattering [35]. Since the Raman scattering is a weak signal the suppression of the Rayleigh scattering is of great importance.

The band pass filter works in the opposite way where only a specific range of frequencies can pass through, while other frequencies are reflected. The band pass filter is used to improve the excitation light. Since Raman scattering is based on the difference between the frequency of the incident and scattered light, changes can be made to reduce the band gap of the incident light to improve the resolution [33]. The strength of a filter is given by the optical density:

$$OD = -\log\left(\frac{I_1}{I_0}\right)$$

The optical density (OD) is related to the ratio of transmitted light (I_1) from the filter to the incident light (I_0).

2.3.3.3.3 Fibers

Fibers enable the possibility of performing Raman analysis in places far away from the instruments or in challenging environments, such as corrosive, sterile, radiation or extreme temperatures [33]. The optical fiber is composed of a material with a high refractive index, surrounded by a shielding material with low refractive index. The fiber transports the light from the source to the excitation probe and from the collection lens to the detector. Advantages with using fibers is the limited interference from outside factors and the possibility of customizing the design of the experiment. The disadvantage with using fibers is the possibility of interference due to fluorescence from the fiber material. This is mostly apparent if a long fiber is used and the Raman signal is weak [33]. The solution to this is the use of coupled fibers for excitation and collection. This increases the amount of information that is carried with the fiber and can be a solution to weaker Raman signals.

The addition of filters in front of the fibers can also be a solution to the issue of interference from the fiber material. The appearance of coupled fiber is shown in figure 5.

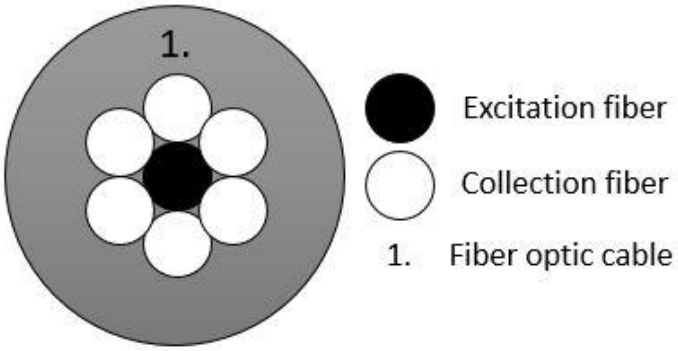

Figure 5: Depiction of a coupled optical fiber, composed of one excitation and six additional collection fibers.

The concept of the coupled fiber shown in figure 5, is that the excitation light is led through the middle fiber and the collected light scattered from the excited sample is led to the spectrometer by the surrounding six fibers. This type of fiber is commonly applied to backscattering Raman spectroscopy in which the excitation and the collection of the signal is carried out using the same probe [33].

2.3.3.4 Detection instrumentation

The detector is the part of the Raman spectroscopy setup in which the collected scatter is processed into accessible data. Since Raman scatter is a relative weak process, the sensitivity of the detector becomes an important factor [33,35]. The sensitivity is related to the signal produced per registered photon, along with a low generated background.

The background is a result of the electrical or dark noise generated from the surroundings and detector. There are numerous types of detectors available for Raman spectroscopic use, each with its individual strengths and weaknesses. A common type of detectors are the single and multi-channel detectors, where the conversion of photons into an electrical signal is obtained using photon multipliers, which is composed of photocathodes. The general disadvantage with photocathodes is the large inherent background and the sensitivity towards light with high frequency [35]. Single channel detectors, such as the linear detector are a simple and efficient type of detector, usually found in handheld devices. The improvement from single detector gave rise to the multi-channel detectors, which enable the possibility of examining several wavelengths at the same time. The use of linear photodetectors has the overall disadvantage of a low signal to noise ratio which led to the use of a semiconducting detector, like a Charge Coupled Device (CCD) [33,35].

Unlike the one-dimensional array used in linear detectors, the CCD is composed of chips of semiconducting photosensitive electrodes arranged in a two dimensional array. Each chip acts as a pixel in the array and records the number of photons received. The photo electrodes generate electrical signals which are translated into a spectrum. The advantages of using a CCD device is the low readout noise and the relative stability at high light intensities.

Noise can be described as a detected signal with no apparent useful information and can possibly be a result from the background, fluorescence or spikes due to external interference. All detectors exhibit an inherent noise, referred to as dark noise, which is a result of the spontaneous buildup of electrons by the detector itself and can be divided into the types- thermal, shot and readout noise. They describe the spontaneous buildup of electrons due to thermal fluctuations, uncertainty of the spectroscopic signal related to photons and electrons and the electrons from the read-out process. Dark noise results in the increase of the background intensity and can be reduced to some extent by cooling the detector [33,35].

3 Experimental

In this work, the catalytic conversion of liquid ortho- to parahydrogen is investigated using Raman spectroscopy. The catalysts used in this study are IONEX® and OXISORB®. The catalytic performance is the subject matter of this study, with the aim to determine the kinetic order of the conversion process and its rate constant. The study also involves the design of a Raman spectroscopy system and the evaluation of its accuracy as an analysis method, for online monitoring of the parahydrogen levels in liquid hydrogen. The following sections provide a description of the experimental setup as well as the procedure and experimental conditions. The chapter will end with a description regarding the treatment and analysis of the obtained experimental spectroscopic data. The complete experimental setup can be divided into two sections, sample setup and Raman setup.

3.1 Sample setup

The sample setup consists of a cryostat to cool the sample cell and control the physical state of the hydrogen inside the sample cell. The sample cell is installed on a stick which can be removed from the cryostat and functions as the connection between the sample cell and gas line. The gas line is designed to handle the flow of hydrogen as well as vacuum to the sample cell. The operating temperature during the catalytic conversion is set to 16K which is in the temperature region of liquid hydrogen.

3.1.1 Cryostat and Sample stick

The cryostat is a closed cycle refrigerator, with a gas-exchange. Made by Janis Research Company [36]. The customized setup is a transportable cryostat, suitable for small experimental areas and available for neutron scattering experiments in the future. The cryostat is illustrated in the figure 6.

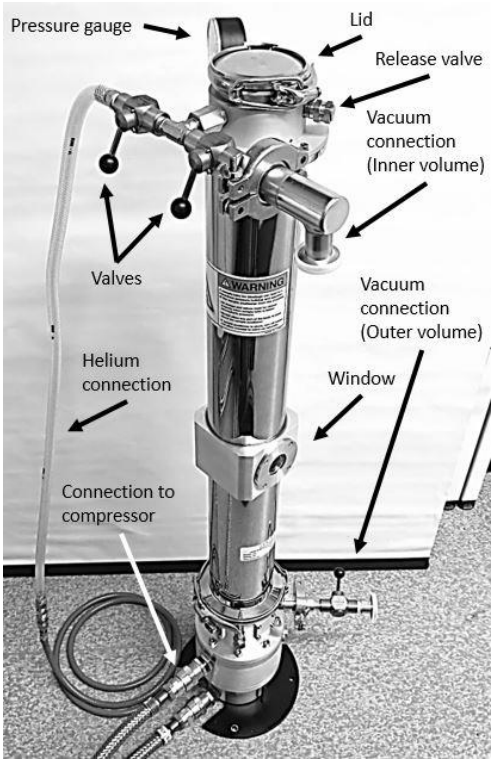

Figure 6: The cryostat tower, with attachments.

The cryostat is composed of a double jacket, where the volume of the outer mantle is connected to vacuum to provide thermal insulation. The volume of the inner mantle surrounding the sample cell, is filled with helium as an exchange gas, to enhance the thermal conductivity inside the inner volume.

With helium as the exchange gas, a medium is provided, which allows thermal conductivity at cryogenic temperatures below the freezing point of hydrogen (<10K). The windows of the cryostat are composed of silica windows (SUPRASIL), O-ring sealed and suitable for spectroscopy using UV-visible light. The cryostat is equipped with two thermal relays, served by an external helium compressor. The first thermal relay is connected to the sample area and the second relay surrounds the inner volume of the cryostat in which the sample cell is placed. The additional cooling provided from the exchange gas greatly reduces the time required for sample cooling.

The cryostat is equipped with a sample stick connected to a thermal mass of copper and composed of heater cartridges and a diode which registers temperature. The sample cell is mounted at the bottom of the thermal mass. A picture of the sample stick is shown in figure 7.

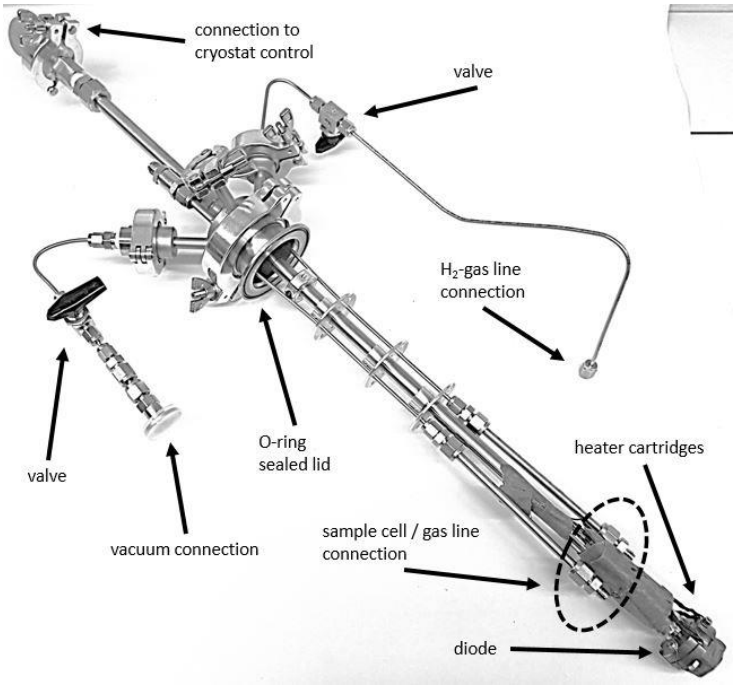

Figure 7:Sample stick, with various components.

The stick is designed with an O-ring sealed lid for easy removal from the cryostat, when a sample change is required. The thermal mass which regulates the temperature of the cell is controlled externally by a temperature control. Connections to hydrogen and vacuum are controlled by valves installed on the gas line connected to the sample cell.

3.1.2 Sample cell

The sample cell is the main part of the sample setup and is composed of modified components made by [37,38]. The sample cell is mounted at the bottom of the sample stick in contact with the thermal mass and connected to the gas line, shown in figure 7. The sample cell is made from stainless steel, with windows classified for spectroscopy. Two types of viewports were available during the experiments, incorporated with widows composed of either quartz or sapphire glass. The volume of the two sample cells along with optical data for the window materials is presented in table 3.

Table 3: Information on the specific characteristics of the two sample cells and their transparent material.

Sample cell (No.)	Window (Material)	Refractive index	Transmittance range (μm)	Glass thickness (mm)	Total cell volume (cm^3)
1	Quartz	1,4607	0.18-3	2.5	3.5
2	Sapphire	1,7717	0.17-5.5	1.5	2.5

The cell dimensions and optical data of the window materials is obtained from the manufacturer and an optical database [37–40]. The final assembly of the sample cell, is composed of three pieces, two window segments and a middle gas line connection. Vacuum annealed copper gaskets are placed in between the segments to prevent leakage. The individual components and the final assembly is presented in figure 8.

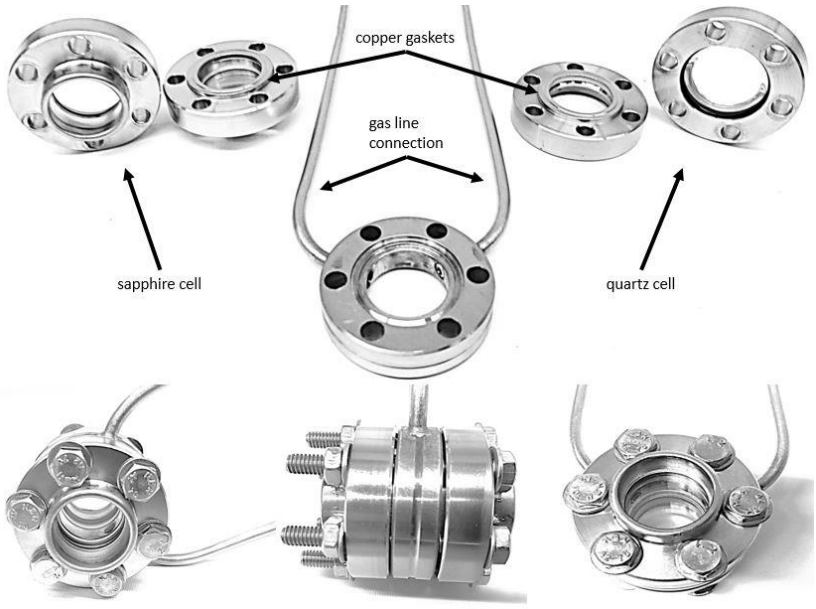

Figure 8:The components of the two sample cells, with the final assembly of the sapphire sample cell.

The assembled sample cell shown in figure 8, is connected to the thermal mass which is located at the bottom of the sample stick. The connection of the gas line and the sample cell is composed of quarter- and eight-inch tubing and is fitted with Teflon seals from Swagelok [41]. The Teflon seals are incorporated to enable the possibility to adjust the position of the sample cell in relation to the thermal mass, as well as the windows of the cryostat.

The finished assembly of the sample stick with the sample cell is shown in figure 9.

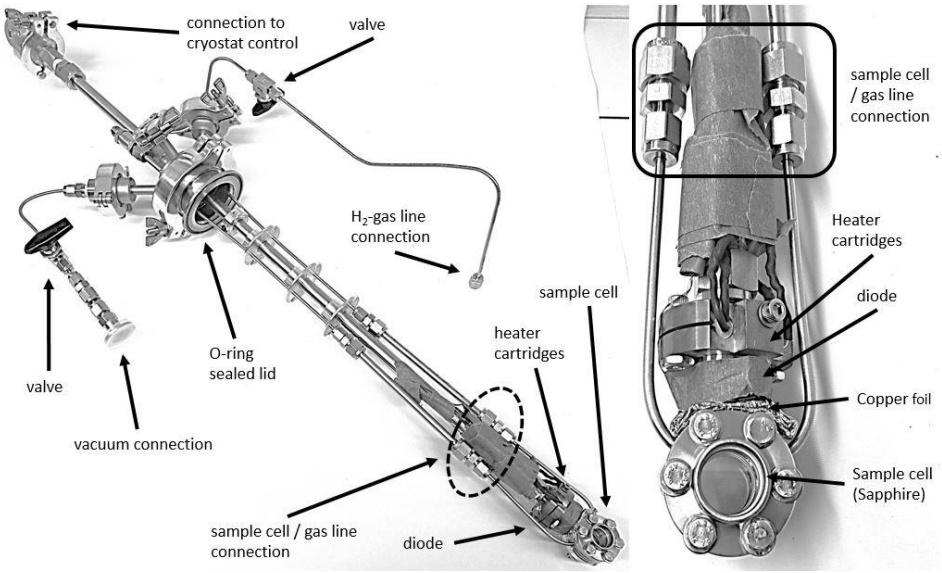

Figure 9: Picture of the completed assembly of the sample stick. Sample stick is attached with the sample cell.

Due to the rounded shape of the cell there is only a small portion of the sample cell surface in contact with the thermocouple. To increase the surface contact is copper foil placed between the thermocouple and the top of the sample cell, shown on the right hand side in figure 9. The final assembly of the sample stick is inserted into the cryostat and connected to the hydrogen storage and vacuum pump. The connections to the cylinder and vacuum is controlled by valves which is shown on the left side of the figure 9.

3.1.3 Gas line

The gas line is designed to control and monitor the hydrogen and vacuum, inside the sample cell. The parts used for the gas line are composed of stainless steel tubing of either quarter or eighth-inch diameter. The tubing and sealing is also made by Swagelok [41]. The gas line can be divided into five key segments. One being the sample cell segment of the gas line depicted in figure 7 and figure 9 and the second one being the vacuum pump. The remaining key segments is represented by the hydrogen inlet, vacuum gauge and the hydrogen storage cylinder with the attached pressure gauge and can be seen in figure 10.

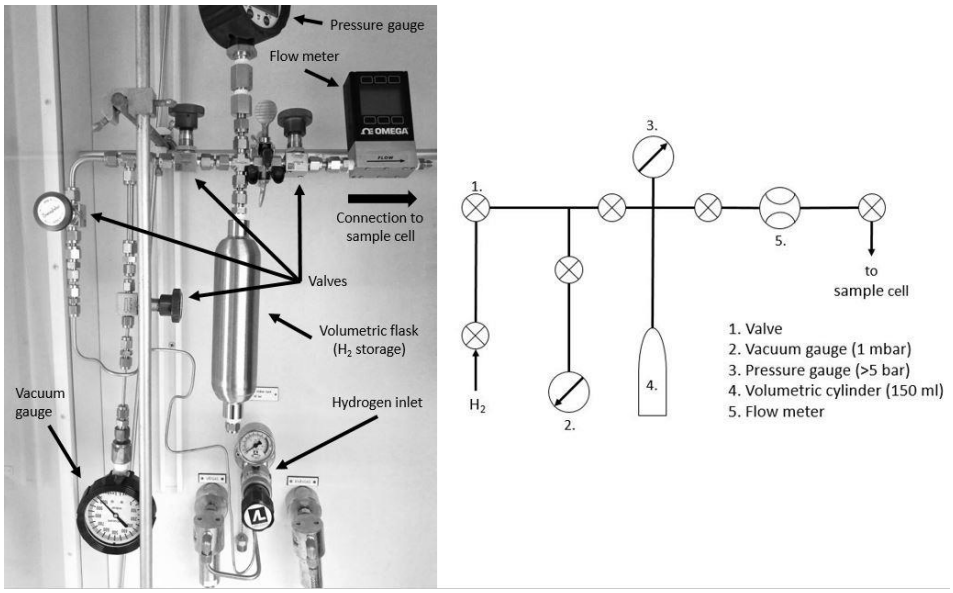

Figure 10:Picture of the gas line along with a schematic drawing of the gas line.

The components shown in figure 10 are crucial for the control of hydrogen as well as vacuum inside the sample cell. These are regulated with needle and ball valves. Most of the valves are shown in figure 10 and the placement of the remaining two valves are shown in figures 7 and 9. The valves are designed to control each individual key segment of the gas line. The storage cylinder is a 150 cm^3 stainless steel vessel, with a pressure gauge to monitor the hydrogen pressure inside the cell. The total amount of hydrogen for the experiments is calculated from the pressure inside the cylinder using the ideal gas law. The cylinder also provides a safety volume during experiments, in case of any malfunction leading to increased hydrogen pressure inside the sample cell. The gas lines are designed to withstand a pressure of six bar and the maximum pressure of hydrogen inside the sample cell is therefore limited to approximately five bar. The vacuum gauge indicates the current vacuum pressure inside the cell and is also used to identify leaks in the gas line. Both analog and digital vacuum gauges have been used during the experiments. The analog vacuum gauge (figure 10), has a range of 10^3 to 0 mbar and the digital gauge has a range from 1 to 10^{-3} bar.

3.2 Raman setup

The parahydrogen concentration is determined using Raman spectroscopy. During the experiments backscattering geometry (reflection, 180° angle) was used. However, transmission Raman spectroscopy was also tested to evaluate the relative differences between the two geometries. The Raman spectroscopy setup is composed of four parts, the laser source, Raman probe, optical components and the Raman spectrometer. A picture of the backscattering geometry setup is shown in figure 11 and is the current design of the online monitoring Raman system for the ESS hydrogen loop.

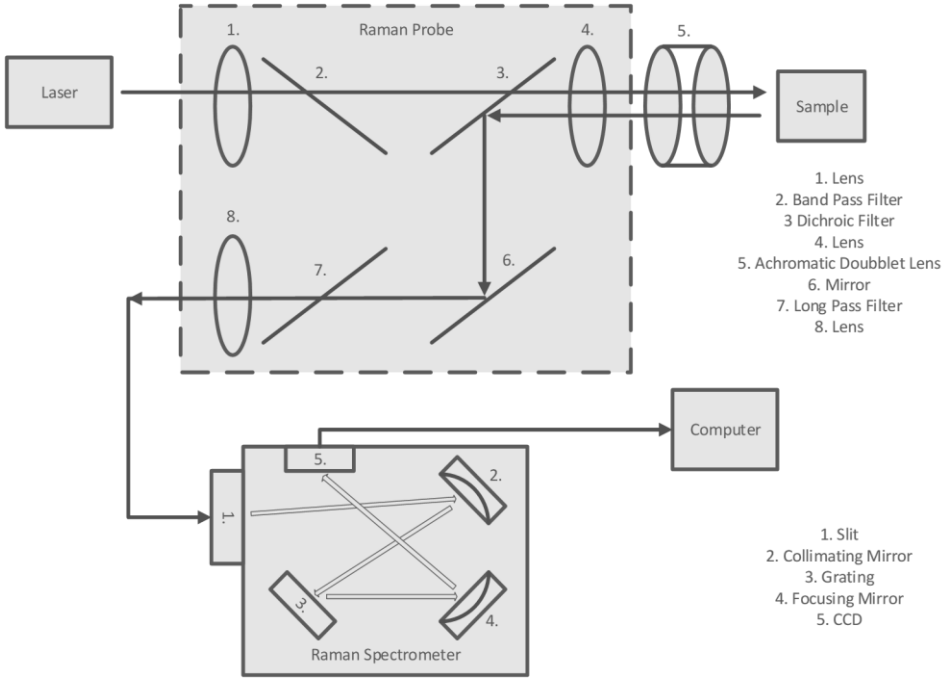

Figure 11: Schematic diagram of the Raman setup.

Figure 11 shows the current Raman setup, with the optical components, which is designed for an excitation wavelength of 532 nm. The equipment, such as the laser and spectrometer, together with the computational software Oceanview is made by Ocean Optics [42]. The Raman probe used for the backscattering geometry was made by InPhotonics [43] and the optical filters inside the probe were configured to the incident laser light.

3.2.1 Laser source

The laser source is a 532 nm multi-mode laser with a fiber coupled output of 50 mW. The laser wavelength of 532 nm results in a laser light in the green region of the visible spectrum. The laser light is led from the laser source to the Raman probe via a 105 µm fiber optic cable and the output power from the probe was determined to be 40 mW.

3.2.2 Raman probe

The Raman probe is a fiber optic sampling probe designed for backscattering spectroscopy (θ=180°), at the excitation wavelength of 532 nm. With backscattering geometry, the probe is designed to facilitate both excitation of the sample as well as sampling of the scattered light, from the excited sample. The connection between the probe, laser source and spectrometer is facilitated using fiber optic cables. A 105 µm fiber optic cable, is used to connect the laser source and Raman probe, referred to as the excitation fiber. The collection fiber, composed of a 200 µm fiber optic cable, is used as a connection between the Raman probe and spectrometer. The size of the collection fiber is set to approximately twice the size of the excitation fiber, to improve the collection of the scattered signal. The Raman probe is composed of two split optical lines, an excitation line and a sampling line. In the excitation line, the laser light is passed through lenses and a long pass filter, before being led out of the probe window by a dichroic filter to irradiate the sample. The collected light scattered from the irradiated sample is focused back into the Raman probe where it passes the dichroic filter to enter the sampling line. In the sampling line, the light passes a band-pass filter and a lens before being led to the Raman spectrometer by the 200 µm fiber optical cable. The focal point of the probe is approximately five millimeters from the exit window of the probe.

3.2.3 Optical components

Due to the short focal distance of the Raman probe, additional lenses are needed to shift the focal point to the center of the sample cell. The shortest distance for the Raman probe is 52.4 mm, which is the distance from the center of the sample cell to the cryostat window. During the experiments, two types of double achromatic lenses were available to shift the focal point. The lenses are manufactured by Thorlabs [44] and shift the focal point by 75 mm and 100 mm respectively.

3.2.4 Raman spectrometer

The Raman spectrometer is of the model QE-Pro high sensitivity fiber optic spectrometer made by Ocean Optics [42]. The spectrometer has a broad sensitivity from ultraviolet (UV) to near infra-red (NIR). The spectrometer is equipped with a FFT-CCD detector with a 2-D pixel arrangement of 1044 X 64 with a response between 200 to 1100 nm. The sampled light from the Raman probe is introduced to the spectrometer through a SMA-connector equipped with an exchangeable slit. Inside the spectrometer, the incoming light is focused on a collimating mirror which reflects the light onto a grating. The grating diffracts the light and directs it towards a focusing mirror which directs the light onto the FFT-CCD detector. The detector is controlled by a computer with the dedicated software (Oceanview) which allows the user to configure specific settings of the spectrometer.

3.2.5 Software

The software Oceanwiew enables the configuration and changes in the specific settings of the spectrometer, as well as the format of the signal, which is obtained from the scatter registered by the detector. Settings that are available for customization to optimize the obtained signal are "integration time", representing the time of a single data collection by the detector, "scans to average", determining how many discrete measurements that a single spectrum will consist of and "boxcar width" which represents smoothing of the obtained data by averaging across adjacent pixels to reduce noise. The time required for a single data collection is described by the following factors:

$$t_{Scan} = t_{integration} * n_{scans\ to\ average}$$

The time (t_{scan}), is the product of integration time ($t_{integration}$) and the number of scans corresponding to each measurement ($n_{scans\,to\,average}$). The computation software allows for a time interval of a single scan down to milliseconds. The data obtained from the spectrometer is presented as a graph representing each individual data collection sequence.

3.2.6 Transmission Raman spectroscopy

The collection of the Raman signal is in the direction of the incident laser beam. The transmission setup is similar to the one used in the backscattering method with a slight difference in configuration. The optical components for the transmission Raman setup are schematically shown in figure 12.

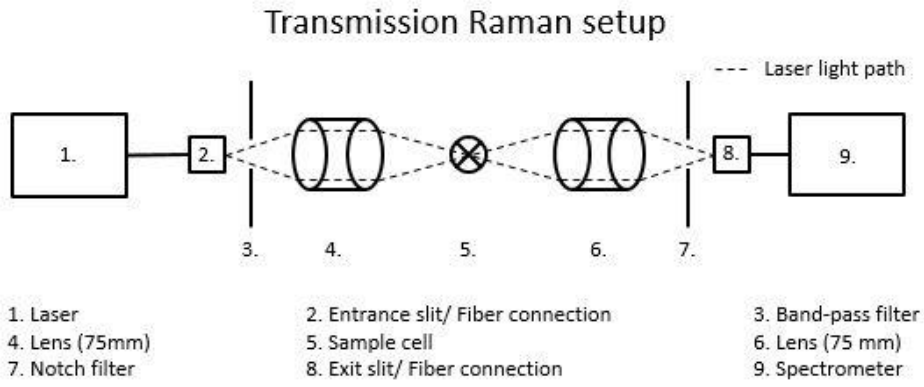

Figure 12: Schematic of the transmission Raman setup.

The difference between the transmission and the backscattering setups is that the combined functionality of the Raman probe is divided into two individual optical enhancement segments.

The excitation segment, contains components 1 to 4 and is placed in front of the sample cell. The sampling segment, illustrated by components 6 to 9 is placed behind the sample cell. The incident laser light and collected scattered light are led through fiber optic cables from the laser source to the excitation segment and from the sampling segment to the spectrometer. The equipment for the optical segments such as filters, lenses and fiber cables were made by Thorlabs [44] and designed for a wavelength of 532 nm.

3.3 Experimental procedure

The remaining sections in this chapter focus on the experimental procedure and treatment of the obtained data. Starting with the calibration of the instrumental Raman shift, followed by the optimization of the Raman signal. The optimization involves modification of the optical alignment and computational settings for the spectrometer in Oceanview. Leading to the evaluation of the sample cells and the collection of the characteristic background, which is followed by the characterization of the hydrogen signal and the analysis of the obtained hydrogen ratio, without the presence of a catalyst. These steps provide a foundation to study the catalytic conversion of ortho- to parahydrogen, where a kinetic expression for the conversion of ortho- to parahydrogen in the presence of the catalysts is determined. The two catalysts, IONEX® and OXISORB® are used in this thesis project. The final section involves the description of the analysis procedure for the obtained data using the software OriginLab.

3.3.1 Calibration of the internal Raman shift

The instrumental Raman shift is determined by comparing the obtained signal of a sample, with a Raman wavenumber standard. The sample is composed of naphthalene powder which is pressed into a pellet and irradiated by the Raman probe. The measurement was conducted in normal atmosphere inside a screening hood covering the Raman setup from interfering light from the outside environment. The obtained spectra of the naphthalene sample was compared to a published standard spectrum of naphthalene [45]. The Raman shift is determined by calculating the difference, in Raman shift, between the peaks from the obtained spectra and the published standard. The calculated difference of the instrumental Raman shift is averaged to a mean value. This is validated through the characterization of the obtained hydrogen signal with published hydrogen Raman spectrum [1].

3.3.2 Signal optimization

Before the measurements begin optimization of the Raman setup is performed, which involves the optical and spectrometer components in the setup.

3.3.2.1 Optical setup

The optimization of the optical setup is focused on increasing the signal to noise ratio of the obtained Raman spectrum. The optimization of the optical setup, involves the alignment and positioning of the Raman probe and lens, with the sample cell. The aim is to place the equipment in an aligned position, where the focal point of the Raman probe is placed inside the sample cell and in the center of the liquid hydrogen bulk. This position is chosen with the intention of minimizing the disturbance of the laser light path, while at the same time irradiating as much as possible of the liquid hydrogen. The optimal arrangement is confirmed through evaluation of the obtained Raman signal. The relative effect of the signal to noise ratio obtained from the optical settings, aligned in focus and out of focus was also evaluated.

The final positions for the components is presented in the schematic of the cryostat and the Raman setup is presented in figure 13.

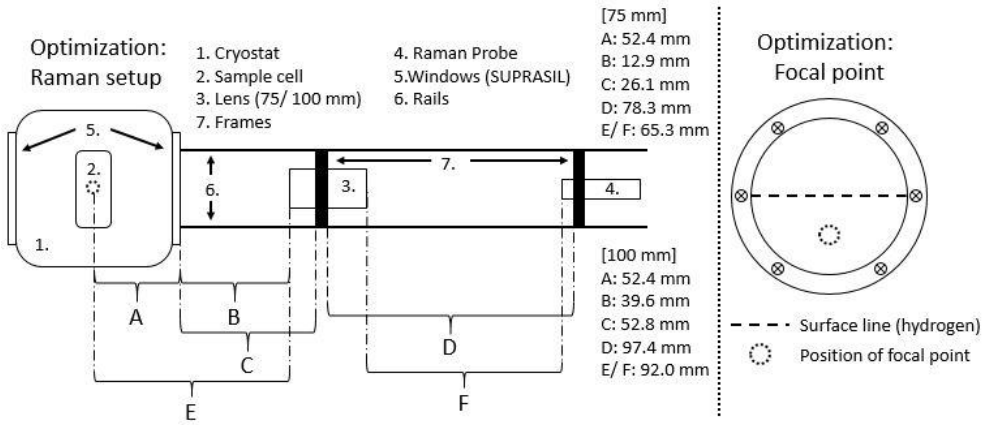

Figure 13: Illustration of the optimized positions for the focal point. Components involved in the optimization are the Raman probe, optical components and the sample cell placed inside the cryostat.

Figure 13 shows the optimized positions of the Raman components based on the two lenses which shifts the focal point by 75 and 100 mm respectively. The distance from the window of the cryostat to the center of the sample cell is 52.4 mm, shown by distance (A). The two lenses have an effective displacement of 65.3 and 92.0 mm respectively, at the edge of the lens shown by distance (E and F) in figure 13. The distance between the cryostat window and lens is given by distance (B).

The entire optical setup is placed in a cage with the possibility to alter the position both vertically and horizontally, for the entire optical assembly as well as each individual component. During the experiments, it was concluded that the position of the focus needs to be below the center of the sample cell. In order to place the focal point of the laser light inside the liquid hydrogen, which is shown on the right-hand side of figure 13.

3.3.2.2 Spectrometer settings

The preliminary settings from the startup of the Raman spectrometer involves corrections of the dark noise. Followed by defining the initial settings, regarding integration time, number of scans recorded per spectrum and the smoothing factor. The dark noise correction involves recording of the signal, when the laser emitted from the active probe is blocked with a cap. The obtained signal is associated to the wavelength of the laser source. For the initial settings of the spectrometer was the acquisition time at first set to one minute per spectrum but was lowered to 25 seconds in order to obtain data in shorter time steps. The acquisition time is the product of the integration time, set to five seconds per scan and the number of scans per spectrum, where five scans were collected for each spectra. The "boxcar width" was set to one and is related to adjacent smoothing, which results in the smoothing of one pixel per side.

3.3.3 Leak rate characterization

The final assembly of the sample equipment composed of the sample cell and sample stick is tested for leaks before being used in experiments. This is performed with a leak test using a Phoenix UL300 leak detector made by Leybold GmbH [46]. The test is in executed by connecting the sample assembly to a vacuum and spraying helium gas onto the surface and around each joint of the sample assembly. The leak rate is determined from helium that leaks into the sample stick and becomes registered by the change of the vacuum level. The vacuum level was set to $1.5*10^{-3}$ mbar and a specific requirement of the leak rate was delimited to $2*10^{-9}$ mbar.

3.3.4 Background data

The background is collected to correct for the contributions by the surrounding environment in the obtained Raman spectra. The characterization of the background also allows for comparison of the optical properties between the two sample cells, which is incorporated with quartz and sapphire windows. The background might change between each measurement, due to eventual changes in the environment or eventual changes in the alignment of the sample cell and optical components. Therefore, is the background recorded before each measurement and at the same experimental conditions. To compensate for any eventual changes which might affect the background. During the measurement of the background, the volume inside the sample cell is put under vacuum. The same spectrometer settings are used for the collection of the background signal as well as during the actual experiments for the catalytic conversion.

3.3.5 Sample cell loading

The loading of the sample cell is divided into two parts. Loading of catalyst and condensing of hydrogen into the sample cell. The catalyst loading is performed during the assembly of the sample cell. The process of loading the catalyst into the sample cell involves specific procedures based on whether IONEX® or OXISORB® is used. The amount of catalyst is determined using an analytical scale with an accuracy of ±0.1 mg. The loading of hydrogen is done after the collection of the background. The connection between the hydrogen storage and the sample cell is regulated by needle valves, where the hydrogen gas is added in sequences from a predetermined volume.

3.3.5.1 IONEX catalyst loading

The IONEX® catalyst requires activation before being used in the conversion experiments. The activation is performed by placing the catalyst into an evacuated furnace at 120°C and a pressure of 8 mbar, for a couple of hours. The time required for activation is based on the catalyst amount and how the catalyst bulk is stored. The activation process is performed to remove additional moisture adsorbed onto the catalyst as well as increase the surface activity. The adsorption of moisture onto the activated catalyst is relatively slow, which allows the loading process to be performed in normal atmosphere. The loading process involves the weighing of the activated catalyst and thereafter added into the sample cell.

3.3.5.2 OXISORB catalyst loading

The catalyst OXISORB® has the inherent disadvantage that it is sensitive to air due to oxidation of the catalytic sites, which consists of Cr(II) oxide bound to a silica gel carrier. The catalytic sites comprise in total 2-3% of the catalyst. Oxidation of the catalytic sites greatly affects the activity of the catalytic sites and due to the low amount of magnetic sites contributes to the sensitivity of the catalyst towards oxidation. This leads to that the catalyst requires loading in inert atmosphere to avoid contamination of the catalyst. Since OXISORB® is provided in sealed packages and always stored in inert environment no activation of the catalyst is required.

The inert atmosphere inside the glovebox is composed of argon. The glovebox is evacuated introducing an argon stream in the bottom of the glovebox. The stream exits from the top of the glovebox at the opposite side of the inlet. The heavier argon stream is assumed to push the air out of the glovebox, providing an acceptable inert atmosphere. However, the glovebox does not have an oxygen or moisture meter so the oxygen content cannot be measured, which results in that a complete inert environment cannot be confirmed. The glovebox is equipped with its own analytical scale with an accuracy of ±0.1 mg. The glovebox cannot accommodate the entire sample stick along with the sample cell, shown in figure 9. This results in that the loading of the catalyst and assembly of the sample cell is performed inside the glovebox and the connection of the sample cell to the sample stick being executed outside of the glovebox, in normal atmosphere. To avoid prolonged exposure to air the sample cell is quickly attached to the stick and connected to vacuum.

3.3.5.3 Hydrogen loading

The hydrogen is deposited as a gas into the sample cell at the temperature of 10K. The hydrogen gas transforms into a solid inside the sample cell. The total amount of hydrogen gas deposited into the cell is between five to six bar from a 150-ml cylinder at room temperature. The loading is conducted in sequences where the volumetric cylinder is loaded with 2 bars of hydrogen at room temperature. The hydrogen is then added into the sample cell in portions of 0.2 to 0.3 bars.

The addition of these portions leads to an increase in temperature, due to the temperature difference between the hydrogen, which is at room temperature and the cryogenic sample cell. The temperature change is monitored and a new portion is added when the temperature of the sample cell has stabilized at 10K. This procedure is repeated until 5.5 ± 0.5 bar of hydrogen have been added into the sample cell. When larger amounts of room tempered hydrogen are added into the cell, the temperature inside the cell increases drastically and the solid hydrogen inside the cell starts to liquefy. This enables the conversion of ortho- to parahydrogen before measurement has started.

Another issue with adding room tempered hydrogen too fast into the sample cell, is the risk of evaporating hydrogen inside the small volume of the sample cell. This is a significant safety risk during the loading procedure, where the increasing pressure inside the cell might cause the sample cell to break. By adding smaller amount of hydrogen into the cell these risks are avoided to a greater extent. When the hydrogen has been deposited into the cell, the solid hydrogen inside the cell is liquefied by increasing the temperature to 16 ± 1K. This elevation in temperature indicates the start of the measurement and the Raman spectroscopy is activated. During the experiments, the connection to the empty volumetric flask is open to provide with additional volume to accommodate for the increased gas pressure of hydrogen, in case of any eventual incidents.

3.3.6 Hydrogen signal

The hydrogen signal is recorded with the purpose to provide information regarding the characteristic peaks of ortho and parahydrogen in the obtained hydrogen spectrum as well as validating the calibration of the instrumental Raman shift of the spectrometer. The second purpose behind the collection of the hydrogen signal is to determine the signal intensity for the initial distribution of ortho- and parahydrogen, without the presence of a catalyst. The obtained signal will represent the initial distribution of ortho- and parahydrogen and is expected to be close to or preferentially identical to normal hydrogen at room temperature, meaning 75 to 25% ortho- to parahydrogen, since no catalyst is present to facilitate conversion. The hydrogen signal is also used to evaluate the differences between the spectroscopic techniques of backscattering Raman and transmission Raman.

The “hydrogen signal” experiment begins with the deposition of hydrogen into the sample cell and the transition of the solid hydrogen to liquid hydrogen by increasing the temperature of the sample cell to 16 ±1K. During the phase transition from solid to liquid the Raman spectroscopy is initiated and the Raman spectra are collected. The settings of the spectrometer for each experiment is presented in the appendix section, see Appendix 1. The hydrogen signal is recorded for 10 to 20 minutes each, with an acquisition time ranging from 25 to 60 seconds. Each spectrum is marked with a time, indicating the elapsed time of the experiment.

3.3.7 Catalytic conversion

The investigation of the catalytic conversion of ortho- to parahydrogen follows the same experimental procedure as previously mentioned for the hydrogen signal. With the difference between recording the catalytic conversion of hydrogen and hydrogen signal, being the presence of a catalyst as well as the number of collected spectra. The conversion is recorded until equilibrium is reached, which is observed as the orthohydrogen signal becoming indistinguishable from the background. The amount of collected spectra varies depending on the acquisition time for a single spectrum and the time required to reach equilibrium, where the elapsed time of the complete data collection depends on the catalyst type and catalyst amount.

3.3.8 Data treatment

The data obtained from the experiments is processed using the software OriginLab. The raw data obtained from the recording of the hydrogen and background signal, is summed up into segments composed of five spectra per segment. The background signal is subtracted from the hydrogen signal by matching the baseline of the background to the baseline of the hydrogen spectra. The background corrected hydrogen spectra are further analyzed in order to determine the ortho- to parahydrogen ratio. The ratio is determined by creating a baseline for the new background corrected spectra and the peaks representing ortho- and parahydrogen are identified. The area of the identified peaks is thereafter integrated and related to the concentration of ortho- and parahydrogen at the time of the recorded spectra.

An illustration on how the raw data is treated along with the procedure of the peak integration is shown in figure 14.

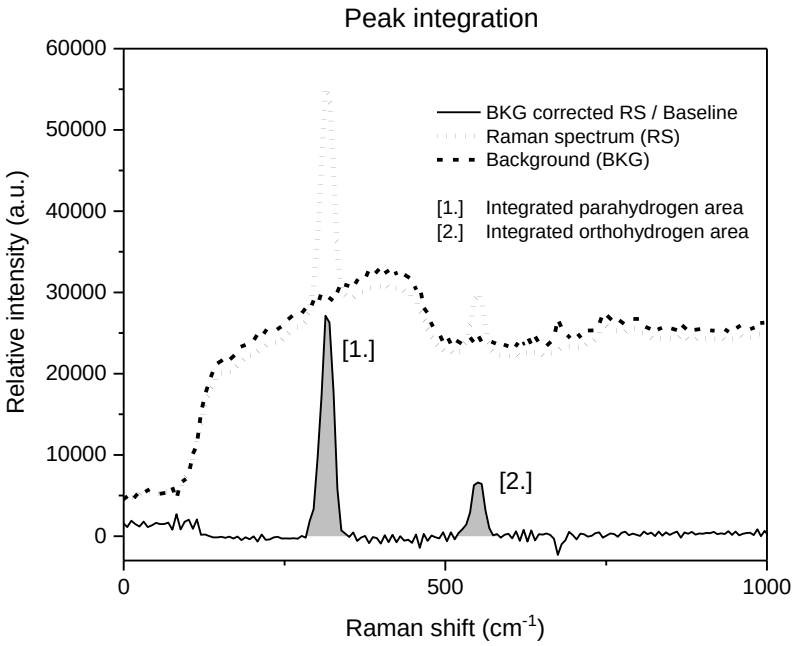

Figure 14: Illustration of the background subtraction and peak integration process. Integrated peaks after background subtraction is highlighted in grey.

Figure 14 shows the background (dashed line) and the hydrogen (dotted line) Raman spectrum. The inherent background in the hydrogen spectrum is subtracted using the background Raman spectrum. From the background corrected spectra, the integration of the ortho- and parahydrogen peaks is performed. The obtained area of the ortho- and parahydrogen peaks is normalized with respect to the total peak area. The resulting ratio of the hydrogen isomers as a function of time is used to determine the kinetics for the catalyzed conversion of ortho- to parahydrogen. The determined rate of conversion is used as a parameter to fit the mathematical function to the experimental data. The catalytic conversion of orthohydrogen is presented in literature as a first order process [1,20,23]. Resulting in that the zero, first and second order rate equation are of particular interest for further investigation. The rate of conversion determined from the catalytic conversion using IONEX® and OXISORB® is compared to one another and thereafter used to evaluate the catalytic efficiency, based on the conditions of the ESS hydrogen loop.

3.3.8.1 Definition of the rate equation

The rate equation is defined by the rate constant along with the concentration of the species which participates in the reaction. The order of the rate equation is given by the sum of exponents of the reactant concentrations. This indicates the number of rate determining reactants in the rate equation [47].

The differential form of the rate equation is given as:

$$\frac{\Delta C}{\Delta t} = k * C^n$$

In the expression above is (C) the concentration of the chemical specie, (k) is the rate constant of the reaction and (n) denotes the order of the rate equation. The simplest versions of the rate equation ranges from a zero order to second order [48]. From the integrated form of the rate equation, can a linear relationship be used to determine the rate constant for the three rate equations is presented in table 4.

Table 4: Integrated rate equation along with the linear relationship for determining the rate constant for the zero, first and second order.

	Zero order	First order	Second order
Integrated rate equation	$C = C_o - kt$	$\ln(C) = \ln(C_0) - kt$	$\frac{1}{C} = C_0 + kt$
Relationship to determine the rate constant	C vs t	ln[C] vs t	1/C vs t
Unit of the rate constant	mol/s	1/s	1/(mol*s)

The following linear relationship is used to determine the rate of the catalytic conversion as well as a method to deduce which order that describes the catalytic conversion of orthohydrogen [49]. The exponential function is fitted to the concentration profile of the experiment using the determined rate of conversion as a fitting parameter.

4 Result and discussion

This chapter is dedicated to the presentation and discussion of the obtained results from this project. Beginning with the results from the calibration of the Raman spectrometer, followed by the background characterization and the sample cell evaluation. Thereafter is the obtained results from the hydrogen Raman spectra, without the presence of a catalyst presented. Along with the results from the kinetic study regarding the catalytic conversion of ortho- to parahydrogen using IONEX® and OXISORB®, where an evaluation of the two catalysts is made, based on the conditions of the future ESS hydrogen loop. The chapter is concluded with a summary from the comparison of the two catalysts.

4.1 Calibration of the Raman spectrometer

The calibration of the Raman spectrometer is performed by comparing the shift in peak position between a spectrum of a naphthalene sample. A pressed pellet consisting of naphthalene flakes with a purity of (99%) procured from Simga-Aldrich [50] and a naphthalene standard reported in literature [45]. Naphthalene is a good wavenumber standard for the calibration of a Raman spectroscopy setup [51]. A spectrum of the naphthalene sample measured with the Raman spectrometer used in this work, is shown in figure 15.

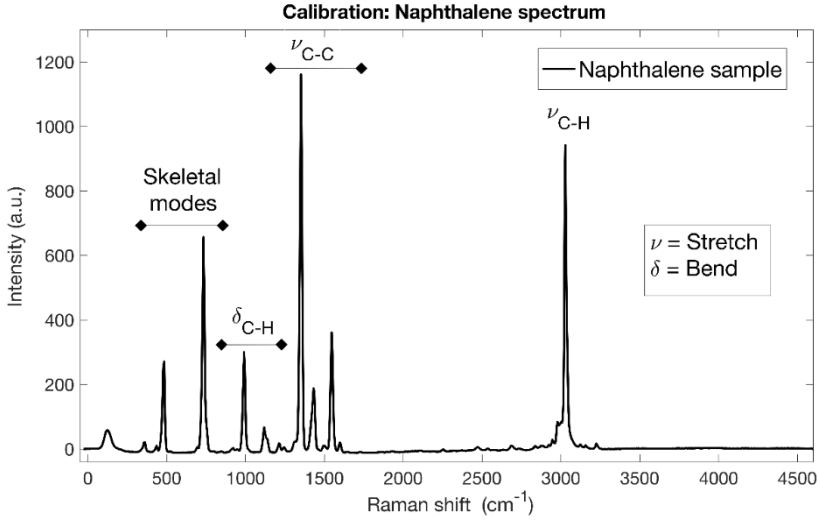

Figure 15: Raman spectrum of the background corrected naphthalene signal used for the calibration of the Raman spectrometer.

As mentioned in the literature survey, see section (2.3.1), Raman scattering is the interaction of light with a sample, resulting in vibrational and rotational movements of the excited molecule. The peak with the highest intensity at 1352 cm^{-1}, along with the following two peaks at 1431 and 1546 cm^{-1} are characteristic for the stretching motion of the carbon-carbon bond in naphthalene [52,53]. The peak at 3028 cm^{-1} represents the stretching of the carbon-hydrogen bond.

The high frequency of vibration is a result of the hydrogen bond strength and the relative mass of the carbon and hydrogen atoms. The region at 700 to 1200 cm^{-1} contains the bending motions of the carbon-hydrogen bonds which requires less energy compared to the stretching motion resulting in a lower Raman shift. The peaks at 485 and 733 cm^{-1}, result from the skeletal distortion of the naphthalene molecule.

The obtained sample spectrum is compared to the naphthalene standard [45]. The chosen standard was recorded using a laser source with the same excitation wavelength of 532 nm. The naphthalene used for the sample [50], is procured in the form of crystal flakes with a purity of 99% and pressed into a pellet. The obtained spectrum of the naphthalene sample along with the spectrum of the naphthalene standard is illustrated by the two curves in figure 16.

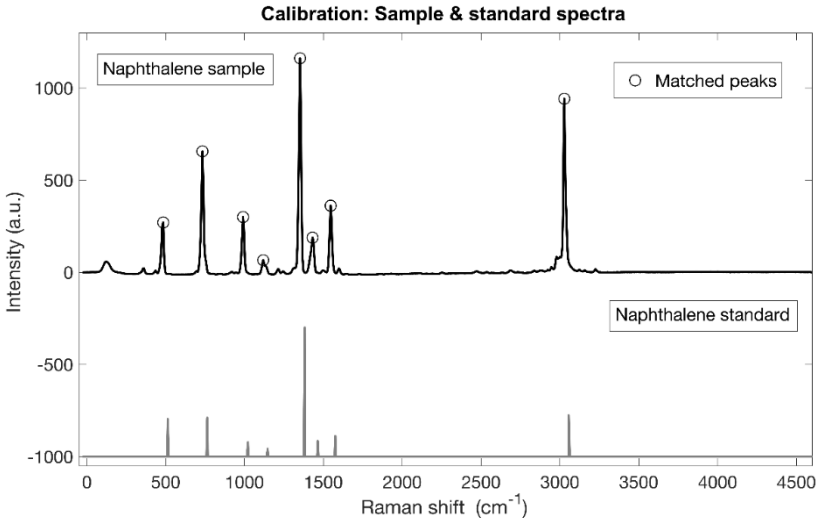

Figure 16: Comparison between the sample spectrum and the standard spectrum of naphthalene. Along with the matched peak positions between the two, marked as circles.

In figure 16, the sample spectrum measured for the present report is illustrated by the top curve and the naphthalene standard is illustrated by the lower curve. The peak intensity of the standard is given as the relative intensity, in relation to the strongest peak, located at 1352 (cm^{-1}). As naphthalene is not used as intensity standard, the important feature of the standard spectrum is the Raman shift of the standard peaks. These are used to calculate the relative shift of the sample and consequently the spectrometer shift. The sample spectrum contains peaks that are not present in the standard spectrum. These extra peaks are relatively small and are a result of reflections from the sample surface, caused by the sample being pressed into a pellet from powders. Through comparison between the sample and standard spectra eight peaks are matched illustrated by the circles in figure 16.

The determined peak positions of the sample and standard along with the resulting difference are presented in table 5.

Table 5: Characterized positions for the individual peaks of the naphthalene sample and naphthalene standard with the calculated difference of the Raman shift.

	Peak position (cm^{-1})							
Sample	484.5	733.3	990.7	1118.7	1351.9	1431.4	1546.4	3028.0
Standard	513.8	763.8	1021.6	1147.2	1382.2	1464.5	1576.6	3056.4
Difference	-29.3	-30.5	-30.9	-28.5	-30.3	-33.1	-30.2	-28.4
Interval	[-33.1 - 28.4]							
Average Raman shift	-30.2							

The instrumental average Raman shift is determined to -30.2 cm^{-1}. The shift is a result of the instrumental differences for the equipment, used in this work and the standard spectrum. The determined shift will be used as a correction factor, to account for the deviation of the Raman instrument to be comparable to spectra in literature.

4.2 Background intensity of the sample cell

The background of the empty sample setup is collected, to determine its impact on the Raman spectrum. Since Raman scattering is a weak process, recording and subtracting the background signal is an important step to improve the Raman spectrum. Any undesirable contributions to the Raman spectrum, can thus be removed. The collection of the background spectrum also provides an evaluation of the sample cell window materials and their contribution to the obtained Raman signal.

The requirements on the sample cell are high, with several different aspects being taken into account. The cell should be able to contain hydrogen, ranging from the solid- to gas-state, without breaking or allowing leakage of hydrogen. This means that the ability to handle unforeseen pressure changes becomes an important factor for the sample cell. The pressure changes might be a result of the phase transitions or eventual evaporation of hydrogen due to insufficient cooling. The sample cell should also enable incident and scattered light to pass through it with a low contribution to the background of the obtained signal.

4.2.1 Evaluaton of sample cells

Two types of sample cells have been examined with widows consisting of sapphire and quartz glass respectively. The properties of the sample cells is given in the experimental section, see section (3.2.1). The two sample cells will be referred to as the sapphire and quartz cell according to the window material of each respective sample cell.

4.2.1.1 Background

The obtained Raman spectra of the sapphire and quartz cell are displayed in figure 17.

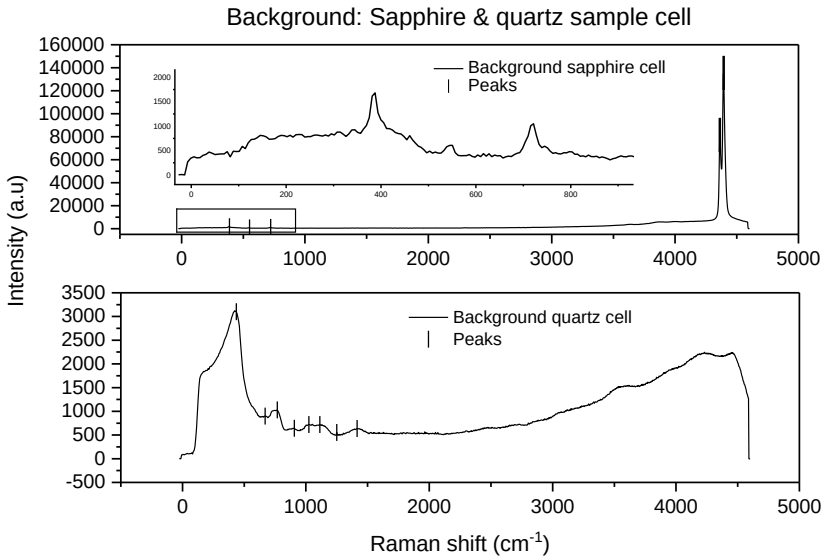

Figure 17: The top graph shows the Raman spectrum from the sapphire sample cell and the bottom spectra illustrates the Raman spectrum obtained for the quartz sample cell.

Figure 17 shows the Raman signal of the two sample cells. The cells are "empty" during the measurement, with the inner volume being under vacuum and the surrounding volume consisting of a low pressure helium gas. The intensity of the obtained spectra is not absolute intensity as the optics were moved between the measurements. However, the obtained spectras can still be used for the comparison of the background between the two sample cells. The most apparent difference between the curves of the two sample cells is found at the lower Raman shift (0-1500 cm^{-1}), shown in figure 17. This is of particular interest since the rotational leves of hydrogen are found in the same region, see section (2.1.7). An increased background might result in the distortion of information from the hydrogen peaks, as well as complicating the processing of the obtained signal.

The two curves share a similar profile untill the Raman shift around 4400 cm^{-1}, where the sapphire spectrum shows two strong peaks while no peaks are observed in the quartz spectrum. These two peaks are related to the material composition of the sapphire windows. From the two curves in figure 17, five peaks were determined for the sapphire spectrum, while eight peaks were found in the spectrum of the quartz cell.

The peaks identfied in the sapphire and quartz cell spectra are corrected for the Raman shift of the spectrometer and presented in table 6.

Table 6: Positions of the characterized peaks from the obtained Raman spectrum of the sapphire and quartz sample cells. Together with a description of the origin for each peak.

Peak position (cm^{-1})			
Sapphire		Quartz	
418	Optical modes (OM)	466	α-quartz
581	OM	700	γ_{sym}
751,885	OM	798	γ_{sym}
4393	R2	936	γ_{assym}
4424	R1	1054	γ_{assym}
-		1143	γ_{assym}
-		1280	γ_{assym}
-		1446	γ_{assym}

Table 6 shows that both sample cells produce signals in the region of 350-800 cm^{-1} which is in the same region as the bands for the transition from first to the second order rotational levels of ortho- and parahydrogen, mentioned in section (2.1.7). These peaks could affect the intensity and alter the obtained information of the hydrogen peaks. Addditional peaks are found at a Raman shift between 900 and 1500 cm^{-1} for the quartz specrtum and above 4400 cm^{-1} for the sappire spectrum. From figure 17 it is observable that the strongest peak is located at 466 cm^{-1} for quartz and 4393 cm^{-1} in the sapphire spectrum. The origin of the respectve peak regions and their relative intesities is due to te crystal lattice of quartz and sapphire.

4.2.1.1.1 Quartz

The bands at low wavenumbers of the quartz spectrum are the symmetric stretching vibrations of the Si-O-Si lattice in solid silica, while the peaks at higher wavenumbers are associated with the anti symmetric stretch of the silicon oxygen bond [54,55]. The strongest peak of the quartz spectrum is located at 466 cm^{-1}. The peak is related to the characteristic peak of α-quartz resulting from the Si-O-Si symmetric stretching movement of SiO_4 tetrahedra connected to six membered rings. The region for the two following peaks at 700 and 798 cm^{-1} is related to the symmetrial stretch of Si-O-Si bonds between structures of n-membered tetraheda. The last region in the quarts Raman spectra represents the assymetric stretch of the Si-O-Si bonds for the n-membered tetreheda [54–58].

4.2.1.1.2 Sapphire

The sapphire Raman spectrum contains five peaks of which three are found in the low frequency region at 350-750 cm^{-1}. These peaks are related to the Raman active phonons of the D_{3d}^6 point group of corundum. These peaks are described as optical modes (OM) of the corundum unit cell. The unit cell is composed of two Al_2O_3 molecules.The three peaks which represent the optical modes are related to specific motions of the lattice inside the corrundum unit cell. The first optical mode which is located at 387 cm^{-1} is the result of the motion of the lattice in the xx, yy and zz directions. The two remaning peaks at 550 cm^{-1} and 721cm^{-1} represents optical modes related to the motion in the xy, xz and yz directions by the corundum lattice [59–61]. The origin of the two larger peaks dominating the sapphire Raman spectrum are R1 and R2 fluorecence emmissions, which originates from the impurities of the chromium ions in the sapphire crystal lattice [62,63]. These two bands are at frequencies above 4300 cm^{-1} (figure 17) and exhibit an intensity decrease with decreased temperature. While the R2 line at (4362 cm^{-1}) exhibits a much stronger dependancy to temperature than R1, both lines are snesitive enough to have been proposed to work as a possible thermal indicator, in the range of 100-10K [62,63].

4.2.1.2 Decision on sample cell

From the comparison between the two sample cells it is obvious that the sapphire sample cell gives a lower background, as well as showing a more narrow half-width of the respective peaks, compared to the quartz sample cell. The sapphire spectrum also contains less peaks which might interfere with the raman spectra of hydrogen than quartz. Based on these aspects the sapphire cell was choosen as sample cell for the experiements and recommended for the online monitoring system at ESS.

4.2.1 Leak rate

The assembled sample setup, which consists of the sapphire cell, sample stick and gas line is examined for leaks using a helium leak detector. The processes are described in more detail in the experimental section, see section (3.3.3). The result of the preformed leak test is presented in table 7.

Table 7: Report sheet obtained from the leak rate test of the complete sample stick setup.

Part identifier Leak detector			Hydrogen loop Phoenix UL300	
Calibrated leak [C_{CL}] (mbar*l/s)			$1.3*10^{-7}$	
Calibrated leak signal [S_{CL}] (mbar*l/s)			$1.5*10^{-7}$	
Equipment name	Residual signal [R_S] (mbar*l/s)	Signal leak [S_L] (mbar*l/s)	Leak evaluation [q_G]	Conformance Yes/No
Hydrogen loop	$1*10^{-8}$	No leak	-	Yes
Level of vacuum pressure during testing (mbar)			$1.5*10^{-3}$	
Leak tightness requirement (mbar*l/s)			$2*10^{-9}$	
Leak testing method			Global Helium vacuum leak test	

From the leak test, no apparent leak could be observerd. The leak tests involving the helium leak detector were performed for the initial assembly of the sample stick and sample cell to validate the procedure of the assembly. After the leak rate test, the unchanged system of the sample stick was installed to the cryostat and gas line. The setup was evacuated in the laboratory envirorment and the vacuum level was measured using a dedicated ion vacuum gauge. A vacuum level of 10^{-5} bar was measured for the hydrogen loop with the leak tested stick. From that point on the assembly was assumed to be leak tight if a vacuum of 10^{-5} bar was achieved and could be kept with closed vales and no pump attached. The use of the helium leak detector is a good method for initial evaluation of new sample cells or how well the system seals, when no air sensitive material is present inside the sample cell of the assembly. The used leak testing setup could not be used when exposure to air is damaging the material inside the sample cell.

4.3 Hydrogen signal

The hydrogen signal is collected without the presence of a catalyst in order to characterize the peaks in the hydrogen spectrum as well as determine the signal intensity for the initial ratio of ortho and parahydrogen. The collection of the hydrogen signal also enables to optimize the signal to noise ratio of the obtained hydrogen spectra. The hydrogen signal was collected using both backscattering and transmission Raman spectroscopy, the list of experiments is presented in table 8.

Table 8: Summary of initial parameters, such as the used hydrogen amount and acquisition time for the hydrogen signal experiment.

Experiment	Amount of hydrogen (Bar*, @ RT, 150 ml)	Amount of hydrogen (mmol)	Acquisition time (min)	Comment
H2B1	5.58 ± 0.1	33.76	10	Focus in front of window
H2B2	5.58 ± 0.1	33.76	10	Longer interval
H2B3	5.59 ± 0.1	33.82	21	Focus inside cell, IL[1]
H2B4	5.59 ± 0.1	33.82	41	Extra position, AL[2]
H2T1	5.57 ± 0.1	33.70	10	200 µm fiber
H2T2	5.57 ± 0.1	33.70	10	400 µm fiber

* ± 0.1 bar, [1] In liquid, [2] Above liquid

From table 8 the following experiments are marked with the letters B or T, which stands for “backscatter” and “transmission” and refers to the geometry of the setup. The focal point is set to three specific positions. The focus of the laser for the two first positions is located in the liquid hydrogen but in front of the sample cell window (H2B1 and H2B2). The third position is located inside the cell (H2B3). The fourth experiment involves two positions of the focal point, where the first position is in the gas phase above the surface of the liquid hydrogen (H2B4 “part 1”) and the second position (H2B4 “part 2”) being at the same position as H2B3. The investigation looks at information regarding how a focused or a dispersed beam changes the obtained Raman spectrum. The difference between a focused and dispersed beam lies in the irradiated volume of the sample, because a dispersed beam spot irradiates a larger sample volume compared to a focused beam.

An illustration of the difference between a focused beam and dispersed beam, along with the focal point positions of the experiments are shown in figure 18.

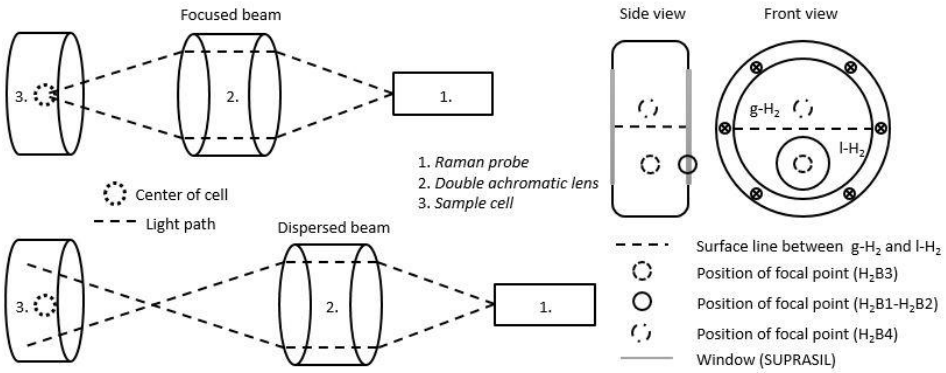

Figure 18: Illustration of the alignment regarding the Raman spectroscopy setup for focus and dispersed beam measurements (left), along with an illustration of the focal position of the hydrogen signal experiments (right).

The liquid hydrogen signal of experiment (H2B3) without a catalyst with a focused beam in the liquid hydrogen present is shown in figure 19.

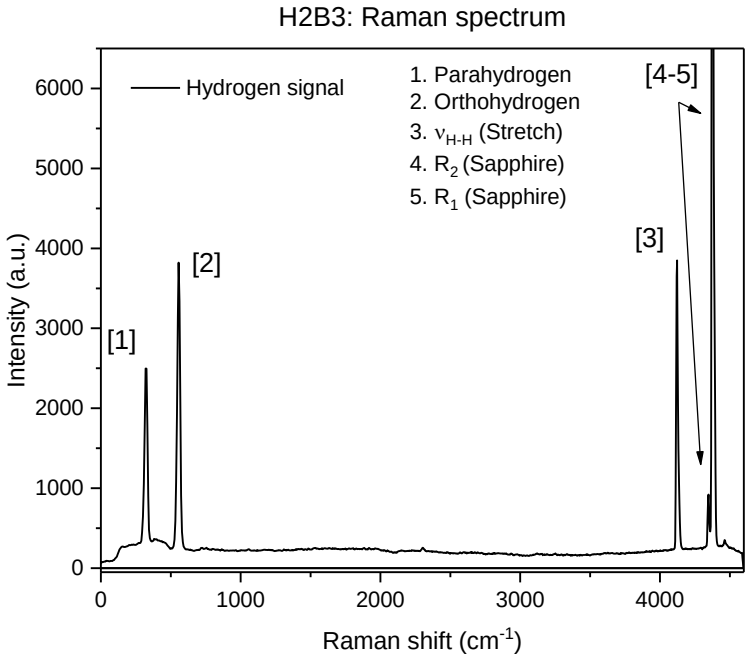

Figure 19: Raman spectrum of experiment (H2B3), with no catalyst present and focus placed in the liquid hydrogen bulk.

A comparison between figure 19 and the background spectrum of the sapphire cell in figure 17, see section (4.2.2), shows that three new peaks are visible in the obtained Raman spectrum. These peaks are labeled (1-3) and are caused by the motion of the excited liquid hydrogen molecules. The hydrogen signal was recorded for 20 minutes and a spectrum was collected every 25 seconds. Since no change in the obtained hydrogen spectra is observed from the experiment, the conclusion can be made that no conversion of ortho- to parahydrogen transpires. This confirms that conversion is not facilitated from the surface of the equipment. Since the natural conversion is extremely slow no conversion is expected from the interaction between orthohydrogen molecules which is mentioned in the literature section (2.1.4) and confirmed from the experiment [13,14].

The specific Raman shift for the peaks determined from the figure 19 are listed in table 9.

*Table 9: The determined Raman shift for the obtained Raman signal of experiment (*H2B3*) with values presented in literature.*

	1	2	3	4	5
	J= 0➔2	J= 1➔3	ν_{H-H}	R2	R1
Raman shift (cm^{-1})	349	580	4149	4370	4401
Literature values	354[1]	587[1]	4162[1]	4360[2]	4389[2]

[1] [1], [2] [57]

The peaks (4) and (5) which are found at high wavenumbers in figure 19 are identified as the R2 and R1 fluorescence emission by the impurities in the sapphire window. These same peaks were identified during the background characterization, see section (4.2.1.1). The temperature for the experiment (H2B3) is at 16K (figure 19), while the background signal (figure 17) was recorded at room temperature.

The intensity of the peaks representing the R2 and R1 fluorescent bands are temperature dependent. During the cooling of the cryostat it becomes apparent that the intensity of the R2 band is affected to a greater extent than the R1 band as a result of the temperature changes. The temperature dependency of the R2 (peak 4) and R1 (peak 5) bands becomes clear in this comparison, where the intensity of the R2 line, in figure 19 has decreased significantly in comparison to the R2 band in figure 17.

Peak 3 is the stretching motion of the hydrogen-hydrogen bond. The symmetric stretch is found at a Raman shift of 4149 cm^{-1} and agrees well with the shift presented in literature [1]. Using the Boltzmann equation, the H-H stretch frequency is determined to show up around 4150-4160 cm^{-1}. The presence of the H-H stretch is expected when hydrogen is examined using Raman spectroscopy. Since only one vibrational mode is possible for diatomic molecules and only one peak in the Raman spectrum can be liked to a vibrational motion. This confirms that the scattered light is due to irradiated liquid hydrogen.

Peaks 1 and 2, which are found in the hydrogen spectrum located at a Raman shift of 319 and 550 cm^{-1} respectively and presented with the corrected peak values in table 9. These peaks correspond to the first order rotational levels for parahydrogen (J=0➔2) and orthohydrogen (J=1➔3). The second order rotational levels (J=2➔4) and (J=3➔5) are not observed in any of the obtained Raman spectra. This is a result of the low intensity of hydrogen molecules present at elevated energetic states, due to the lower energy levels being favored at lower temperatures.

The shift of the hydrogen peaks in figure 19, corrected for the internal Raman shift of the spectrometer (30.2 cm^{-1}) agrees well with values presented in literature for the rotational and vibrational modes of the hydrogen molecule [1]. This confirms the value of the spectrometer Raman shift is consistent and independent to the sample temperature. The small deviance which is still present between the experimental and literature values can be regarded as a result of the difference of the experimental equipment or a statistical error.

After the hydrogen signal is recorded, the characterization of the ortho-parahydrogen ratio follows. The signals are amplified by recording and summing up a number of hydrogen and background spectra. Then the background is subtracted from the hydrogen Raman spectra.

An illustration of a background subtracted liquid hydrogen Raman spectrum is shown in figure 20.

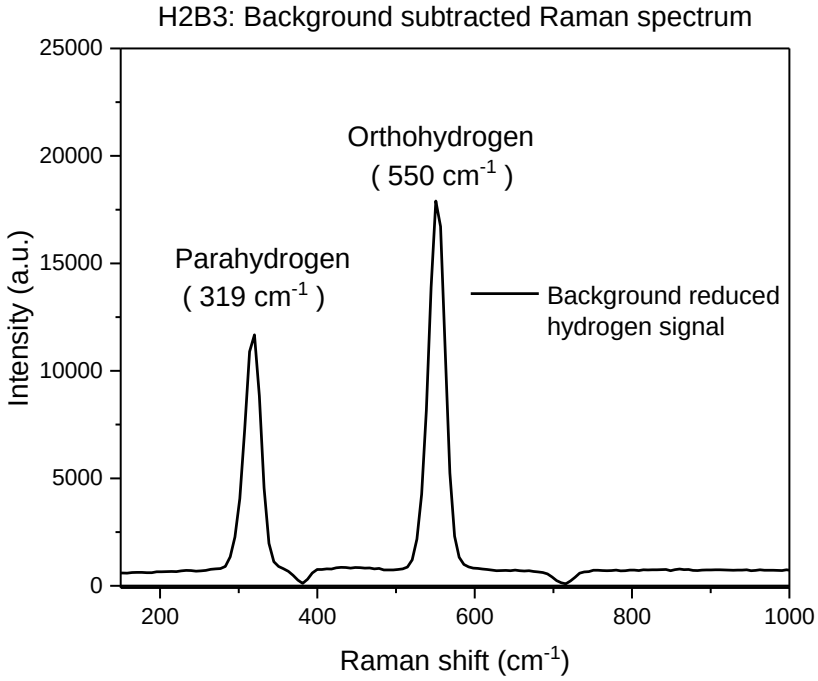

Figure 20: Background subtracted Raman spectrum. Illustrating the ortho- and parahydrogen peaks of the hydrogen signal obtained from experiment (H2B3).

The foreground and background signals are enhanced by compiling five individual spectra respectively. The background is then subtracted from the foreground, resulting in the following spectra shown in figure 20. The negative peaks are the result of over subtraction by the background, caused by the three small peaks in the sapphire background spectrum in the region 350 to 750 cm^{-1}. The ratio of ortho- and parahydrogen is then determined by defining a baseline under the peaks and integrate the area of the peaks. The integrated area is a measure of to the concentration of each isomer in the irradiated hydrogen bulk at the time of the recorded signal, see section 3.3.8.

The calculated ratio of the hydrogen isomers from the backscattering measurements of the hydrogen signal is shown in table 10.

Table 10: Ortho-parahydrogen ratio, determined from backscattering Raman spectroscopy.

Experiment	Parahydrogen ratio (mol%)	Orthohydrogen ratio (mol%)	Comment
H2B1	37.5	62.5	Not in focus
H2B2	36.8	63.2	Not in focus
H2B3	38.8	61.2	In focus
H2B4 “part 1”	41.2	58.8	Focus above surface line
H2B4 “part 2”	38.8	61.2	In focus

The ortho-para ratio in hydrogen is that of normal hydrogen composition (3:1), since it is the distribution of hydrogen thermodynamically favored at room temperature. When hydrogen is condensed, the ratio of normal hydrogen will still be maintained since no catalyst is present and natural conversion is extremely slow.

From the acquired hydrogen spectra, the following distribution of the ortho- and parahydrogen signal is displayed as a 2:1 (67:33 mol%) relationship. This phenomenon has been observed and the relationship between the observed and true ratio of ortho- and parahydrogen has been reported in literature [1,27,64]. The relationship between the presented and true ratio of the hydrogen isomers is further discussed in section 4.4.3.2. From the observed ratio presented in table 10 along with that no apparent change is observed for the peak intensities of the hydrogen isomers, indicating that orthohydrogen is not converted into parahydrogen during the experiment the following conclusion can be made: That the observed ratio of the hydrogen signal is related to the true value of normal hydrogen.

The reason for the deviation of the observed ratio and the normal hydrogen distribution is believed to be a result of the instrumental response function (IRF). The IRF is related to the response of the scattered light by the spectrometer over the experimental wavelength range. It is also dependent on the collective disturbances of the light path by the equipment of the setup. These disturbances can be a result of several optical effects which are dependent on the wavelength of the incident and scattered light, such as mirrors absorbing light, the efficiency of lenses, gratings and the transmission of filters, fiber optical cables weakening the signal of the light or from the sensitivity of the detector [65,66].

In table 10 the hydrogen isomer distribution is shown for each focal point position. The obtained ratio is lower when the beam irradiating the liquid hydrogen is dispersed (out of focus) compared to when the laser is in focus. This is likely just an effect of smaller signal to noise ratio and that information is lost.

The Raman spectra of measurement (H2B2) is shown in figure 21.

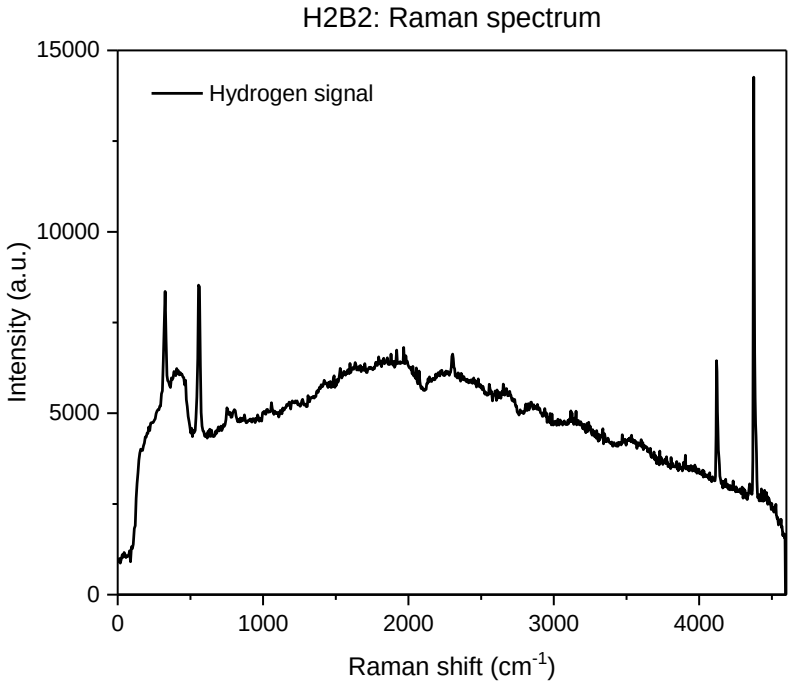

Figure 21: Raman spectrum of the experiment (H2B2).

The focus laser beam for H2B2 is aligned with the liquid hydrogen but placed in front of the sample cell. No change in intensity was observed during the recording of the hydrogen signal, which was conducted for 10 minutes. The increased background however, dilutes the information of the hydrogen signal and leads to a higher uncertainty of the ortho- and parahydrogen peak areas, which is illustrated nicely in figure 21. The significant increase of the background in the region of the hydrogen peaks leads to deviating results when determining the hydrogen ratio.

The result form the measurement (H2B4 “above surface line”) seemingly shows a significant increase of the parahydrogen ratio. The increase is a result of the information being lost due to the focal point of the laser not being in line with the liquid hydrogen. This shows that a dispersed beam in line with the hydrogen provides a more accurate signal compared to a focused beam where the alignment is slightly out of the liquid hydrogen.

The hydrogen signal was also examined using transmission Raman spectroscopy, to validate the relative intensities of backscattering Raman spectroscopy. The focus is inside the center of the bulk liquid hydrogen. Since the transmission measurement use an entirely different setup compared to the backscattering Raman, there is an opportunity to examine the signal to noise ratio based on the relative size of the fiber optic cable, ranging from 200 µm (H2T1) to 400 µm (H2T2).

The obtained Raman spectra from the transmission Raman measurements is shown in figure 22.

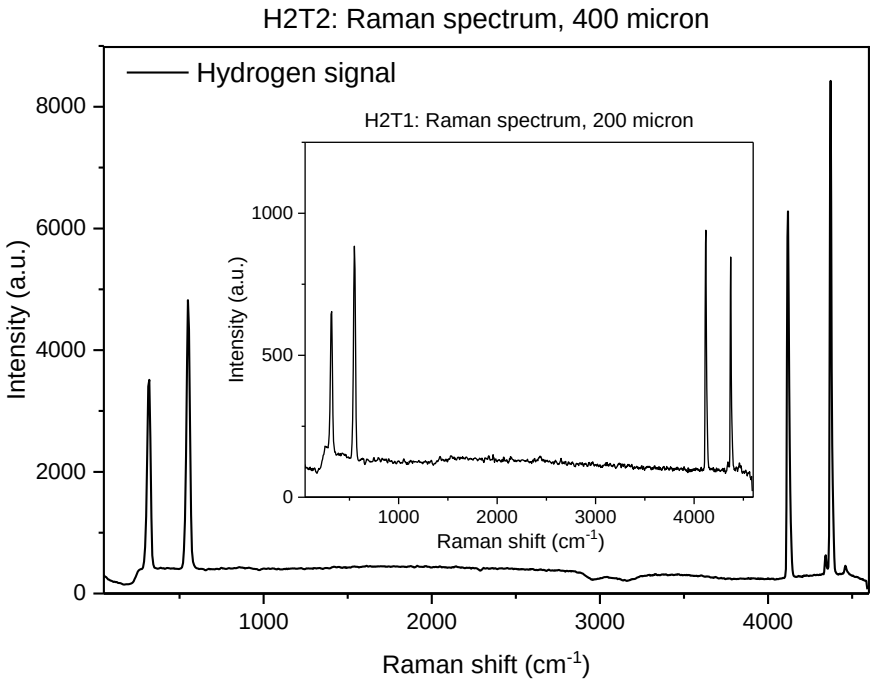

Figure 22: Obtained transmission Raman spectra based on measurements with 200-micrometer fiber (center curve) and 400 micrometer fiber optic cables (outer curve).

Using a larger optical fiber, results in a stronger signal and better signal to noise ratio, which is seen in figure 22 by the relative intensity of the peaks. The intensity of the ortho- and parahydrogen peak along with the integrated area is presented in table 11.

Table 11: Peak and background intensity (peak maximum) along with the determined ortho: parahydrogen ratio for the transmission Raman measurements.

Experiment	H_2^P [Intensity] (a.u.)	H_2^O [Intensity] (a.u)	Background [Intensity] (a.u)	H_2^P [Ratio] (mol%)	H_2^O [Ratio] (mol%)
H2T1	650	880	130	39.6	60.4
H2T2	3510	4820	420	41.5	58.5

The table confirms that the signal to noise ratio increases with the size of the fiber cable. An increase of the fiber size by a factor two gives an approximate increase of the hydrogen signal by a factor five and the background by a factor three. The difference in signal intensity is an effect from the size of the optical fiber, where the increased size of the fiber would result in the collection of more scattered light resulting in the increased intensity

The observed ratio of the hydrogen isomers from the transmission Raman measurement agrees with the distribution of the isomers obtained from the experiments using the backscattering Raman setup. The relationship between the observed deviation from the true ratio id further discussed in section 4.4.3.2. The slight deviation between the observed ration from the transmission and backscattering geometries is a result of the instrumental differences from the filters incorporated in the Raman probe and the filters used in the transmission Raman setup. The difference in the ratio of the isomer could be a result of the increased background as a result of the scattered light being transported in a fiber with larger diameter causing more dispersion of the collected information, which results in a lower resolution of the obtained spectra leading to the observed deviation.

The peak positons of the characterized hydrogen signal at 16K shows to be consistent with the hydrogen signal presented in literature, when accounting for the internal Raman shift of the spectrometer. That was determined using naphthalene at room temperature. The hydrogen ratio is determined to an interval of [39.6-41.5] mol% parahydrogen and [60.4-58.5] mol % orthohydrogen respectively, which deviates from the normal hydrogen distribution of 75:25 mol%. The deviation is most likely due to the instrumental response function of the spectrometer.

The investigation regarding the spectroscopy geometry resulted in the same distribution of the hydrogen isomers, along with an additional observation that the intensity can be enhanced when increasing the size of the fiber inside the fiber optic cable.

4.4 Ortho- to parahydrogen conversion

The catalytic conversion of ortho- to parahydrogen has been investigated for the two catalysts, IONEX® and OXISORB®. In order to present the results of the conducted experiments in an informative manner, only relevant data is shown in this chapter. A summary of all results can be found in the appendices of this report. Each experiment is labeled with a specific index, indicating the type of catalyst involved and numbered following the order of the experiment. Experiments which involves the IONEX® catalyst are labeled, ION (i) where (i) is the index for experiment, ranging from 1 to 9. Experiment regarding the OXISORB® catalyst is labeled as OXI (i) where (i), with an index of 1 to 6. The scattered light during each experiments was continuously recorded with specific settings of the spectrometer, presented in the appendix section, see Appendix 1. The raw experimental data is obtained as multiple spectra, from which the change in ortho- and parahydrogen concentration is reported as a function of elapsed time.

4.4.1 IONEX®

The first catalyst examined is the iron oxide catalyst IONEX®. In this section, a comparison will be made between the catalytic conversion in two experiments. Table 12 shows the initial parameters regarding the amount of hydrogen, catalyst as well as the acquisition time for the experiments ION 3 and ION 9.

The time column in table 12 is divided up into "full time" and "in liquid state", where the "full time" also accounts for the time in which the solid hydrogen transitions to liquid hydrogen. The transition from solid to liquid is shown as a significant spike in intensity of the Raman spectrum. The obtained spectra for solid hydrogen has a low signal to noise ratio, as well as the main interest of this thesis being the study of the catalytic conversion in liquid hydrogen, therefore is the solid hydrogen spectra removed from further study. This leads to the second part of the time column describing the time of conversion in liquid hydrogen.

A complete table of the initial parameters for all experiments involving IONEX® is presented in the appendix section, see Appendix 2.

Table 12: Initial parameters regarding the hydrogen amount, catalyst amount and acquisition time for the experiments ION 3 and ION 9.

	Amount of hydrogen (Bar*, @ RT, 150 ml)	Hydrogen amount (mmol)	Catalyst amount (mg)	Time [Full time]/[liquid state] (min)
ION 3	5.58 ±0.01	33.76	21.0 ±0.1	180/175
ION 9	5.56 ±0.01	33.64	20.8 ±0.1	180/175

* ± 0.1 bar

The amount of hydrogen added into the sample cell, was determined based on the pressure limit of the gas line in case of emergency, as well as obtaining a reasonable amount of liquid hydrogen inside the cell, so the laser could pass straight through the liquid without interference from the cell. The amount of hydrogen was decided to 5.5 ± 0.1 bar based on a 150 ml vessel. The catalyst amount was determined to 21 ± 0.2 mg. The catalyst was changed once to assure optimal activity of the catalyst, due to an interruption causing a longer stop in the experimental phase. The amount of catalyst used in the first load resulted in acceptable times with respect to the complete conversion of the deposited hydrogen as well as a reasonable rate of conversion in the early stage of orthohydrogen conversion. The same catalyst amount was chosen with the desire to further investigate the kinetics with a comparable catalyst amount to the first experiments. The first catalyst load involved the investigation of signal to noise ratio as a result of the focal point position, while the second load was mainly focused on the conversion with optimal focal settings. The catalyst amount of 21 mg provided a suitable pace of conversion in the early stages, along with a total conversion time in the range of 150 to 200 minutes.

4.4.1.1 Raman spectrum

The following two figures shows the Raman spectra of the catalyzed orthohydrogen conversion using IONEX, where the spectra ION 9 is presented first followed by ION 3.

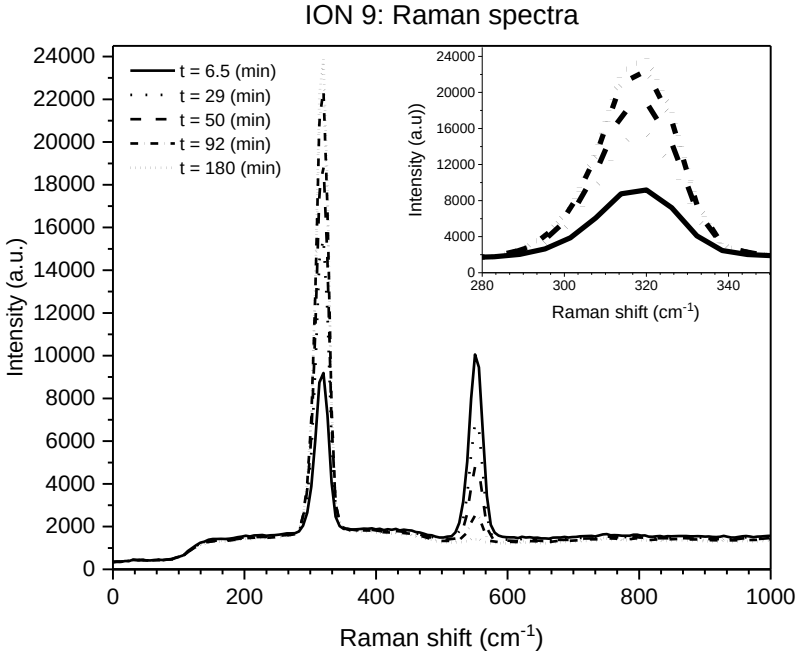

Figure 23: Raman spectra of the orthohydrogen conversion for ION 9. Illustrating the relative change of the peak intensities at a specific point in time: Orthohydrogen (right peak) and parahydrogen (left peak).

Figure 23 shows the Raman spectra obtained of a catalytic ortho- to parahydrogen conversion (ION 9). The initial parameters are presented in table 12. From each curve the relative ratio of ortho- and parahydrogen at the time of the collected spectra can be determined. By compiling the ratio of the hydrogen isomers obtained from each spectrum as a function of the conversion time for each measurement, will provide information with respect to the process of the catalytic conversion of ortho- to parahydrogen. A selection of the obtained spectra from the experiment ION 9 is shown in figure 23, illustrating the decrease in intensity of the peak located at 550 cm^{-1} representing orthohydrogen, and the increase in peak intensity at 319 cm^{-1} which represents parahydrogen.

The obtained spectra of experiment ION 3 is shown in figure 24.

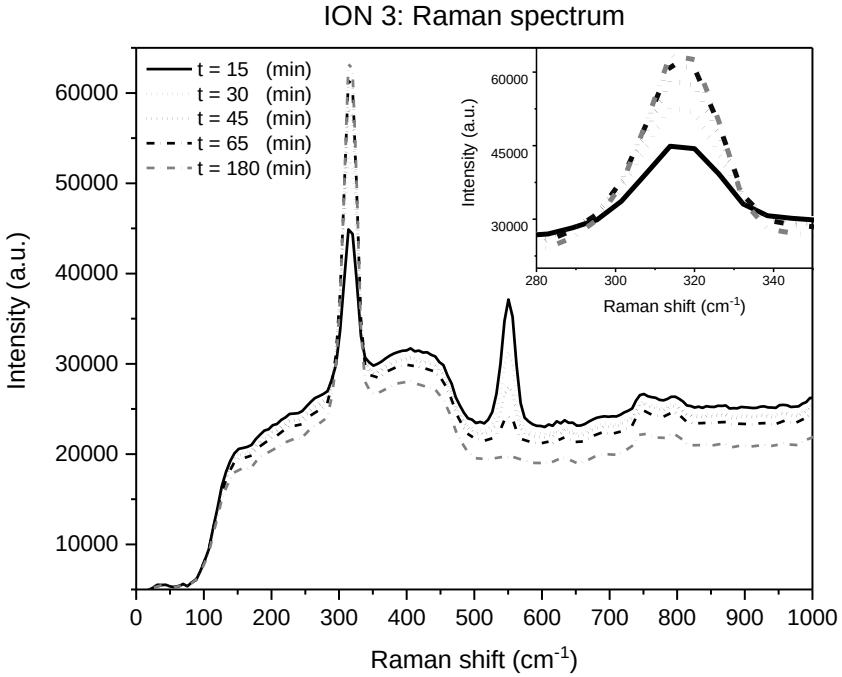

Figure 24: Raman spectra of the orthohydrogen conversion for ION 3. Illustrating the relative change of the peak intensities at a specific point in time: Orthohydrogen (right peak) and parahydrogen (left peak).

From a comparison of the background intensity between figure 23 and 24, some differences can be observed. Firstly, the relative intensity of the background in figure 24 is significantly larger compared to the background of figure 23. Secondly the background in figure 24 also appears to decrease in intensity during conversion, which is not observed in figure 23. These two observations can be related to the focal point positioning of the laser. For ION 9 the focal point of the laser beam was set to be inside the sample cell, while for ION 3 the focus was fixed at the same altitude but outside of the sample cell.

With the focus outside of the cell, the surrounding environment contributes to the background of the obtained Raman spectra which weakens the hydrogen signal. This results in the decreased resolution of the hydrogen peaks and increases the uncertainty of the baseline. When focus is placed inside the cell, possible interferences from the surroundings are reduced. This leads to a spectrum with higher resolution and smaller changes of the baseline. A similar observation was made in section (4.3), regarding the focal point positioning effect on the pure hydrogen signal. The loss of information, due to the increased background is shown to be of less significance in the early stages of conversion when the signal of ortho- and parahydrogen is stronger and therefore more easily distinguishable in the Raman spectra. The focal point effect becomes more apparent along the conversion process as the orthohydrogen peak becomes concealed by the background. This concealment complicates the integration of the orthohydrogen peak area, which in turn contributes to an increase of the relative error for the calculated ratio. The reduction of the relative background is an important feature for optimizing the relative error of the ortho-parahydrogen ratio.

The observed change of the ortho- and parahydrogen peaks with time shows that conversion of ortho- to parahydrogen transpires. During the experiment formation of bubbles in the liquid hydrogen could be observed by eye. These bubbles consist of hydrogen gas, formed from liquid hydrogen as a result of the heat emitted by the exothermic reaction of ortho- to parahydrogen formation. The conversion is shown as the growth of the parahydrogen peak while the orthohydrogen peak grows smaller with time until it becomes almost indistinguishable from the background. The first peak representing parahydrogen reaches its maximum intensity. The maximum intensity is shown for the parahydrogen peak by the curve representing 180 minutes of conversion, which suggest that the conversion process has reached the thermodynamic equilibrium of ortho- and parahydrogen.

The two experiments of ION 9 and ION 3 were recorded using different collection times. The time scale shows to only affect the relative intensity of the spectra with no significant improvement on the resolution of the improved spectra. The time for the starting curve of figure 24 is equal to 15 minutes of conversion. This is due to the measurement being initiated before the hydrogen inside the cell had transitioned from solid to liquid. The obtained Raman of solid hydrogen generates a scatter with much lower intensity compared to liquid hydrogen, which is a result to the different mobility of the hydrogen molecules in liquid and solid state. Since the kinetic study is focused on the conversion in liquid hydrogen the following data obtained from solid hydrogen is excluded from further study. The final observation from the figures 23 and 24 is that the relative relationship between the peaks is closer to 1:1 distribution of (ortho: parahydrogen) rather than the previously determined ratio of 2:1, obtained from the hydrogen signal, see section (4.3). This suggests that conversion of ortho- to parahydrogen already begins during the deposition of hydrogen gas into the sample cell, before the start of the measurements. Some of the solid hydrogen transitions into liquid hydrogen, when room temperature hydrogen gas is introduced into the cell. The melting was found to be a difficult issue to avoid due to the difficulties to control the precise amount of hydrogen added into the sample cell in each loading sequence.

4.4.1.2 Concentration profile and curve fitting

From the measured spectra of the Raman scattering, it is possible to define the ratio between the ortho- and parahydrogen concentrations as a function of time. The concentration is determined by integration of the ortho- and parahydrogen peak area. This is performed for each individual spectrum, acquired from the conducted experiment. The relative ratio of ortho- and parahydrogen is obtained as a function of conversion time. The complete procedure is presented in the experimental section, see section (3.3.8), regarding the processing of the raw Raman scattering data. The concentration profile of the experiments is shown in the figures below.

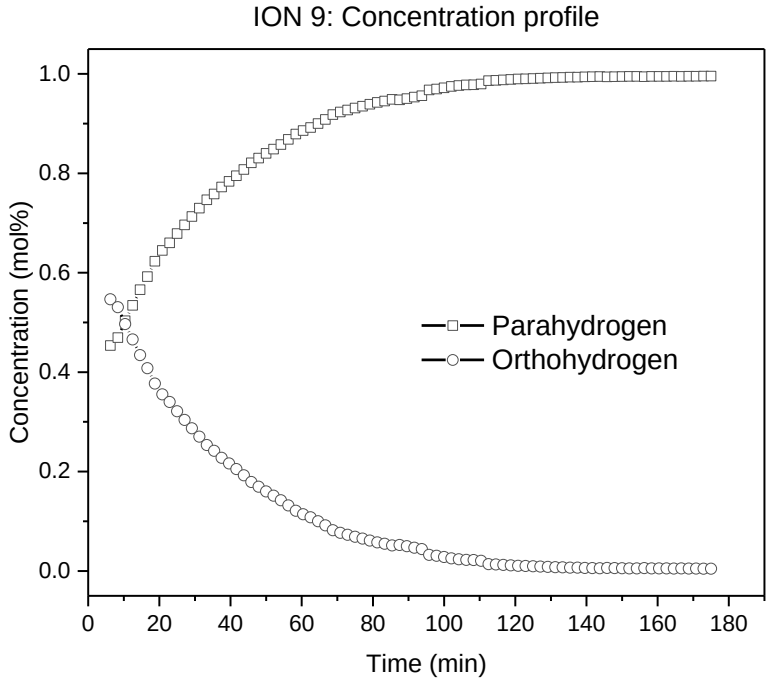

Figure 25: Concentration profiles of ortho- and parahydrogen for the experiment ION 9. The profiles are based on the obtained data from the catalytic conversion in liquid hydrogen.

Figure 25 shows the change of the ortho-and parahydrogen concentration as a function of the acquisition time, for experiment ION 9. The concentration profiles are created from the determined ratio of the hydrogen isomers, which has been determined from the acquired Raman spectra. The profiles describe the process of conversion and formation of the hydrogen isomers in the liquid state, where the parahydrogen profile is represented by the upper curve (boxes) and the lower curve (circles) represents the orthohydrogen profile.

The concentration profile of the experiment ION 3 is presented in figure 26.

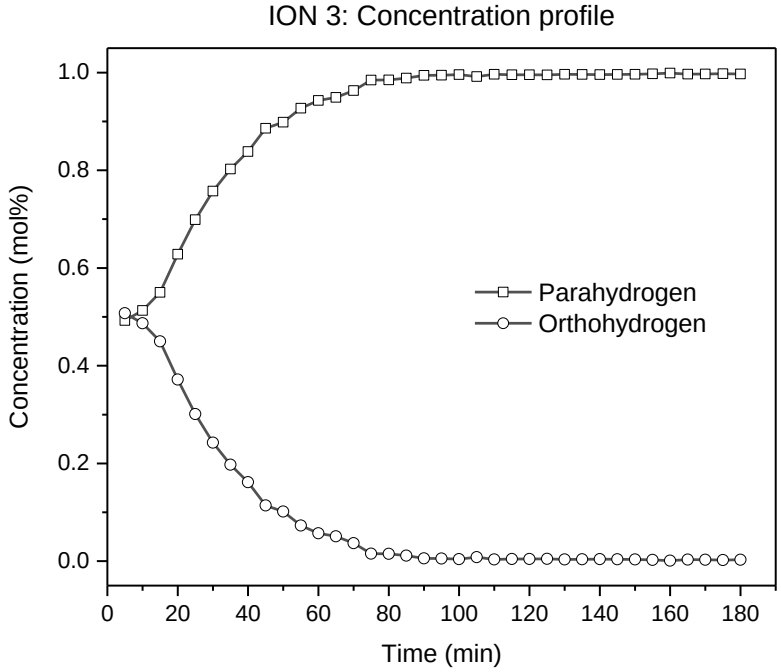

Figure 26: Concentration profiles of ortho- and parahydrogen for the experiment ION 3. The profiles are based on the obtained data from the catalytic conversion in liquid hydrogen.

A first observation from the figures 25 and 26, shows that the orthohydrogen profile of ION 3 (figure 26), becomes linear at 80 minutes of conversion, while the orthohydrogen curve of ION 9 seems to become linear after 110 minutes (figure 25). The linear segment of the concentration profile indicates that the hydrogen distribution inside the sample cell has reached the thermodynamic equilibrium, at the specific temperature of the experiment (16K). The equilibrium at 16K is around 99.8% parahydrogen [17].

From the comparison, it is obvious that the equilibrium is reached faster for the experiment ION 3 compared to ION 9. This is a result of the focal point, where the increased background of the Raman spectra for ION 3 leads to a higher uncertainty of the orthohydrogen peak. The increased uncertainty is a result of the peak being concealed by the background. This becomes more apparent at lower concentrations of orthohydrogen, which will result in the appearance that the equilibrium is reached at an earlier stage.

The initial and final ratio for the concentration profiles of ION 9 and ION 3 is presented in the table 13.

Table 13: Initial and final concentration of ortho- and parahydrogen for ION 9 and ION 3.

Sample	$H_{2_{INIT}}^{P}$ (mol%)	$H_{2_{INIT}}^{O}$ (mol %)	$H_{2_{END}}^{P}$ (mol %)	$H_{2_{END}}^{O}$ (mol %)
ION 9	45.4	54.6	99.6	0.4
ION 3	49.3	50.7	99.7	0.3

The final concentration shows that a parahydrogen content is above 99.5 mol%, is for both ION 9 and ION 3. As mentioned in the literature study (see section (2.1.3)) the parahydrogen concentration reaches an equilibrium value of 99.8% at 20 K. The obtained values agree with the equilibrium, when taking the uncertainty into consideration. The uncertainty to the signal is a result of the inherent error from the analysis equipment, external factors such as contribution from the sample cell and the analysis procedure of the obtained data.

4.4.1.3 Reaction rate and kinetic order

After analyzing the data acquired from the experiments fit attempts were made to determine the reaction rate and kinetic order of the catalytic conversion, using IONEX®. The kinetics and reaction rate was determined by plotting the natural logarithm of the concentration as a function of time. The natural logarithm of ION 9 and ION 3 is shown in the following figures.

A first order reaction depends linearly on one reactant concentration, in this case being the orthohydrogen concentration.

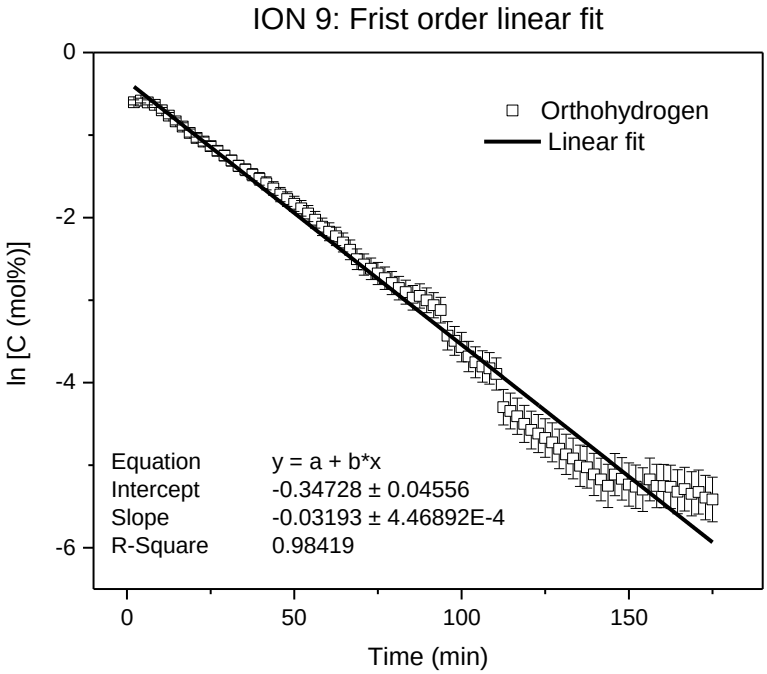

Figure 27: Natural logarithm of the orthohydrogen concentration as a function of acquisition time with a linear fit for the experiment ION 9. The error bars represent a 5% deviation of the concentration.

Figure 27 shows the natural logarithm of the orthohydrogen concentration as a function of time, for the experiment ION 9. One observation is that the concentration profile fits to a linear equation. The linear dependency indicates that the conversion of orthohydrogen is a first order reaction. In the last 30 minutes of the conversion, a change can be observed. The curve begins to follow a single value indicating that the reaction is completed.

At this point the driving force for the conversion of orthohydrogen approaches zero. This is a result of the hydrogen isomer distribution approaching the thermodynamic equilibrium at the temperature of the experiments (16K). This trend is more evident for the plot of the natural logarithm of ION 3 illustrated in figure 28 below.

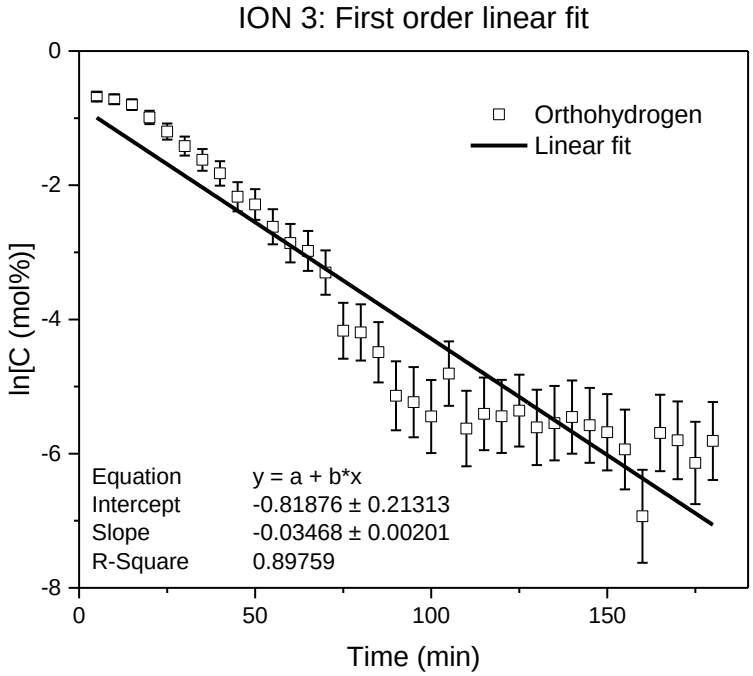

Figure 28: Natural logarithm of the orthohydrogen as a function of acquisition time with a linear fit for the experiment ION 3. The error bars represent a 10% deviation of the concentration.

The concentration profile for ION 3 (figure 28), is less linear than ION 9 (figure 27). The change-over point to a horizontal line can be observed at an earlier stage, after approximately 100 minutes of conversion.

The most significant difference between the two experiments is related to the focal point position. Its effects have been observed throughout this section. The position of the focal point affects the resolution and intensity of the obtained spectra. The out of focus configuration results in the background becoming overemphasized, leading to the increased uncertainty of the obtained data which results in the observed difference. To account for this increased uncertainty has the relative error bars for in figure 28 been increased to represent a deviation of the relative concentration by 10 percent

The reaction rate for the orthohydrogen conversion is determined from the natural logarithm of the orthohydrogen concentration. The rate of conversion is obtained by linear fitting of the concentration profile, in which the slope represents the rate of conversion. This rate is used as a fixed parameter for the fitting of an exponential equation based on the determined first order kinetics, to the concentration profiles. The orthohydrogen profile is fitted to a fist order kinetic exponential decay function, which describes the decrease in concentration. The parahydrogen concentration is fitted to an equivalent exponential growth function. The results of the fit of the two first order kinetic exponential equations onto the concentration profiles is shown in the figures 29 and 30.

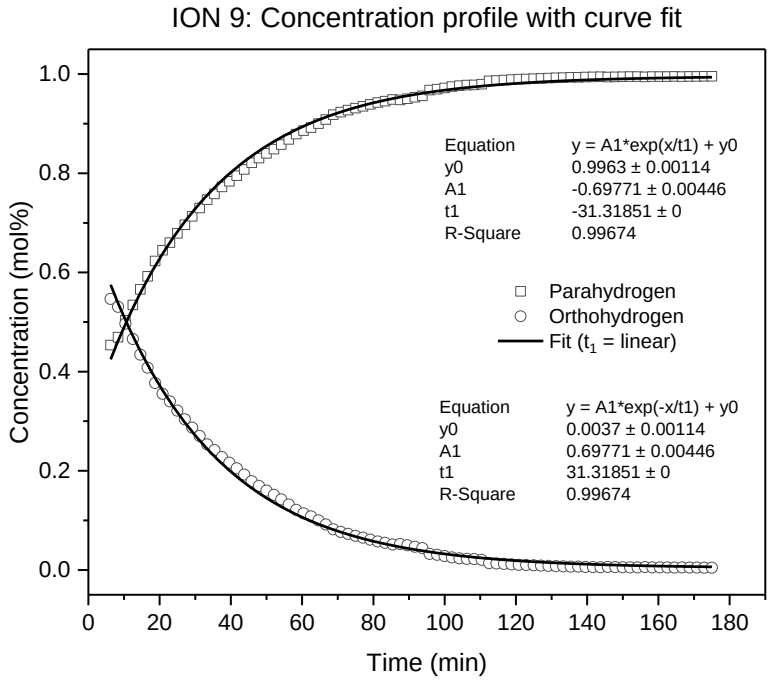

Figure 29: Concentration profile of ortho- and parahydrogen for experiment ION 9. With the fitted exponential decay (ortho) and exponential growth (para) functions based on first order kinetics.

The solid black lines represent the fit of the exponential functions to the ortho- and parahydrogen data points of ION 9, displayed as circles and squares, respectively. The result of the fits is presented in the text boxes, above and below the legend in the figure. The upper box is the fit result of the parahydrogen data and the lower box the fit of the orthohydrogen data.

The two equations used for fitting are given by the following relationship:

$$y^{Isomer} = A_1 * e^{\left(\pm x / t_1\right)} + y_0^{Isomer} \quad \begin{matrix} +x : growth, H_2^P \\ -x : decrease, H_2^O \end{matrix}$$

The equation provides a percentage of the respective hydrogen isomer (y^{Isomer}) at any given time (x) after the start of the conversion. The time of conversion (x) has a positive sign while it is describing the change of the parahydrogen ratio and a negative sign, when representing the orthohydrogen ratio. The variable (y_0) represents the offset and (A_1) is the amplitude of the equation, where the initial concentration is the sum of these two terms.

From the previous fit an equation of the rate constant is determined. The time factor (t_1) in the first order equation, is the inverse of the rate constant (τ) as its inverse of the time factor. The following relationship is illustrated below:

$$\tau = \frac{1}{t_1}$$

From the time factor can the half-life ($t_{\frac{1}{2}}$) of the reaction be determined. The half-life represents the time required for the concentration to be halved with respect to the initial concentration. For a first order reaction the half-life is related to the rate constant by the following relationship:

$$t_{1/2} = \ln(2) * t_1$$

A complete table of the results obtained from the fitting related to the experiments using IONEX® as catalyst, can be found in the appendix section, see Appendix 3.

The fit for ION 3 is shown in figure 30.

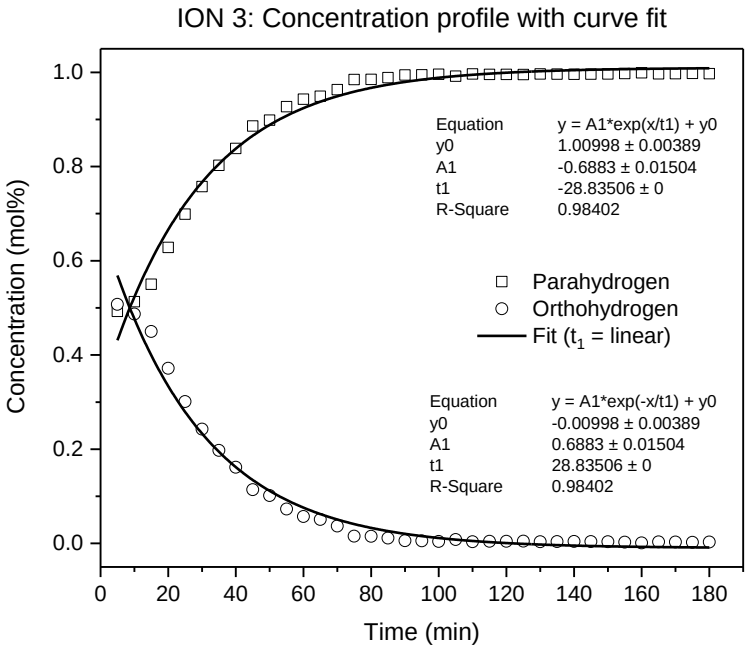

Figure 30: Concentration profile of ortho- and parahydrogen for experiment ION 3. With fitted equations of a first order exponential decay (ortho) and a first order exponential growth (para).

The of fit of the concentration function of ION 3 (figure 30) shows to be not as good as the fitting of ION 9 (figure 29). However, the quality of fit is still at an acceptable level ($R^2 = 0.984$) and confirms the argument that the conversion follows a first order exponential function. This trend in observed throughout the experiments with IONEX® and comparisons are made between ION 3 and ION 9. The comparison shows how the fitting is affected as a result of the increased uncertainty between the concentration profile of ortho- and parahydrogen for ION 9 and ION 3. The time factor along with the determined rate constant, obtained from the linear fit of the natural logarithm and the calculated half-life is presented in table 14.

Table 14: Time factors, rate constants and half-life of the conversion process of experiment ION 9 and ION 3.

	Time factor $[t_1]$ (min)	Rate constant $[\tau]$ (min^{-1})	Half-life $[t_{\frac{1}{2}}]$ (min)
ION 9	31.32	0.032	21.71
ION 3	28.84	0.035	19.99

A comparison of the values given in table 13 indicates that the time factor and half-life for ION 3 is lower compared to ION 9, which is a result of the larger rate constant. The observed difference is below 10 percent and is an effect of the increased background interfering with the hydrogen signal. The uncertainty of the orthohydrogen peak area increases, at later stages of conversion, which has an effect on the determined rate. The other possibilities that the different rates of ION 3 and ION 9 can be regarded as a statistical deviation as well as due to the small differences in the catalyst and hydrogen amount of the two experiments

Additional information obtained from the curve fitting is the amplitude (A_1) and the offset (y_0), which provides information regarding the initial ratio of the hydrogen isomers when no conversion has transpired. The result in the obtained values from the curve fitting along with the initial distribution of ortho-and parahydrogen for ION 3 and ION 9 presented in the table 15.

Table 15: Amplitude and offset determined from the fitting of the exponential decay and growth functions for ION 9 and ION 3, along with the extrapolated initial concentration at (x = 0).

	Isomer	Amplitude [A_1]	Offset [y_0]	Extrapolated ratio [y_E] at time (x = 0)
ION 9	Ortho	0.698	0.004	0.704
ION 9	Para	-0.698	0.996	0.296
ION 3	Ortho	0.688	-0.009	0.679
ION 3	Para	-0.688	1.009	0.321

The extrapolated ratio (y_E) obtained for experiment ION 9 is observed to be closer to the ratio of normal hydrogen. Suggesting that the contribution of the response function is compensated by the fitted exponential function. The extrapolated ratio of ION 9 can be considered to agree with the normal hydrogen distribution. The small deviation still remaining between the extrapolated and normal hydrogen ratio is likely a result of the orthohydrogen conversion that transpires during the loading procedure of hydrogen into the sample cell. The probability that the orthohydrogen conversion is a first order process is strengthened by the degree of fit of the first order exponential equation to the concentration profile of orthohydrogen. Along with the linear shape of the profile in the plot of the natural logarithm as a function of time.

The implementation of a first order equation for the formation of parahydrogen appears to coincide well from an observation of the mathematical curve and the concentration profile, illustrated in figures 29 and 30. The fit of the exponential curve shows that the effect of the response function appears to be less significant at higher degrees of conversion. The ratio obtained at the end of conversion agree well with the equilibrium distribution of the hydrogen isomers at 16K. This can be observed in figure 29 and 30, where the fit of the exponential function becomes better with conversion time.

4.4.1.3.1 Preferential adsorption

The information obtained from the Raman spectroscopy is related to the irradiated volume inside the sample cell. Preferential adsorption is proposed as a probable cause to the observed deviation between the observed and true hydrogen ratio is related to the interaction between the hydrogen isomers and catalyst surface.

Preferential adsorption describes a reaction, which takes place during the conversion process. The bond strength of orthohydrogen onto the catalyst surface is greater compared to parahydrogen. This results in orthohydrogen being more favorably adsorbed on the catalyst surface compared to parahydrogen. The increased bond strength is mentioned to be a result of the polarizability, due to the elevated rotational state of the orthohydrogen molecule [21].

This means that the observed concentration of the hydrogen isomers inside the bulk liquid is pushed towards parahydrogen, since the orthohydrogen is preferentially adsorbed on the catalyst. This causes a concentration gradient between the liquid bulk and the catalyst surface, which in turn gives the impression of a more rapid formation of parahydrogen in the liquid. When the orthohydrogen, is in fact only concealed by being adsorbed on the catalyst. During the conversion process the amount of orthohydrogen will decrease which will eventually lead to the second process of the preferential adsorption.

The second process describes the moment in time when parahydrogen is the majority of the liquid bulk as well as on the catalyst surface. The continued conversion depends on the diffusion of single orthohydrogen molecules from the liquid bulk to the catalyst surface. The observed conversion of orthohydrogen is more accurately observed by the Raman spectroscopy.

The preferential adsorption is more prominent in IONEX® compared to OXISORB® based on the relative bond strength of iron ions being stronger towards hydrogen compared to chromium ions [24] An illustration of the observed change in the liquid bulk is shown in figure 31.

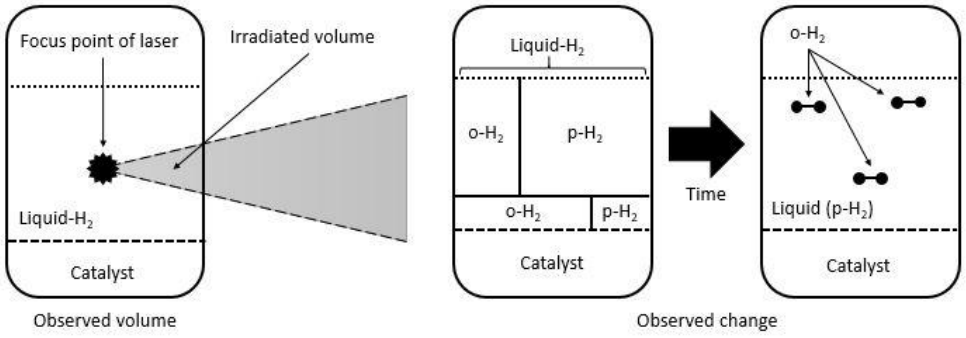

Figure 31: Illustration of the observed volume in the sample cell (left). Along with the appearance of the observed hydrogen ratio during the conversion process. Illustrating the preferential adsorption (middle) and the diffusion of orthohydrogen (right).)

4.4.1.4 Space velocity and extrapolations to the ESS hydrogen loop

The space velocity is calculated from the previously determined rate and based on the conditions of the experiments. The space velocity is a measure of the amount of hydrogen which is converted as a function of time and amount of catalyst and is given by the following relationship:

$$R_{Sp} = \frac{n_{H_2} * \tau}{m_{Cat}}$$

The term (R_{Sp}) represents the space velocity which is the specific conversion rate of the reaction when a catalyst is used. The term (R_{Sp}) has the unit (mol H_2/min/g catalyst), where the time is related to the rate of conversion (τ) determined from the linear fitting of the Rama data and the amount of hydrogen and catalyst is presented in mol and gram respectively. Additional equations used in this section is presented in the appendix, see Appendix 5.

The calculated space velocities for the experiments are presented in table 16.

Table 16: Calculated space velocity for the IONEX® experiments as well as a calculated mean space velocity, along with the amount of hydrogen, determined rate of conversion and amount of IONEX® used.

	Space velocity [R_{Sp}] (mol H_2/min/g IONEX®)	Hydrogen amount (mol)	Rate of conversion (min^{-1})	Catalyst amount (g)
ION 1	0.0337	0.0332	0.0213	0.021
ION 2	0.0455	0.0330	0.0289	0.021
ION 3	0.0558	0.0338	0.0347	0.021
ION 4	0.0388	0.0335	0.0243	0.021
ION 5	0.0479	0.0333	0.0302	0.021
ION 6	0.0556	0.0330	0.0351	0.0208
ION 7	0.0620	0.0335	0.0385	0.0208
ION 8	0.0637	0.0335	0.0395	0.0208
ION 9	0.0515	0.0336	0.0319	0.0208
Mean [R_{Sp}]		0.0505		

Table 16 shows the space velocities obtained from all experiments using IONEX®. The space velocities are in a range between 0.034 and 0.064. The range is a combined result of the inherent error form measuring the hydrogen signal, difference in catalyst amount and the obtained rate in which limitations of the spectrometer might contribute to the divergence between single measurements. A mean value of the space velocities is determined to (R_{Sp} = 0.0505). The mean value of the space velocities is compared to the presented space velocity from the manufacturer of IONEX®, which is reported as 1200 ml H_2/min/ml IONEX® which is equal to 0.34 mol H_2/min/g IONEX®. The experimental conditions used by the manufacturer was 1.4 bar and 77K under continuous flow.

The difference between the space velocity determined by the experiments in this thesis and the reported velocity from the manufacturer differs by a factor of 6.7. The differences are a result of the differences in the experimental conditions of this report and those used by the manufacturer. The greatest difference is that the experiments in this thesis is conducted in a static setup with no possibility of creating a continuous flow of hydrogen over the catalyst, as well as lower mobility of liquid hydrogen compared to gaseous hydrogen. Allowing a flow over the catalyst will increase the conversion rate, due to the increased mobility of reactants and products over the catalyst surface.

The difference in temperature and pressure will also contribute to the difference between the two space velocities but is likely a minor factor in comparison to the condition of a static setup. From the specific space velocity of the catalyst follows the calculations regarding the efficiency, based on the conditions for the ESS hydrogen loop in which the catalyst will be used.

The conditions for the hydrogen loop is presented in the table 17.

Table 17: Conditions of the future ESS hydrogen loop based on the use of IONEX® as catalyst material.

Hydrogen amount (kg)	Catalyst amount (kg)	Bypass flow (g/s)	Moderator flow (g/s)	Back conversion rate (mol H_2^P/min)	Operating temperature (K)
24	37.5	50	1000	10	20

The total hydrogen amount is determined to 24 kg which is equivalent to 12 kmol of hydrogen. The hydrogen will initially be composed of normal hydrogen (75:25), ortho: parahydrogen. It is converted by the catalyst during the cooling of the hydrogen to the operation temperature of the hydrogen loop (20K). In equilibrium at 20K, exists 99.8 percent of the hydrogen isomers as parahydrogen. This ratio of 99.8 mol% has been proven to be achievable from the conducted experiments. From the mean specific rate of conversion for the experiments, presented in table 16 follows the rate of conversion per minute, when the total catalyst amount is taken into account. The predetermined amount of catalyst is set to 37.5 kg, which accounts for a safety factor of 1.5. The catalytic rate (R_{Tot}), which represents the rate of conversion for orthohydrogen based on the weight of the catalyst bulk (37.5kg). The catalytic rate for the reaction using IONEX® catalyst is determined to 1894 mol H_2/min in this work. The time required to convert the 12 kmol of normal hydrogen to the equilibrium ratio at 20K is achieved in 4.75 minutes based on the obtained rate of conversion for the 37.5 kg catalyst bulk. The following results has been determined using the formulas listed in the appendix (appendix 5).

The parahydrogen is used as moderating material for the production of cold and thermal neutrons. The hydrogen will be circulated in the moderation loop with a flow of 1000 g/s. This means that the same hydrogen molecule will enter the moderator every 24 seconds. From the circulating hydrogen, a small bypass of the flow will be passed over the catalyst. The catalyst will experience a hydrogen flow of maximum 50 g/s. The full hydrogen storage of 24 kg is circulated through the catalyst every 8 minutes or 7.5 times per hour. Each hydrogen molecule passes through the catalyst 20 times less frequently compared to the moderator. The catalyst need to accommodate for the back conversion of parahydrogen which occurs when parahydrogen is used as a moderating material. The rate of the back conversion accounted by a safety factor of 3, which results in the estimated back conversion rate of 10 mol para-H_2/min. This is well below the calculated catalytic rate of 1893 mol H_2/min for the bypass flow, based on a catalyst amount of 37.5 kg IONEX®.

4.4.2 OXISORB®

The catalytic conversion of orthohydrogen is investigated using the chromium(II) oxide doped silica, OXISORB®. The details regarding the hydrogen and catalyst amount along with the time for full conversion is presented in table 18.

Table 18: Initial parameters regarding the hydrogen amount, catalyst amount and acquisition time for the hydrogen conversion experiments using OXISORB® as a catalyst.

	Amount of hydrogen (Bar* @ RT, 150 ml)	Hydrogen amount (mmol)	Catalyst amount (mg)	Time [Full time]/[liquid state] (min)
OXI 1	5.53 ±0.1	33.46	10 ±5	180/169
OXI 2	5.61 ±0.1	33.95	34.9 ±0.1	470/465
OXI 3	5.57 ±0.1	33.70	71.8 ±0.1	300/294
OXI 4	5.58 ±0.1	33.76	71.8 ±0.1	300/278
OXI 5	5.52 ±0.1	33.40	142.8±0.1	150/136
OXI 6	5.51 ±0.1	33.34	142.8±0.1	180/167

* ± 0.1 bar

Two things can be observed from table 18, which deviate from the experiments in the IONEX® section. The first thing is that the catalyst amount has been changed multiple times. The second observation is that the full acquisition time for the conversion, using OXSORB® is much greater, in comparison with the acquisition time for the conversion experiments using IONEX®, see table 12 in section (4.4.1). Conversion times similar to the ones obtained for IONEX® are obtained for the experiments OXI 5 and OXI 6 where the catalyst amount has been increased by a factor 7.

The design of the initial experiment using OXISORB® was based on the relative surface area of the catalyst. The OXISORB® catalyst has a surface area of 560 m^2/g in comparison to the IONEX® catalyst, with a surface area of 216 m^2/g. Hence the initial catalyst amount of OXISORB® was halved in comparison to the previous experiments involving IONEX®, to 10 mg of catalyst.

This was conducted with the desire to obtain a conversion, which is progressing at a suitable pace while minimizing the conversion of orthohydrogen during loading. The resulting conversion process was observed to be much slower in comparison to the experiments of the IONEX® and the conversion of OXI 1 was stopped after 180 minutes of conversion. During that time, the ratio of orthohydrogen had changed from 63 to approximately 51 percent.

In the next experiment the catalyst amount was increased roughly by a factor of 1.75, in which full conversion was achieved in 470 minutes. The catalyst amount was thereafter doubled in two intervals for the following experiments and a conversion time, around 180 minutes was achieved with 142.8 mg of OXISORB®. An increase of the catalyst amount by a factor seven in comparison to the catalysts amount used for IONEX®.

The relative change in acquisition time as a function of the increased catalyst amount is presented in the table 19.

Table 19: Comparison of relative effect of the amount of catalyst on the conversion time. the experiment OXI 2 is chosen as the reference.

	Increase of catalyst (mg OXI (i)/mg OXI 2)	Reduced time of conversion $[1 - (t_{eq}(i)/t_{eq}(2)]$
OXI 1	0.287*	0.617*
OXI 2	1	0
OXI 3	2.057	0.362
OXI 4	2.057	0.362
OXI 5	4.092	0.681
OXI 6	4.092	0.617

* Measurement stopped before equilibrium was reached.

From table 19 it is possible to observe that by doubling the catalyst amount the conversion time is reduced by approximately 36%. This indicates that the reduction in conversion time does not linearly dependent on the catalyst amount, which is an effect due to the large surface area of OXISORB®. Catalytic conversions are in general independent of stoichiometry, based on the requirement that the catalyst has enough surface area to facilitate the conversion. This means that the conversion is not dependent on the amount of reactants or products that is either adsorbed and desorbed from the catalyst, which results in the observed difference between the increased catalyst amount and reduced time of conversion (table 19).

The deviation in acquisition time between OXI 5 and OXI 6, is a result of hydrogen freezing in the gas line during the loading procedure of experiment OXI 5. The system had to be brought up in temperature, in order to melt the solidified hydrogen trapped in the gas line and thereafter retuned back down to the loading temperature continue the loading of hydrogen. This procedure of bringing the sample cell up in temperature, causes some conversion to occur before the experiment is initiated. This results in an initial lower ratio of orthohydrogen and thus a faster conversion.

4.4.2.1 Raman spectrum

A Raman spectrum, obtained from the catalytic conversion of experiment OXI 6 is presented in figure 32.

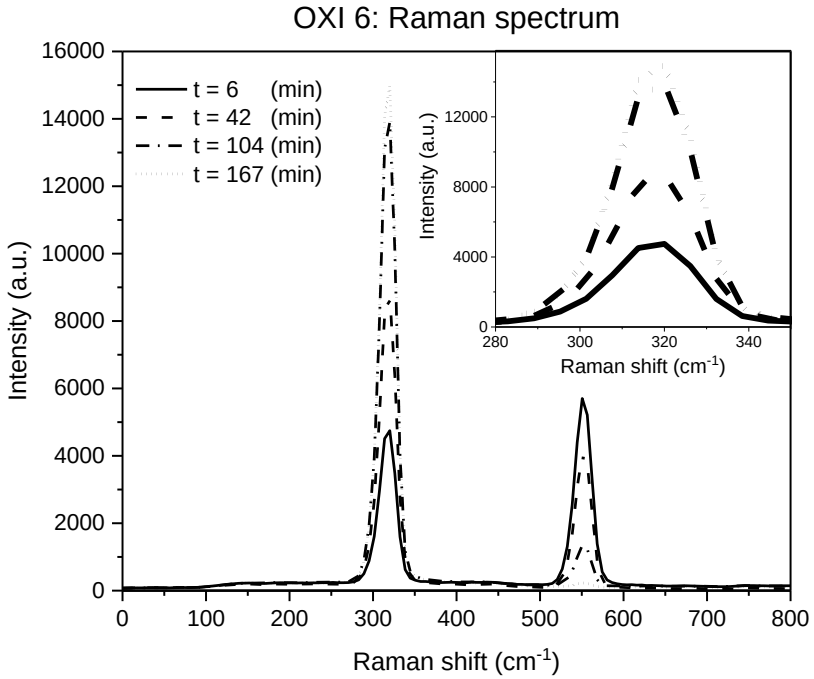

Figure 32: Raman spectrum illustrating the conversion process of ortho- to parahydrogen for experiment OXI 6. It shows the relative change of the peaks at a certain acquisition time. Orthohydrogen (right peak) and parahydrogen (left peak).

Only the two first order rotational levels are observable in the obtained spectra, shown in figure 32. The spectra show that the parahydrogen peak (left), increases while the orthohydrogen peak (right) decreases.

This confirms that the OXISORB® catalyst is able to facilitate conversion of orthohydrogen. The final curve indicating 167 minutes of conversion is indifferent to the baseline, which is an indication that the conversion has reached the equilibrium at the operating temperature of 16K. The equilibrium distribution is referred to in the theory section to be at 0.2% orthohydrogen ad 99.8% parahydrogen at 20K. The conversion of orthohydrogen is presented as a concentration profile, in which the curve shows the change in concentration as a function of time.

4.4.2.2 Concentration profile and curve fitting

The orthohydrogen concentration profiles for all experiments using OXIOSRB is presented in the figure 33.

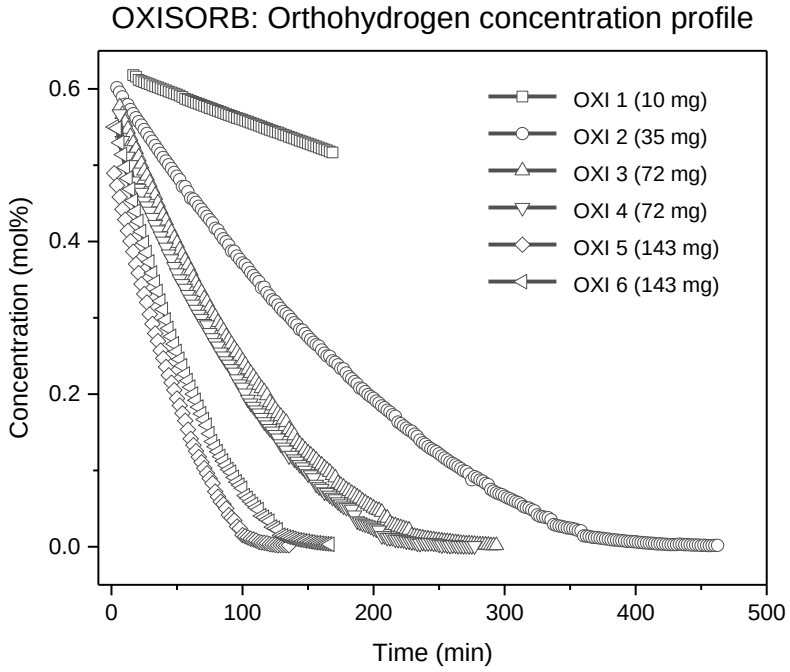

Figure 33: Comparison of the orthohydrogen concentration profiles.

In figure 33 are all obtained concentration profiles compared to one another. An observation from the curves is that the time required to reach the equilibrium decreases with increased amount of catalyst. The increased rate of the conversion seen in figure 33 with the addition of more catalyst is a result of the presence of more magnetic sites which facilitates the spin flip of the orthohydrogen molecules. Another observation is regarding the curves representing OXI 5 and OXI 6, where conversion times similar to the IONEX® experiments are obtained. The general difference is that the catalyst amount is a factor 7 higher compared to the catalyst amount of the experiments involving IONEX®.

This result suggests that the conversion rate using OXISORB® is much slower compared to the conversion rate using IONEX®, when equal amounts of catalyst are used. This can be related to the general aspects of the catalyst. The OXISORB® catalyst despite its larger surface area only contains 2-3% of magnetic impurities which can facilitate the spin flip. IONEX® on the other hand is smaller in surface area but is in its entirely composed of iron oxide. This leads to that more hydrogen can be adsorbed by the OXISORB® catalyst but less of the adsorbed hydrogen is converted due to the lower number of magnetic sites.

Another possibility is that the catalyst is contaminated during the handling and loading procedure. The glovebox is assumed to be in inert atmosphere. However, since there is no oxygen meter present in the glovebox the presence of oxygen in the glove box cannot be measured. A weakness with OXISORB® is the sensitivity towards oxygen and moisture, where a contaminated catalyst would display a lower catalytic strength. The initial and final concentrations of ortho and parahydrogen is presented in the table 20.

Table 20: Initial and final concentration of ortho- and parahydrogen for the experiments using OXISORB®.

	$H^P_{2_{INIT}}$ (mol%)	$H^O_{2_{INIT}}$ (mol%)	$H^P_{2_{END}}$ (mol%)	$H^O_{2_{END}}$ (mol%)
OXI 1	38.2	61.8	48.3	51.7
OXI 2	39.8	60.2	99.8	0.2
OXI 3	42.3	57.7	99.8	0.2
OXI 4	43.3	56.7	99.9	0.1
OXI 5	51.0	49.0	99.8	0.2
OXI 6	45.0	55.0	99.7	0.3

The results shown in table 20 confirms the earlier assumptions that equilibrium is reached. The obtained values correspond well with the equilibrium concentration of hydrogen at 20K (0.2: 99.8 mol%) ortho: parahydrogen. This validates OXISORB® as a potential catalyst to be used in the future ESS hydrogen loop. The experiment labeled OXI 1 was stopped after three hours of conversion, in which the parahydrogen amount had only reached 48 %. Due to the slow conversion the decision was made to increase the catalyst amount. The catalyst amount was increased three times before similar conversion times to the IONEX® experiments were obtained. The amount of OXISORB® used in the experiments are resented in table 18. The initial concentration observed for the earlier experiments using OXISORB®, agrees well with the obtained ratio from the characterization of the hydrogen signal. The initial ratio was determined to be near a 2:1 relationship for ortho: parahydrogen. This could be a result of a more careful deposition of hydrogen, where less hydrogen becomes converted during the loading process. However, a more likely reason is the lower catalyst amount which results in a slower conversion process.

4.4.2.3 Reaction rate and kinetic order

The kinetic order of the catalytic conversion using OXISORB®, along with the rate of conversion are determined by the same procedure used for IONEX®. The natural logarithms of the orthohydrogen concentration is compared to one another in figure 34.

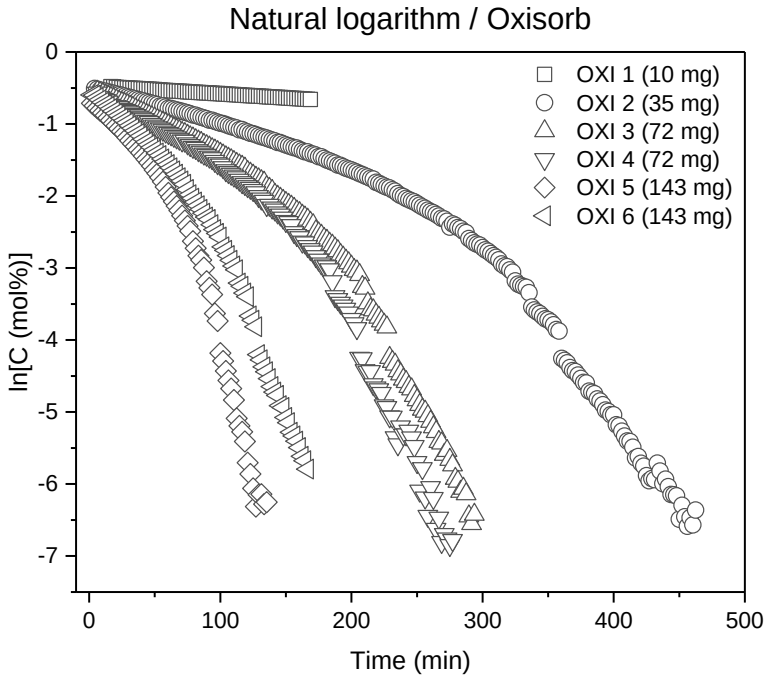

Figure 34: Comparison of the natural logarithm of the orthohydrogen concentration as a function of conversion time for the experiments with OXISORB®.

From the figure, it is possible to observe a difference in the general shape of the natural logarithm, which deviates from the linear appearance observed for IONEX®.

The shape of the profiles in figure 34, displays two linear segments. This suggests that the conversion is dependent on two separate first order functions. The two segments seem to exhibit both independency as well as codependency on one another. The catalyst amount, appears to have a significant effect on the profiles. The increased amount of catalyst appears to make the incline of the linear segments more similar to one another. This can be observed by the smoother transition between the linear segments of the profiles in figure 34. This suggests that the difference in rate of conversion between the two segments decreases with an increased amount of catalyst.

The investigation is conducted for the experiment OXI 6. The linear segments are defined and fitted with linear functions, which is illustrated in figure 35.

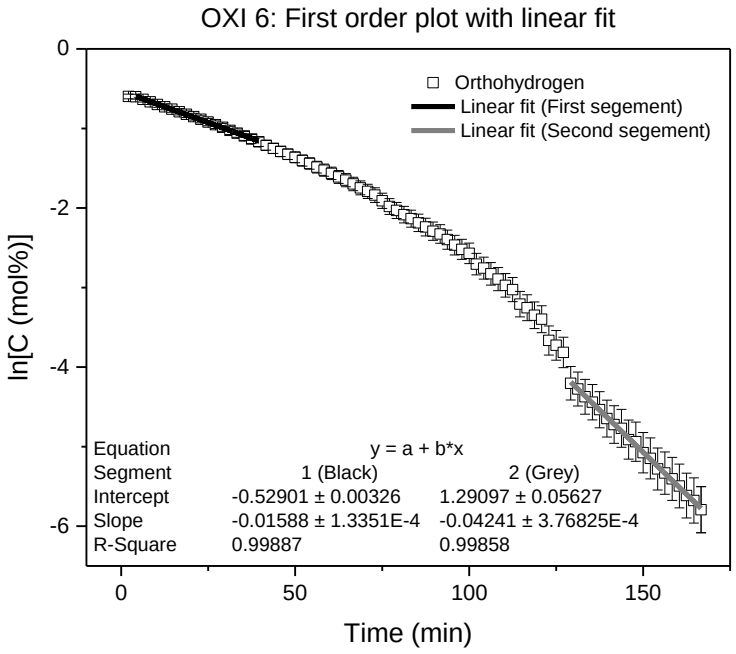

Figure 35: Natural logarithm of the orthohydrogen concentration as a function of acquisition time with two linear fittings for each linear segment in experiment OXI 6. Attached error bars represents 5% of the concentration.

Figure 35 shows the fit of the two linear segments. The first segment transitions from a linear function with increased conversion time. The transition to the second linear segment is observed after an apparent drop in the profile around 130 minutes of conversion. These linear segments are determined by comparing the resulting degree of fit, from the exponential functions to the normal orthohydrogen curve. The following linear segments, shown in figure 35, had the best fit to the orthohydrogen profile.

The drop is present for all experiments involving OXISORB®, see figure 34. This drop is confirmed to not be a result of the data treatment, background subtraction or peak integration of the obtained data. The reason for this drop is not determined but suggest a reaction in the conversion process which significantly increases the rate of conversion. Suggestions on potential causes to this drop, is related to preferential adsorption or that the catalyst has been poisoned and becomes activated due to becoming regenerated during the conversion process. The theory regarding the catalyst becoming activated, is based on the assumption that the catalyst might have been contaminated during the loading of the catalyst, where the regeneration of the contaminated catalyst is represented by transition of the linear function.

Preferential adsorption results in the appearance of an accelerated conversion and is due to the stronger bond between a orthohydrogen molecule and the catalyst surface, compared to a parahydrogen molecule. At a certain point in time, most of the orthohydrogen will have been adsorbed on the catalyst surface giving the impression of a faster ortho- to parahydrogen conversion.

The kinetic order of the catalytic conversion for OXI 6 is determined to be assembled by two first order functions. The kinetics for the catalytic conversion has been tried to fitted both zero and second order which did not work. Due to the resulting fit of the orthohydrogen profile, deviating further form a linear expression. Since no expression can be determined for the entire concentration profile, regarding the rate of conversion. The following conversion rates for the experiments using OXISORB® as a catalyst, will be determined from the two linear segments obtained from the natural logarithm (figure 35). The two segments represent the start –and endpoint of the profile generated form the orthohydrogen data points.

The following slopes of the linear fitting is presented in the table 21.

Table 21: Determined rates of the two linear segments (1 & 2) for the OXISORB® experiments.

	Rate segment 1 [τ] (min^{-1})	Rate segment 2 [τ] (min^{-1})	Factor (segment 2/segment 1)
OXI 1	0.00114	*	
OXI 2	0.00529	0.0233	4.406
OXI 3	0.00942	0.0349	3.705
OXI 4	0,00993	0.0383	3.857
OXI 5	0.0181	0.0662	3.657
OXI 6	0.0159	0.0423	2.660

*: No secondary segment could be observed.

The following table shows the determined slopes from the linear fitting of the natural logarithm, based on the obtained curves presented in figure 34. The linear fit of the first segment shows small differences in the value of the slope, with varying number of points of the linear segment. However, to be consistent when defining the first linear segment for the OXISORB® experiments a requirement was set at an R^2 value above 0.995. The fit of the second segment was set to begin at the drop of the natural logarithm curve. This is a phenomenon which is observed in all of the curves of the natural logarithm, for the experiments involving OXISORB® as a catalyst.

The experiment OXI 1 has only one linear fit because the experiment was stopped before full conversion. A general observation is that the conversion rates increases significantly for segment 2 compared to segment 1, which is given by the factor between the two segments. This factor shows that the phenomena causing the observed drop has a tremendous effect on the conversion rate. The origin of this drop whether it is due to an experimental error or that the kinetics for OXISORB is not of a first order, will become an important feature for further study. If the drop is due to contamination of the catalysts, this can be solved by a change in loading procedure and improving the environment of the glovebox. To determine if the kinetics is of a first order or not will require further study on the catalytic conversion. This will be left out of this thesis due to the limited time of the project.

4.4.2.3.1 Empirical modeling of the orthohydrogen profile

The two linear segments appear to exhibit a codependency on one another. Based on the assumption that the catalytic conversion is described by two first order functions. An empirical modeling of the conversion profile was made to illustrate a possible expression of this codependency. From the linear fitting two individual first order exponential functions can be created. Describing the change of orthohydrogen based on the obtained rates. These two exponential functions dare presented together with the normal orthohydrogen curve, in figure 36.

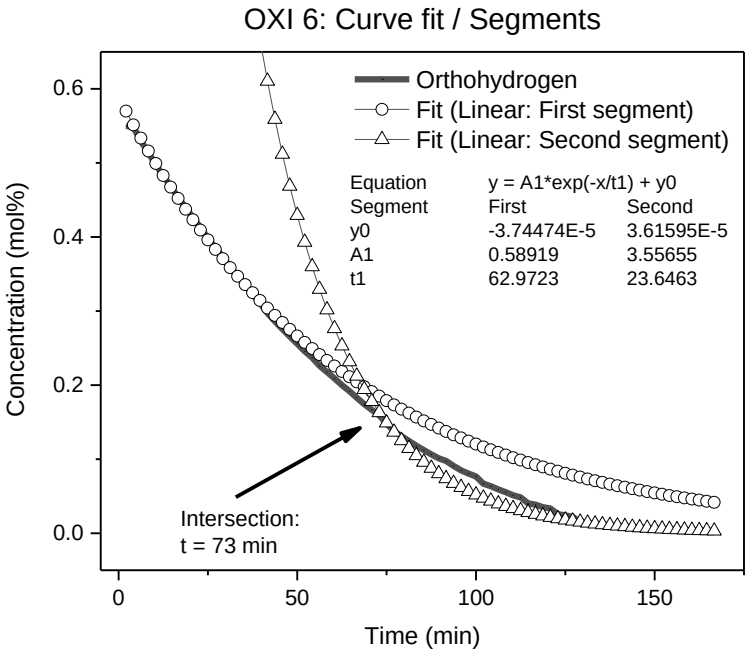

Figure 36: Illustration of the fit for the two exponential decay functions based on the time factors derived from the linear fitting of the natural logarithm. The two functions intersect at t = 73 min.

The two exponential equations, shown in figure 35 results in the exponential curves, which seems to fit well to the respective region of each segment in figure 36. The functions start to deviate from the orthohydrogen curve in between the two linear segments, to become completely unrepresentative to the curve in the region of the opposite linear segment. Based on the assumption that the two functions are codependent on one another in-between the two linear regions. This implies that there is a relationship between the two segments which describes the two exponential functions dependency on one another. It is also possible to observe that the curve of the second segment intersects the orthohydrogen curve at 73 minutes. This results in that the two segments will affect the combined function to different degrees based on which side of the intersection the combined function represents. A conversion times before the intersection (73 minutes) segment 1 will be more significant, while segment 2 will be more important to the combined function at conversion times above 73 minutes

The middle segment will be described by two combined functions where the assumption is made, that the second segment is weak in the first combined function and stronger in the second combined function and vice versa for the first segment. The following combined functions are presented below:

$$CF_1 = Seg_1 * \left(1 - \left(\frac{0.3580}{\left(16 * \left(\frac{(25 * 5)}{60}\right)\right)}\right) * t\right) + Seg_2 * \left(0 + \left(\frac{0.041}{\left(16 * \left(\frac{(25 * 5)}{60}\right)\right)}\right) * t\right)$$

$$CF_2 = Seg_1 * \left(1 - \left(\frac{0.3660}{\left(26 * \left(\frac{(25 * 5)}{60}\right)\right)}\right) * t\right) + Seg_2 * \left(0 + \left(\frac{0.2870}{\left(26 * \left(\frac{(25 * 5)}{60}\right)\right)}\right) * t\right)$$

The two combined functions are based on (Seg_1), which represents the exponential decay function based on the linear fit of segment 1 and (Seg_2) representing the exponential function based on segment 2. Each segment is weighted by an arbitrary factor. The weight is determined from manual fitting and the weight is normalized by the number of data points of each region. This is shown in the inner brackets of the combined functions. The scaling of the weighted factor is performed as function of conversion time (t).

The relative fit of the combined functions to the orthohydrogen curve is shown in figure 37.

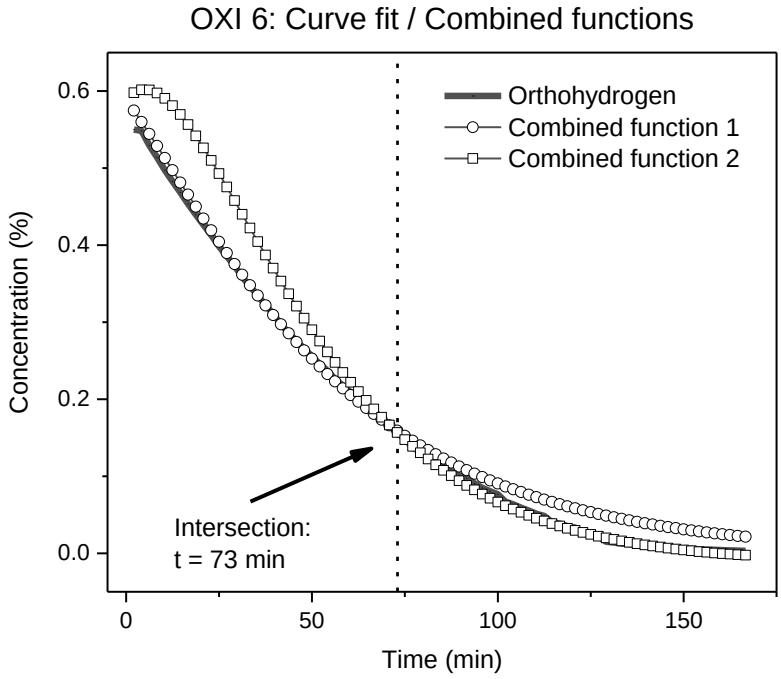

Figure 37: The fit of the resulting combined functions based on the scaled contribution of the two exponential decay functions of segment 1 & 2.

In figure 37 it is possible to observe that the equations of the combined functions exhibit a good fit to their respective half of the region with the intersection at 73 minutes.

The combined function of the first segment (CF_1) is illustrated by the line with circles, in figure 37 and describes the region before the intersection at 73 minutes of conversion. The combined function of segment 2 (CF_2) represented by the line with squares, describes the region after 73 minutes. The accelerating process becomes more and more significant with time and the accelerated conversion is believed to be due to the preferential adsorption of orthohydrogen onto the catalyst or potential regeneration of a contaminated catalyst.

The following combined functions along with the exponential functions of the two linear segments are made into a simulated curve which is shown in figure 38.

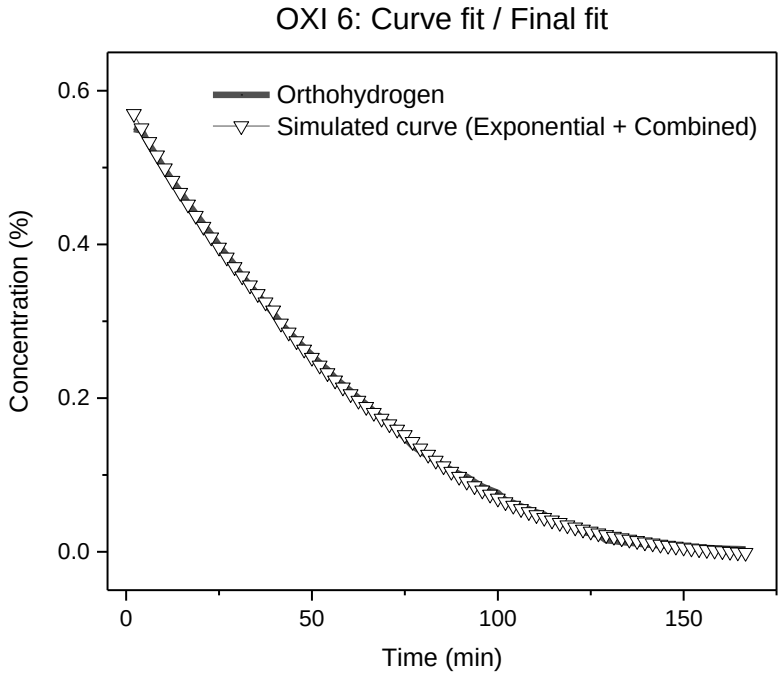

Figure 38:The final empirical curve composed of the two segments (1 & 2) and the two combined functions (1 & 2).

The empirical curve shows a good fit to the orthohydrogen profile and is composed of the two linear equations (Seg_1 and Seg_2) along with the scaled combined functions (CF_1 and CF_2), where the combined functions are weighted and normalized and the weight is changed at the point of the intersection found at 73 minutes of conversion.

However, a rate of conversion from the empirical function was not determined. Because no physical explanation could be found which describes the origin of the combined functions in order to confirm the empirical curve. Therefore, was the decision made that the rate of conversion for the OXISORB® experiments will be determined from the linear fitting of the two linear segments, respectively.

4.4.2.4 Space velocity and extrapolations to the ESS hydrogen loop

The space velocity is calculated using the rates of conversion obtained by the slope from the linear fitting of the two segments (Seg_1 and Seg_2), shown in figure 35. This is presented along with the hydrogen and catalyst amount in table 22. The following calculations are made based on the equations listed in the appendix section, see Appendix 5.

Table 22: The resulting space velocities for the two segments based on the experiment using OXISORB® as a catalyst, along with a calculated mean space velocity and the initial amount of hydrogen and catalyst used to determine the space velocities.

	Space velocity "Segment 1" [R_{Sp}] (mol H_2/min/g OXISORB®)	Space velocity "Segment 2"	Hydrogen amount (mol)	Catalyst amount (g)
OXI 1	0.00468		0.0335	0.0100
OXI 2	0.00516	0.0224	0.0340	0.0349
OXI 3	0.00441	0.0164	0.0337	0.0718
OXI 4	0.00466	0.0179	0.0338	0.0718
OXI 5	0.00421	0.0154	0.0334	0.0143
OXI 6	0.00374	0.00981	0.0333	0.0143
Mean [R_{Sp}]	0.00448	0.0164		

The space velocities determined for the two segments shows, that the space velocity for segment 2 is about a factor 4 higher than the space velocity of segment 1. Indicating that the second process, which is described by segment 2 would be a faster process in comparison to the process representing segment 1.

For IONEX® the only process which is significant to the observed first order function is the conversion of orthohydrogen. However, for the OXISORB® the first order process has changed into a relationship between two first order processes. The rate appears to become accelerated with increased degree of conversion. The cause of this behavior has not been determined from this project and is not mentioned in literature. The expected rate would be of first or second order kinetics however, neither of those fully describe the conversion process. Suggestions to what might cause this deviation has been argued to be a result of the preferential adsorption or catalyst contamination.

An observation of the space velocity for segment 1 resembles the theoretical rate reported in literature regarding the conversion of hydrogen using chromium doped silica. The rate is determined to 4 mmol H_2/min/g catalyst. This value is determined from the study [18], in which two monolayers of hydrogen is converted in approximately five minutes. This agrees well with the determined rate for the conversion based on segment 1.

The conditions for the ESS hydrogen loop based on the use of OXISORB® as a catalyst, are presented in table 23.

Table 23: Conditions for the future hydrogen loop with OXISORB® as catalyst material.

Hydrogen amount (kg)	Catalyst amount (kg)	Bypass flow (g/s)	Moderator flow (g/s)	Back conversion rate (mol H_2^P /min)	Operating temperature (K)
24	20	50	1000	10	20

The amount of catalyst for the hydrogen loop is now changed to 20 kg, which represents a safety factor of 2. The hydrogen amount in storage, flow rates and rate of back conversion is still unchanged. The same calculations used to extrapolate the space velocities to the conditions of the ESS hydrogen loop, and is presented in appendix 5. The following conversion rate is based on the catalyst amount and the time for full conversion of the hydrogen storage during the cooling process is presented in table 24.

Table 24: The determined catalytic rate based on the catalyst amount in the ESS hydrogen loop along with the time for full conversion of the hydrogen storage used as a moderator.

	Catalytic rate [R_{Tot}] (mol H_2^O /min)	Time for full conversion of H_2-storage (min)	Able to sustain back conversion (Yes/No)
Segment 1	89.6	100	Yes
Segment 2	328	27	Yes

The result from table 24 shows that the catalytic rate of OXISORB® is good enough to counteract for the back conversion of parahydrogen into orthohydrogen during operation. The back conversion for the moderator is assessed to 10 mol/min, based on a safety factor of 3. This results in that the OXISORB®, based on the catalytic rate of segment 1 and 2 is approximately 9 and 33 times greater respectively, compared to the back conversion. The hydrogen storage will be converted to the equilibrium at 20 K within the range of 1.5 hours to ½ hour, based on the rates determined from the linear segments. This confirms that OXISORB® is an acceptable catalyst for the ESS hydrogen loop. However, the obtained rates based on the amount of catalyst is lower compared to the rate determined for IONEX®. The relative amount of catalyst is lower for OXISORB® compared to IONEX®, which affects the obtained catalytic rate. The difference in catalyst amount is based on the relative volume by the catalysts. OXISORB® has a lower density compared to IONEX® which results in a lower catalyst amount.

4.4.3 Comparison between IONEX® and OXISORB®

The following rates obtained from the mean space velocities of the IONEX® and OXISORB® catalysts along with the extrapolated space velocities are presented in table 25.

Table 25: Summary of the specific space velocity and the catalytic rate based of the conditions of the hydrogen loop.

	Space velocity [R_{Sp}] (mol H_2^O /min/g Catalyst)	Catalytic rate [R_{Tot}] (mol H_2^O /min)
IONEX®	0.0505	1894
OXISORB® (Seg_1)	0.00448	89.6
OXISORB® (Seg_2)	0.0164	328

From table 25 it is possible to observe that the space velocity and catalytic rate is greater for IONEX® compared to OXISORB®. The space velocity of the IONEX® catalyst is approximately 11 times greater than segment 1 and 3 times greater that segment 2 of OXISORB®, based on the relative amount of catalyst in the ESS hydrogen loop. The true rate of conversion for OXISORB® is likely somewhere in the region of the two obtained rate expressions. To determine the true rate of conversion as well as defining the source of the apparent kinetics observed for OXISORB®, will require additional research. However, based on the obtained rates from the experiments, the IONEX® catalyst appears to be stronger compared to OXISORB®. The strength of IONEX® is reasoned to be a result of the magnetic moment from the iron ions and the magnetic density of IONEX®, which is higher compared to OXISORB®. The magnetic moment of chromium ions is weaker and the number of magnetic sites is significantly lower.

However, both catalysts have showed the capability of converting the hydrogen storage into the desired ratio of 99.8% parahydrogen. The catalytic rate is sufficient enough for both catalysts to compensate for the back conversion, in which parahydrogen is transformed into orthohydrogen in a radiation field. Based on the results IONEX® shows to be a more suitable catalyst. The catalytic rate obtained using IONEX®, based on the catalyst amount of the hydrogen loop, is a factor 21 and 5 greater than the determined rates of the two linear segments, (Seg_1 and Seg_2) in OXISORB®. However, to make a complete assessment of the suitable catalyst other factors needs to be taken into account, where catalyst degradation over long time exposure is an important factor. IONEX® is mentioned to be more prominent for deactivation due to repeated use [18]. This would require the need for the catalyst to be regenerated or even replaced more frequently. This could result in the OXISORB® being the most suitable catalyst.

The final assessment would therefore include the result regarding the rate of catalyst deactivation. Due to limited time this was not further investigated, from the IONEX® measurements could no significant deactivation be observed. The same conclusion can be made with the OXISORB® experiments where the catalyst amount was changed 3 times from the original amount in which no relationship can be observed.

4.4.3.1 Integrated area IONEX® versus OXISORB®

The observed change of the hydrogen isomers along with the total hydrogen concentration for the three measurements is shown in figure 40.

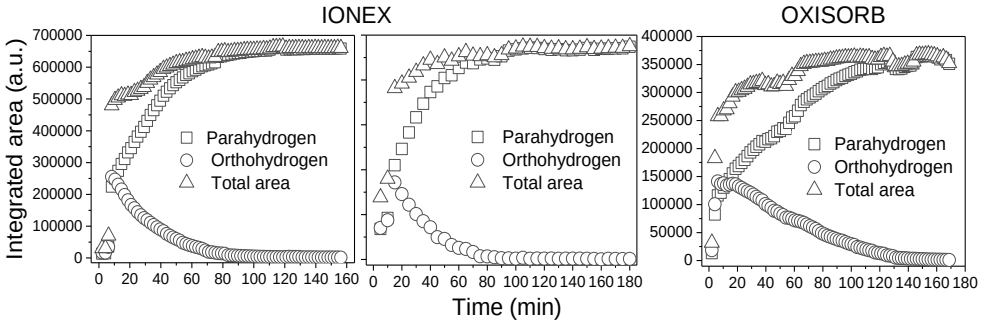

Figure 40: Change in integrated area as a function of conversion time for the three experiments, (From the left) ION 9, ION 3 and OXI 6.

Figure 40 shows the integrated area for the ortho- and parahydrogen peaks, illustrated by the circles and squares respectively. The total area is shown by the triangle line in the figure. From this figure, it is possible to observe that the total area increases with time and reaches an equilibrium, which is about the same as the observed equilibrium for the parahydrogen curve. The increase in the integrated area can be explained by the preferential adsorption. The adsorbed hydrogen is not observed by the Raman spectroscopy, which results in the increase of the integrated area.

The appearances of the ortho- and parahydrogen profiles shows a significant difference between the IONEX® and OXISORB®. This would suggest that the conversion of orthohydrogen are described by different kinetics based on the catalyst type. There is also possible to observe a difference between the ortho and parahydrogen profiles within the experiments which is clearly shown by the OXISORB® spectrum in figure 40. The parahydrogen curves increase faster compared to the orthohydrogen curves, which is the likely cause to the fluctuations of the total hydrogen curve in the spectra of figure 40. These anomalies are possibly a result of the previously mentioned sources of error, which is the preferential adsorption and especially in the case of the OXISORB® contamination of the catalyst.

The reason to why the kinetic study is performed using the relative ratio of the hydrogen isomers instead of integrated area, is that the relative ratio obtained from the hydrogen isomers is normalized irregularities in the hydrogen amount. These irregularities are observed in figure 40 as the fluctuations in the hydrogen amount. By using the relative ratio rather than the total hydrogen amount additional uncertainties are accounted for in the data, which is used to determine the catalytic rate of conversion.

4.4.3.2 Corrections for the deviation in initial ratio

The initial ratio of the hydrogen signal, without the presence of a catalyst was found to deviate from the expected ratio of normal hydrogen (75:25%, ortho: parahydrogen). To determine the relative effect of this deviation, the relationship between the observed rate and theoretical rate is assumed to be linear. The linear relationship is shown in figure 41.

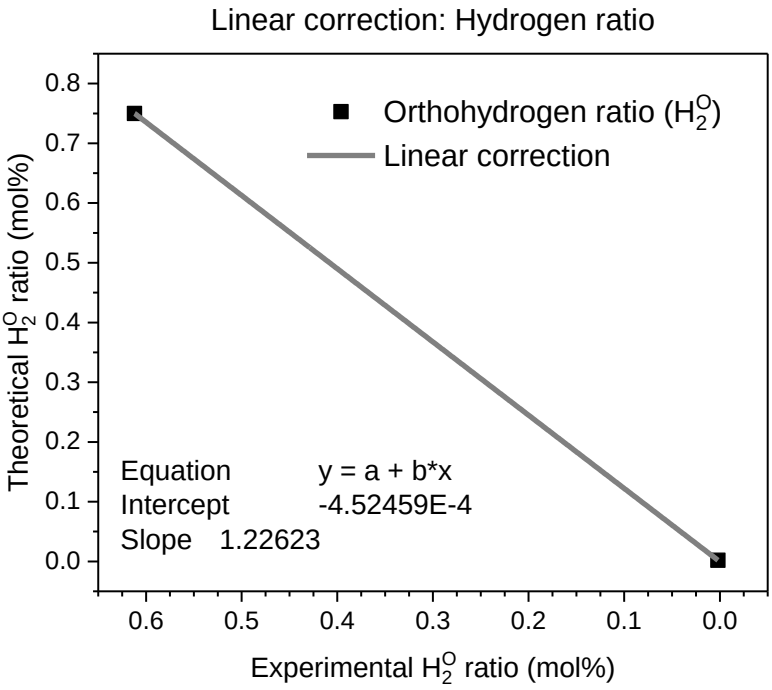

Figure 41: Linear relationship between the observed and true ratio of hydrogen.

The correction is based on the two points that are know with certainty to be correlated to both the theoretical and experimental ratio. These points are related to the initial and equilibrium ratio of the hydrogen isomers. The following relationship shown in figure 41 is related to the orthohydrogen ratio. The correction is based solely on the assumption that it is possible to describe the deviation by a linear relationship.

The experimental data corrected by the linear function obtained from figure 41 and the resulting rates from the corrected orthohydrogen curves is presented in table 26.

Table 26: Experimental and corrected rate of conversion for the experiments ION 9, ION 3 and OXI 6

	ION 9	ION 3	OXI 6 (Seg_1)	OXI 6 (Seg_2)
Rate	0.032	0.035	0.0159	0.0423
Corrected rate	0.033	0.036	0.0156	0.0451

From the table it is possible to observe that the linear correction shows a small difference in the rate of conversion, for IONEX® and segment 1 of OXISORB®. The biggest difference is observed for the second segment of OXI 6 which is related to the concentration obtained at higher degrees of conversion. The difference due to the linear corrections is however fairly small and does not affect the rate to any greater significance. This suggest that the deviation of the initial ratio has a small effect on the obtained rates for the catalytic conversion. To confirm this theory and the relative fit of these linear corrections, requires that the need to determine the response function of the spectrometer.

The observed initial distribution between the hydrogen isomers, from the hydrogen signal, has been reported in this study to be closer to a 2:1 ratio instead of the expected 3:1 distribution. The deviation between the observed and theoretical ratio is reported in literature and mathematical equations describing this relationship have been proposed [1,27,64]. From the equations presented in literature the following expression has been presented by [64] which describes the relationship in solid hydrogen.:

$$C_{Ortho} = \frac{5}{3} * \left(\frac{I_{Para}}{I_{Ortho}} + \frac{5}{3}\right)^{-1}$$

In this expression (C_{Ortho}) represents the orthohydrogen ratio which has been corrected for the deviation. The correction is performed using the integrated intensities of the ortho- and parahydrogen peaks (I_{Ortho} and I_{Para}) that is observed in the obtained Raman spectrum. the corrected value can be used to evaluate the fit of the observed ratio to the expected distribution. The following table shows the relationship between the observed ratio and the expected ratio of normal hydrogen (3:1) using the previously presented mathematical expression.

The experiments presented in table 27 are the observed hydrogen signal H2B3 (table 10) and the determined ratio from the experiments ION 3, ION 9 (table 13) and OXI 6 (table 20).

Table 27: Comparison of the experimental and theoretical ratio of ortho- and parahydrogen. Along with the determined fraction and the relative difference to the fraction of the mathematical relationship.

Experiment	I_{Ortho} (%)	I_{Para} (%)	C_{Ortho} (mol%)	Difference (%)
H2B3	61.2	38.8	72.4	96.6
ION 3	50.7	49.3	63.2	84.2
ION 9	54.6	45.4	66.7	89.0
OXI 6	55	45	67.1	89.4

From table 27 it is obvious that the hydrogen signal of (H2B3) can be regarded to agree within the margin of the experimental error while the observed ratio for the conversion experiments (ION and OXI) shows a much larger deviation. This deviation has been confirmed as the conversion of orthohydrogen during the loading process. The two methods which are presented in this chapter to correct for the deviation of the hydrogen ratio shows similar results regarding the relationship between the obtained signal and the true distribution of the hydrogen isomers. This suggest that the obtained hydrogen signal is in agreement with the true ratio. The mathematical expression used for solid hydrogen also appears to be applicable for the correction of the observed hydrogen ratio for liquid hydrogen data.

5 Conclusion

The final design of the experimental setup, allows the acquisition a Raman spectrum with an acceptable resolution of the hydrogen signal. The resolution is good enough for the characterization and integration of the peaks for use in liquid hydrogen and provides reliable information regarding the conversion of ortho- to parahydrogen. The obtained spectrum includes three peaks, which are characteristic to hydrogen. These peaks represent the first order rotational levels of ortho- and parahydrogen as well as the first order vibrational level. The optimization of the experimental system has shown the importance of the positioning of the optical components. Another important conclusion is that sapphire is the best transparent material for the window of the sample cell. An internal Raman shift was observed for the Raman spectroscopy system. The shift was determined to 30.2 cm^{-1}. The internal shift is due to the interference of the scattered light by the surrounding environment as well as the equipment used in the spectroscopy setup.

The kinetics of the catalytic conversion of orthohydrogen using IONEX® and OXISORB® catalyst was studied. From the study it became evident that the two catalysts exhibit different characteristics. The OXISORB® requires approximately 7 times more catalyst, to perform a full conversion in the same time frame as the IONEX®. A full conversion is obtained when hydrogen with normal distribution (25% parahydrogen) is converted to the equilibrium distribution of hydrogen at 20K (99.8% parahydrogen)

The rate of conversion using IONEX® was found to fit an exponential first order function which showed a good fit for the catalytic process of both the ortho- and parahydrogen The reaction kinetics while using the OXISORB® catalyst, it was not possible to describe the entire conversion process with a single mathematical equation. The conversion is characterized to be of two first order processes which are dominant individually at the beginning and the end of the reaction. In the intermediate region a combination of these two seems to dominate. This was studied by empirical modeling of the concentration profile of orthohydrogen, in which the intermediate region is described by two additional weighted functions. However, the physics behind this is not clear and the catalytic rate is determined based on the two linear segments.

The conversion rates while using IONEX® and OXISORB® catalysts were determined from the kinetic study, which showed that the conversion of orthohydrogen using IONEX® is faster compared to the conversion while using OXISORB®, based on equivalent amounts of the catalysts. The space velocities were determined for the two catalysts, where the space velocity corresponding to IONEX® was 6.7 times lower compared to the space velocity reported by the manufacturer. This deviation is possibly a result of the experimental conditions. The experiments in this thesis have been conducted in a static setup and at 16K, while the manufacturer determined the space velocity in a continuous flow of hydrogen gas at 77K. The space velocity determined from the OXISORB® trials showed a resemblance to the conversion rate by similar catalysts of chromium doped silica. The extrapolation of the space velocities shows that both catalysts are suitable for the conversion of orthohydrogen and can compensate for the estimated back conversion of para- to orthohydrogen during the operation of the ESS liquid hydrogen moderator. The comparison of the catalysts shows that the IONEX® catalyst is more efficient compared to the OXISORB® catalyst. However, to make a definitive assessment of the most optimal catalyst, there is a need to study the relative long-term effects of the catalytic conversion using the two catalysts and to determine the life times of the catalysts.

6 Future work

This thesis has presented an initial structure for the analysis of the ortho- and parahydrogen ratio in liquid hydrogen and provided with an initial assessment of the relative kinetics for the two catalysts. However, there is still room for improvement in this field to further improve the experimental setup and the implementation of additional experiments for the definitive assessment of the catalytic performance.

For the Raman spectroscopy system are enhancement of the resolution a continuous desired feature. The relative effect on the resolution by implementing a laser with a higher power output or a stronger excitation wavelength are possible features for future experiments.

Optimization of the signal to noise ratio, by determining the response function of the spectrometer. If the response function is known, the signal to noise can be corrected in relation to the inherent factor which would provide with more precise data.

The kinetics regarding OXISORB requires to be further studied to determine if the observed two linear kinetics are correct of if they are a result of interfering factors. By confirming the kinetics, the following rate of conversion will be confirmed in which a better comparison between the IONEX® and OXISORB® can be performed.

The investigations of the long-term degradation of the catalyst could be further investigate to determine the relative stability of the catalytic activity which would provide with valuable information for the assessment of the most suitable catalyst.

The effect on the relative gain in intensity due to coupled optical fibers in comparison with the currently used single fiber is also a point for possible improvement of the Raman spectroscopy system. Providing with information on the relative improvement of the resolution by the addition of optical fibers.

Another possible investigation is the relative effect on the intensity by the emission of the excitation laser through vacuum feedthroughs which was not implemented in this experimental setup but will be an addition to the future ESS hydrogen loop.

The kinetic study of the catalytic conversion could be further analyzed, based on a continuous setup, where the hydrogen is circulated over the catalyst.

References

[1] I. F. Silvera, “The solid molecular hydrogens in the condensed phase: Fundamentals and static properties,” *Rev. Mod. Phys.*, vol. 52, no. 2, pp. 393–452, Apr. 1980.

[2] “Hydrogen,” *National Center for Biotechnology Information. PubChem Compound Database*, 16-Jun-2004. [Online]. Available: https://pubchem.ncbi.nlm.nih.gov/compound/783. [Accessed: 05-Apr-2017].

[3] “Hydrogen - Element information, properties and uses,” *Rsc.org*. [Online]. Available: http://www.rsc.org/periodic-table/element/1/hydrogen. [Accessed: 05-Apr-2017].

[4] M. Hartl *et al.*, “Hydrogen adsorption on two catalysts for the ortho- to parahydrogen conversion: Cr-doped silica and ferric oxide gel,” *Phys Chem Chem Phys*, vol. 18, no. 26, pp. 17281–17293, 2016.

[5] B. S. Burkholder, “Catalysis of Conversion Between the Spin Isomers of H2 by MOF-74,” *Oberlin Coll. Honors Thesis*, 2009.

[6] M. Teshigawara *et al.*, “Experimental verification of equilibrium para-hydrogen levels in hydrogen moderators irradiated by spallation neutrons at J-PARC,” *Nucl. Instrum. Methods Phys. Res. Sect. B Beam Interact. Mater. At.*, vol. 368, pp. 66–70, Feb. 2016.

[7] N. Watanabe, “Neutronics of pulsed spallation neutron sources,” *Rep. Prog. Phys.*, vol. 66, no. 3, pp. 339–381, Mar. 2003.

[8] T. Kai, M. Harada, M. Teshigawara, N. Watanabe, and Y. Ikeda, “Coupled hydrogen moderator optimization with ortho/para hydrogen ratio,” *Nucl. Instrum. Methods Phys. Res. Sect. Accel. Spectrometers Detect. Assoc. Equip.*, vol. 523, no. 3, pp. 398–414, May 2004.

[9] Y. Kiyanagi, N. Watanabe, and H. Iwasa, “Experimental studies on neutronic performance of coupled liquid-hydrogen moderator for pulsed spallation neutron sources,” *Nucl. Instrum. Methods Phys. Res. Sect. Accel. Spectrometers Detect. Assoc. Equip.*, vol. 312, no. 3, pp. 561–570, 1992.

[10] K. Batkov, A. Takibayev, L. Zanini, and F. Mezei, “Unperturbed moderator brightness in pulsed neutron sources,” *Nucl. Instrum. Methods Phys. Res. Sect. Accel. Spectrometers Detect. Assoc. Equip.*, vol. 729, pp. 500–505, Nov. 2013.

[11] B. F. Minaev and H. Aagren, “Spin catalysis of ortho-para hydrogen conversion,” *J Phys Chem*, vol. 99, no. 21, pp. 8936–8940, 1995.

[12] L.-M. Sutherland, J. N. Knudson, M. Mocko, and R. M. Renneke, “Practical in-situ determination of ortho-para hydrogen ratios via fiber-optic based Raman spectroscopy,” *Nucl. Instrum. Methods Phys. Res. Sect. Accel. Spectrometers Detect. Assoc. Equip.*, vol. 810, pp. 182–185, Feb. 2016.

[13] J. W. Leachman, R. T. Jacobsen, S. G. Penoncello, and E. W. Lemmon, “Fundamental Equations of State for Parahydrogen, Normal Hydrogen, and Orthohydrogen,” *J. Phys. Chem. Ref. Data*, vol. 38, no. 3, pp. 721–748, Sep. 2009.

[14] G. Buntkowsky, B. Walaszek, A. Adamczyk, Y. Xu, H.-H. Limbach, and B. Chaudret, “Mechanism of nuclear spin initiated para-H2 to ortho-H2 conversion,” *Phys. Chem. Chem. Phys.*, vol. 8, no. 16, p. 1929, 2006.
[15] J. Natterer and J. Bargon, “Parahydrogen induced polarization,” *Prog. Nucl. Magn. Reson. Spectrosc.*, vol. 31, no. 4, pp. 293–315, 1997.
[16] T. R. Prisk, M. S. Bryan, and P. E. Sokol, “Diffusive and rotational dynamics of condensed n-H $_2$ confined in MCM-41,” *Phys. Chem. Chem. Phys.*, vol. 16, no. 33, p. 17960, Jul. 2014.
[17] B. I. Verkin, T. B. Selover, and J. I. Ghojel, Eds., *Handbook of properties of condensed phases of hydrogen and oxygen*, Rev. and augm. English ed. New York: Hemisphere Pub. Corp, 1991.
[18] N. S. Sullivan, D. Zhou, and C. M. Edwards, “Precise and efficient in situ ortho — para-hydrogen converter,” *Cryogenics*, vol. 30, no. 8, pp. 734–735, Aug. 1990.
[19] E. Ilisca, “Ortho-para conversion of hydrogen molecules physisorbed on surfaces,” *Prog. Surf. Sci.*, vol. 41, no. 3, pp. 217–335, Nov. 1992.
[20] C. M. Cunningham and H. L. Johnston, “The Surface Catalysis of the Ortho- to Para-Conversion in Liquid Hydrogen by Paramagnetic Oxides on Alumina,” *J. Am. Chem. Soc.*, vol. 80, no. 10, pp. 2377–2382, May 1958.
[21] Y. L. Sandler, “The Adsorption and the Magnetic Ortho–Para Conversion of Hydrogen on Diamagnetic Solids. I. Some Experiments in Surface Paramagnetism,” *J. Phys. Chem.*, vol. 58, no. 1, pp. 54–57, 1954.
[22] J. W. Conant, F. J. Edeskuty, J. E. Huston, and F. V. Thome, “The conversion of para to orthohydrogen in a gamma-ray and neutron radiation field,” *Cryogenics*, vol. 15, no. 1, pp. 12–16, Jan. 1975.
[23] D. H. Weitzel, W. V. Loebenstein, J. W. Draper, and O. E. Park, “Ortho-para catalysis in liquid-hydrogen production,” *J. Res. Natl. Bur. Stand.*, vol. 60, no. 3, pp. 221–227, 1958.
[24] “Magnetic Moments of Transition Metals,” *Chemistry LibreTexts*. [Online]. Available: https://chem.libretexts.org/Core/Inorganic_Chemistry/Crystal_Field_Theory/Magnetic_Moments_of_Transition_Metals. [Accessed: 05-Apr-2017].
[25] H. Kasai, W. A. Diño, and R. Muhida, “Surface science-based reaction design: increasing the ortho–para hydrogen conversion yield via molecular orientation, a case study,” *Prog. Surf. Sci.*, vol. 72, no. 1–4, pp. 53–86, Jun. 2003.
[26] E. B. Iverson and J. M. Carpenter, “Kinetics of irradiated liquid hydrogen,” in *Proceedings of the International Collaboration on Advanced Neutron Sources*, Neuss, Germany, 2003.
[27] M. J. Matthews, G. Petitpas, and S. M. Aceves, “A study of spin isomer conversion kinetics in supercritical fluid hydrogen for cyrogenic fuel storage technologies,” *Appl. Phys. Lett.*, vol. 99, no. 8, p. 081906, 2011.
[28] E. Ilisca, “Theoretical Calculation of a New Effect in Ortho-Para H 2 Conversion on Magnetic Surfaces,” *Phys. Rev. Lett.*, vol. 24, no. 15, pp. 797–798, Apr. 1970.

[29] J. R. Ferraro, K. Nakamoto, and C. W. Brown, “Introductory Raman spectroscopy,” in *Introductory Raman spectroscopy*, 2nd ed., Amsterdam ; Boston: Academic Press, 2003, pp. 1–32.
[30] E. Smith and G. Dent, “Modern Raman spectroscopy: a practical approach,” in *Modern Raman spectroscopy: a practical approach*, Hoboken, NJ: J. Wiley, 2005, pp. 1–21.
[31] E. Smith and G. Dent, “Modern Raman spectroscopy: a practical approach,” in *Modern Raman spectroscopy: a practical approach*, Hoboken, NJ: J. Wiley, 2005, pp. 71–92.
[32] P. Vandenabeele, “Practical Raman spectroscopy: an introduction,” The Atrium, Southern Gate, Chichester, West Sussex, United Kingdom: Wiley, 2013, pp. 1–38.
[33] E. Smith and G. Dent, “Modern Raman spectroscopy: a practical approach,” in *Modern Raman spectroscopy: a practical approach*, Hoboken, NJ: J. Wiley, 2005, pp. 23–41.
[34] J. R. Ferraro, K. Nakamoto, and C. W. Brown, “Introductory Raman spectroscopy,” in *Introductory Raman spectroscopy*, 2nd ed., Amsterdam ; Boston: Academic Press, 2003, pp. 103–137.
[35] P. Vandenabeele, “Practical Raman spectroscopy: an introduction,” The Atrium, Southern Gate, Chichester, West Sussex, United Kingdom: Wiley, 2013, pp. 61–100.
[36] “Cryogenic Research Equipment by Janis Research Company,” *Janis.com*. [Online]. Available: https://www.janis.com/. [Accessed: 20-Apr-2017].
[37] “Kurt J. Lesker Company | CF Flanged Zero Length Quartz (Fused Silica) Glass Viewports | Vacuum Science is our Busines,” *Lesker.com*. [Online]. Available: http://www.lesker.com/newweb/flanges/viewports_cf_quartz.cfm?pgid=0. [Accessed: 20-Apr-2017].
[38] “Kurt J. Lesker Company | CF Flanged Zero Length Sapphire Viewports | Vacuum Science is our Business,” *Lesker.com*. [Online]. Available: http://www.lesker.com/newweb/flanges/viewports_cf_sapphire.cfm?pgid=0. [Accessed: 20-Apr-2017].
[39] “Silica Glass (SiO2) Optical Material,” *Crystran.co.uk*. [Online]. Available: https://www.crystran.co.uk/optical-materials/silica-glass-sio2. [Accessed: 21-Apr-2017].
[40] “Sapphire Optical Material,” *Crystran.co.uk*. [Online]. Available: https://www.crystran.co.uk/optical-materials/sapphire-al2o3. [Accessed: 21-Apr-2017].
[41] “Swagelok.com the source for tube fittings, valves, and other fluid system components | Swagelok,” *Swagelok.com*. [Online]. Available: https://www.swagelok.com/en. [Accessed: 03-Apr-2017].
[42] “The All New OCEANOPTICS.COM,” *Ocean Optics*. [Online]. Available: https://oceanoptics.com/. [Accessed: 03-Apr-2017].

[43] “InPhotonics: Makers of the Raman Probe (TM) and Raman spectrometer Raman spectroscopy,” *Inphotonics.com*. [Online]. Available: http://www.inphotonics.com/. [Accessed: 05-Apr-2017].
[44] “Thorlabs, Inc. - Your Source for Fiber Optics, Laser Diodes, Optical Instrumentation and Polarization Measurement & Control,” *Thorlabs.com*. [Online]. Available: https://www.thorlabs.com/. [Accessed: 05-Apr-2017].
[45] “ASTM E1840-96(2014), Standard Guide for Raman Shift Standards for Spectrometer Calibration,” vol. 2014. ASTM International, West Conshohocken, PA, p. 11.
[46] Leybold GmbH, “PHOENIX L300i MODUL | Leybold,” *Leybold Online Shop*. [Online]. Available: https://www.leyboldproducts.com/products/leak-detecting-instruments/leak-detectors/751/phoenix-l300i-modul. [Accessed: 10-May-2017].
[47] “Reaction Order - Chemistry LibreTexts,” *Chemistry LibreTexts*. [Online]. Available: https://chem.libretexts.org/Core/Physical_and_Theoretical_Chemistry/Kinetics/Rate_Laws/The_Rate_Law/Reaction_Order. [Accessed: 20-Oct-2017].
[48] “First-Order Reactions - Chemistry LibreTexts,” *Chemistry LibreTexts*. [Online]. Available: https://chem.libretexts.org/Core/Physical_and_Theoretical_Chemistry/Kinetics/Reaction_Rates/First-Order_Reactions. [Accessed: 20-Oct-2017].
[49] “Using Graphs to Determine Integrated Rate Laws - Chemistry LibreTexts,” *Chemistry LibreTexts*. [Online]. Available: https://chem.libretexts.org/Core/Physical_and_Theoretical_Chemistry/Kinetics/Experimental_Methods/Using_Graphs_to_Determine_Integrated_Rate_Laws. [Accessed: 20-Oct-2017].
[50] “Naphthalene 147141,” *Sigma-Aldrich*. [Online]. Available: http://www.sigmaaldrich.com/catalog/product/aldrich/147141?lang=en&region=SE. [Accessed: 28-Apr-2017].
[51] I. R. Lewis and H. G. M. Edwards, *Handbook of Raman spectroscopy: from the research laboratory to the process line*. New York: Marcel Dekker, 2001.
[52] E. R. Lippincott and E. J. O’Reilly, “Vibrational Spectra and Assignment of Naphthalene and Naphthalene- *d* -8,” *J. Chem. Phys.*, vol. 23, no. 2, pp. 238–244, Feb. 1955.
[53] S. S. Mitra and H. J. Bernstein, “VIBRATIONAL SPECTRA OF NAPHTHALENE- d_0 , -α- d_4 , AND - d_8 MOLECULES,” *Can. J. Chem.*, vol. 37, no. 3, pp. 553–562, Mar. 1959.
[54] A. K. Yadav and P. Singh, “A review of the structures of oxide glasses by Raman spectroscopy,” *RSC Adv*, vol. 5, no. 83, pp. 67583–67609, 2015.
[55] M. Wang, J. CHeng, M. Li, and F. He, “Raman spectra of soda–lime–silicate glass doped with rare earth,” *Phys. B Condens. Matter*, vol. 406, no. 20, pp. 3865–3869, Oct. 2011.
[56] F. L. Galeener, “Planar rings in vitreous silica,” *J. Non-Cryst. Solids*, vol. 49, no. 1–3, pp. 53–62, 1982.

[57] S. K. Sharma, A. K. Misra, S. M. Clegg, J. E. Barefield, R. C. Wiens, and T. Acosta, “Time-resolved remote Raman study of minerals under supercritical CO2 and high temperatures relevant to Venus exploration,” *Philos. Trans. R. Soc. Math. Phys. Eng. Sci.*, vol. 368, no. 1922, pp. 3167–3191, Jul. 2010.
[58] M. H. Manghnani, A. Hushur, T. Sekine, J. Wu, J. F. Stebbins, and Q. Williams, “Raman, Brillouin, and nuclear magnetic resonance spectroscopic studies on shocked borosilicate glass,” *J. Appl. Phys.*, vol. 109, no. 11, p. 113509, Jun. 2011.
[59] S. P. S. Porto and R. S. Krishnan, “Raman Effect of Corundum,” *J. Chem. Phys.*, vol. 47, no. 3, pp. 1009–1012, Aug. 1967.
[60] M. Kadleíková, J. Breza, and M. Veselý, “Raman spectra of synthetic sapphire,” *Microelectron. J.*, vol. 32, no. 12, pp. 955–958, Dec. 2001.
[61] A. Aminzadeh and H. Sarikhani-fard, “Raman spectroscopic study of Ni/Al2O3 catalyst,” *Spectrochim. Acta. A. Mol. Biomol. Spectrosc.*, vol. 55, no. 7–8, pp. 1421–1425, Jul. 1999.
[62] H. Yamaoka *et al.*, “Ruby pressure scale in a low-temperature diamond anvil cell,” *J. Appl. Phys.*, vol. 112, no. 12, p. 124503, Dec. 2012.
[63] D. D. Ragan, R. Gustavsen, and D. Schiferl, “Calibration of the ruby R_1 and R_2 fluorescence shifts as a function of temperature from 0 to 600 K,” *J. Appl. Phys.*, vol. 72, no. 12, pp. 5539–5544, Dec. 1992.
[64] J. H. Eggert, E. Karmon, R. J. Hemley, H. K. Mao, and A. F. Goncharov, “Pressure-enhanced ortho-para conversion in solid hydrogen up to 58 GPa,” *Proc. Natl. Acad. Sci. U. S. A.*, vol. 96, no. 22, pp. 12269–12272, 1999.
[65] P. A. Jansson, “Method for determining the response function of a high-resolution infrared spectrometer,” *JOSA*, vol. 60, no. 2, pp. 184–191, 1970.
[66] “A Glossary of Spectroscopic Terms - Ocean Optics,” *Ocean Optics*. [Online]. Available: https://oceanoptics.com/glossary/. [Accessed: 10-May-2017].

Appendix

Appendix 1 – The optimized settings of the Raman spectrometer.

Table A1: Optimized settings for the Raman spectrometer for the conducted experiments.

	Integration time ($t_{integration}$)	Scans to average ($n_{scans\,to\,average}$)	Boxcar width (n_{box})	Temperature (K)	Lens [Focal length] (mm)	
ION						
1	7 & 60	5 & 1	0	16 ± 1	75	OoF
2	60	5	0	16 ± 1	100	OoF
3	60	1	1	16 ± 1	100	OoF
4	5	5	1	16 ± 1	100	
5	5	5	1	16 ± 1	100	
6	5	5	1	16 ± 1	75	
7	5	5	1	16 ± 1	75	
8	5	5	1	16 ± 1	75	
9	5	5	1	16 ± 1	75	
OXI						
1	5	5	1	16 ± 1	75	
2	5	5	1	16 ± 1	75	
3	5	5	1	16 ± 1	75	
4	5	5	1	16 ± 1	75	
5	5	5	1	16 ± 1	75	
6	5	5	1	16 ± 1	75	
H2B						
B1	7	5	1	16 ± 1	100	OoF
B2	60	1	1	16 ± 1	100	OoF
B3	5	5	1	16 ± 1	75	
B4	5	5	1	16 ± 1	75	AL
H2T						
1	5	1	1	16 ± 1	75	200 µm
2	5	1	1	16 ± 1	75	400 µm
3	5	1	1	16 ± 1	75	200 µm, AL
4	5	1	1	16 ± 1	75	400 µm, AL

OoF: Out of focus
AL: Above liquid surface
200 µm: 200 micrometer fiber
400 µm: 400 micrometer fiber

Appendix 2 – Complete table of the initial parameters for the catalytic conversion using IONEX®

Table A2: Initial parameters regarding the hydrogen amount, catalyst amount and acquisition time for the Catalytic conversion experiments using IONEX®.

	Amount of hydrogen (Bar, @ RT, 150 ml)	Hydrogen amount (mmol)	Catalyst amount (mg)	Time [Full time]/[liquid state] (min)
ION 1	5.49 ±0.01	33.22	21.0 ±0.1	195/191
ION 2	5.46 ±0.01	33.04	21.0 ±0.1	200/195
ION 3	5.58 ±0.01	33.76	21.0 ±0.1	180/100
ION 4	5.53 ±0.01	33.46	21.0 ±0.1	180/167
ION 5	5.50 ±0.01	33.28	21.0 ±0.1	150/144
ION 6	5.45 ±0.01	32.98	20.8 ±0.1	160/157
ION 7	5.54 ±0.01	33.52	20.8 ±0.1	160/154
ION 8	5.54 ±0.01	33.52	20.8 ±0.1	160/156
ION 9	5.56 ±0.01	33.64	20.8 ±0.1	180/175

Appendix 3 – Complete set of the obtained variables from the fitting of the exponential functions on the concentration profiles of the IONEX® experiments.

Table A3: The complete information regarding the obtained variable form the fitting of the exponential functions of the IONEX® concentration profiles.

	Isomer	Model fit	Offset [y_0] (a.u.)	Amplitude [A_1] (a.u.)	Time factor [t_1] (min)	Half-life [$t_{\frac{1}{2}}$] (min)	Rate [τ] (min^{-1})
ION 1	Ortho	ExpDec1	0.005	0.528	46.95	32.54	0.021
ION 1	Para	ExpGro1	0.995	-0.528	46.95	32.54	0.021
ION 2	Ortho	ExpDec1	0.004	0.568	34.60	23.98	0.029
ION 2	Para	ExpGro1	0.996	-0.568	34.60	23.98	0.029
ION 3	Ortho	ExpDec1	-0.009	0.688	28.84	19.99	0.035
ION 3	Para	ExpGro1	1.009	-0.688	28.84	19.99	0.035
ION 4	Ortho	ExpDec1	-0.025	0.581	41.09	28.48	0.024
ION 4	Para	ExpGro1	1.025	-0.581	41.09	28.48	0.024
ION 5	Ortho	ExpDec1	0.015	0.633	33.11	22.95	0.030
ION 5	Para	ExpGro1	0.985	-0.633	33.11	22.95	0.030
ION 6	Ortho	ExpDec1	0.002	0.667	28.51	19.76	0.035
ION 6	Para	ExpGro1	0.998	-0.667	28.51	19.76	0.035
ION 7	Ortho	ExpDec1	0.000	0.656	25.98	18.01	0.038
ION 7	Para	ExpGro1	1.000	-0.656	25.98	18.01	0.038
ION 8	Ortho	ExpDec1	-0.005	0.754	25.31	17.54	0.040
ION 8	Para	ExpGro1	1.005	-0.754	25.31	17.54	0.040
ION 9	Ortho	ExpDec1	0.004	0.698	31.32	21.71	0.032
ION 9	Para	ExpGro1	0.996	-0.698	31.32	21.71	0.032

Appendix 4 – Initial and final concentration of the ortho- and parahydrogen ratio for the IONEX® experiments.

Table A3: Initial and final concentration of the ortho- and parahydrogen concentration for the IONEX® experiments.

Sample	$H_{2_{INIT}}^{P}$ (mol%)	$H_{2_{INIT}}^{O}$ (mol%)	$H_{2_{END}}^{P}$ (mol%)	$H_{2_{END}}^{O}$ (mol%)
ION 1	52.4	47.6	99.4	0.6
ION 2	53.2	46.8	99.4	0.6
ION 3	49.3	50.7	99.7	0.3
ION 4	48.0	52.0	99.7	0.3
ION 5	49.7	50.3	99.1	0.9
ION 6	44.2	55.8	99.7	0.3
ION 7	51.3	48.7	99.7	0.3
ION 8	46.8	53.2	99.8	0.2
ION 9	45.4	54.6	99.6	0.4

Appendix 5 – Formulas for the calculation of space velocity and extrapolation to the future ESS hydrogen loop.

Calculated space velocity [R_{Sp}] for the catalytic conversion measured in the experiments:

$$R_{Sp} = \frac{\left(\frac{P_{H_2} * V_{Cyl}}{R * T}\right) * \tau}{m_{Cat}}$$

Conversion rate for orthohydrogen (based on the total catalyst amount used):

$$R_{Tot} = R_{Sp} * m_{Cat,Tot}$$

Time required for full conversion of the orthohydrogen amount (based on the catalytic rate of the total catalyst amount):

$$t_{Tot} = \frac{n_{H2}}{R_{Tot}} * 0.75$$

Time for full circulation of hydrogen via the moderator loop.

$$t_{Mod} = \frac{m_{H2}}{F_{Mod}}$$

Time for full circulation of hydrogen over the catalyst bypass:

$$t_{Bypass} = \frac{m_{H2}}{F_{Bypass}}$$

Flow rate relationship between moderator and catalyst loop:

$$n_{\frac{Bypass}{Moderator}} = \frac{t_{Bypass}}{t_{Moderator}} = \frac{F_{Mod}}{F_{Bypass}}$$